University of Nevada, Reno

The Use of Nonlocal Static Stability to Determine Mixing Height from NCEP Eta Model Output over the Western U.S.

A thesis submitted in partial fulfillment of the
requirements for the degree of Master of Science in
Atmospheric Science

by

Matthew G. Fearon

Dr. Timothy J. Brown/Thesis Advisor

December, 2000

ABSTRACT

Planetary boundary layer (PBL) structure is of great importance when predicting localized air quality. Knowledge of its depth can provide information about lower atmospheric transport and dispersion that strongly influence the vertical extent of pollutants. Forecasting the mixing layer height (the altitude above ground within which pollutants are dispersed) and mean transport (the average wind speed and direction within the determined mixing layer) is a common method of assessing localized air quality. Prediction of these variables is also an essential guidance tool for the wildland fire agencies as decision-makers can utilize such forecasts to monitor smoke dispersion resulting from wildfire and prescribed burning.

For this study, mixing height values are computed at 00 and 12 UTC for the period September 1997 through August 1999 using NCEP Eta model output and atmospheric sounding data. Values are determined from both data sets using a nonlocal static stability method (Stull), and an operational NWS method (Holzworth). The principal objectives of this study are:

(1) To introduce the Stull method and statistically compare it to the Holzworth procedure.

(2) To examine and compare mixing height differences computed from NCEP Eta model output and atmospheric sounding data.

(3) To address the poor spatial and temporal representation of mixing height values produced from soundings over the western U.S. by using NCEP Eta model output.

ACKNOWLEDGEMENTS

By far, writing this thesis is one of the most challenging things I have done in my lifetime. There were many instances where I was extremely frustrated and annoyed with this project and graduate school in general. I will never forget the times I had to force myself physically and mentally to continue to achieve my goal, especially during beautiful summer weather. Even though it took tremendous efforts on my part to complete this Masters Degree, there are many people to whom I must show great appreciation and thanks.

I would first like to thank my research advisor, Tim Brown. Tim allowed me to become much more exposed to the scientific computing world, which was something I was in desperate lack of when I arrived at the Desert Research Institute in August 1998. He showed a great deal of patience with me when I struggled with computing concepts that in reality were not that difficult to grasp. Tim was also inviting to my research opinions and always encouraged me to explore my ideas. I should not forget to mention the kindness and patience Tim should me when I took four weeks off after my first semester of graduate school to move my fiancée across country. Tim Brown has been an excellent mentor and I owe him a great deal of thanks.

Next, I would like to thank John Lewis for taking the time to be on my research committee. John often provided extra time for me to discuss my research ideas and problems with him. We also had friendly conversations about John's past experiences as a graduate student that often helped me continue when I was academically frustrated over

the last year and half. John is a great person and has become a good friend of mine. His advice and encouragement is unforgettable.

I would like to thank Scott Mensing who took the time and patience to sit on my research committee. Scott was patient with me when I had to change my oral defense date a couple of times and he was very helpful in allowing me additional time prior to the scheduled defense. I greatly appreciate his advice and suggestions toward finalizing this research. Beth Hall, a Research Assistant here at DRI, also took extra time to assist me with numerous computing concepts that were plaguing to me while I performed this research. She is great person and I am very appreciative of her assistance.

Since this research project would not have been possible without the two rather large data sets that were supplied. I need to extend great deal of thanks to National Weather Service Cooperative Program for Operational Meteorology, Education and Training (COMET), specifically Elizabeth Page, for providing the NCEP Eta model output used in this study. I would also like to thank the Western Regional Climate Center, specifically James Ashby, who made the atmospheric sounding data used for this research easily attainable.

Lastly, I would like to thank my family, close friends, and my beautiful fiancée Erin for their strong love and support while I completed this Master's Degree. Erin, who I owe the most personal appreciation to, put her life on hold for me for two years and always put up with me when I was extremely frustrated. I am forever thankful for her strong love and encouragement. She is the most precious part of my life. Forever love and thanks!

“You know if you put your mind to it, you can accomplish anything.”

– Movie: Back to the Future, 1985

CONTENTS

TABLES

FIGURES

CHAPTER ONE

INTRODUCTION

One of the most important aspects of air quality monitoring involves examination of the planetary boundary layer (PBL) structure. The PBL is defined as the atmospheric layer that extends from the earth's surface to the geostrophic wind level, the upper limit of frictional influence from earth's surface (Huschke, 1959). Assessment of PBL can provide information about lower atmospheric transport and diffusion that strongly influence the amount of pollutants present in an environment. For many years, forecasting the mixing layer height (the altitude above ground to which pollutants are vertically dispersed; Beyrich et al. 1996) and mean transport (the average wind speed and direction within the determined mixing layer) has been a common method for estimating localized air quality. Prediction of these boundary layer variables is also an essential guidance tool for the wildland fire community as decision-makers can utilize such forecasts to monitor smoke dispersion resulting from wildfire and prescribed burning.

Prescribed burning is a method of re-introducing fire back into the ecosystem life cycle. Prior to the late 1970s, non-anthropogenic fire ignition was not often viewed as a natural environmental occurrence and full suppression measures were the only response to its onset. Planned burns are used to reduce hazard during future fire suppression of unplanned wildfires since control of the burning terrain is generally more predictable (Pyne et al. 1996). Part of the strategy involved with prescribed burning is managing the resulting smoke. Many National Weather Service Forecast Offices (NWSFOs) issue daily forecasts of mixing height and mean transport specifically for fire agency managers

and decision-makers by using atmospheric profile measurements available from radiosondes or model derived profiles (typically only extracted at radiosonde launch locations; Figure 1-1). These height and wind estimates are used as a guidance tool to assess the vertical dispersion of smoke and its transport in order to comply with visibility and air quality guidelines that are within the acceptable limits of the Clean Air Act (NWS, 2000).

The practice of prescribed burning began in the late 1970s, however it is being utilized much more often nowadays. Due to the increased usage of burn planning, fire agencies (e.g., U.S. Forest Service, National Park Service, and Bureau of Land Management) have been requesting more timely (i.e., beyond 12 hours) and spatially specific smoke management forecasts. However, radiosonde measurements currently used for prediction are available at 00 and 12 UTC which only allows 12 hour forecasts to be issued unless model derived soundings are utilized. Therefore, in order to address this problem, this study explores using a more comprehensive data source to provide better spatial and time resolution forecasts of mixing height and mean transport wind over the western United States.

Problem definition

The current problem with operational forecasts of mixing height and mean transport may be divided into three areas: 1) methodology used to generate forecasts, 2) spatial representation of values over a large geographical area (e.g., western United States), and 3) temporal availability of forecasts which typically are not greater than 12 hours.

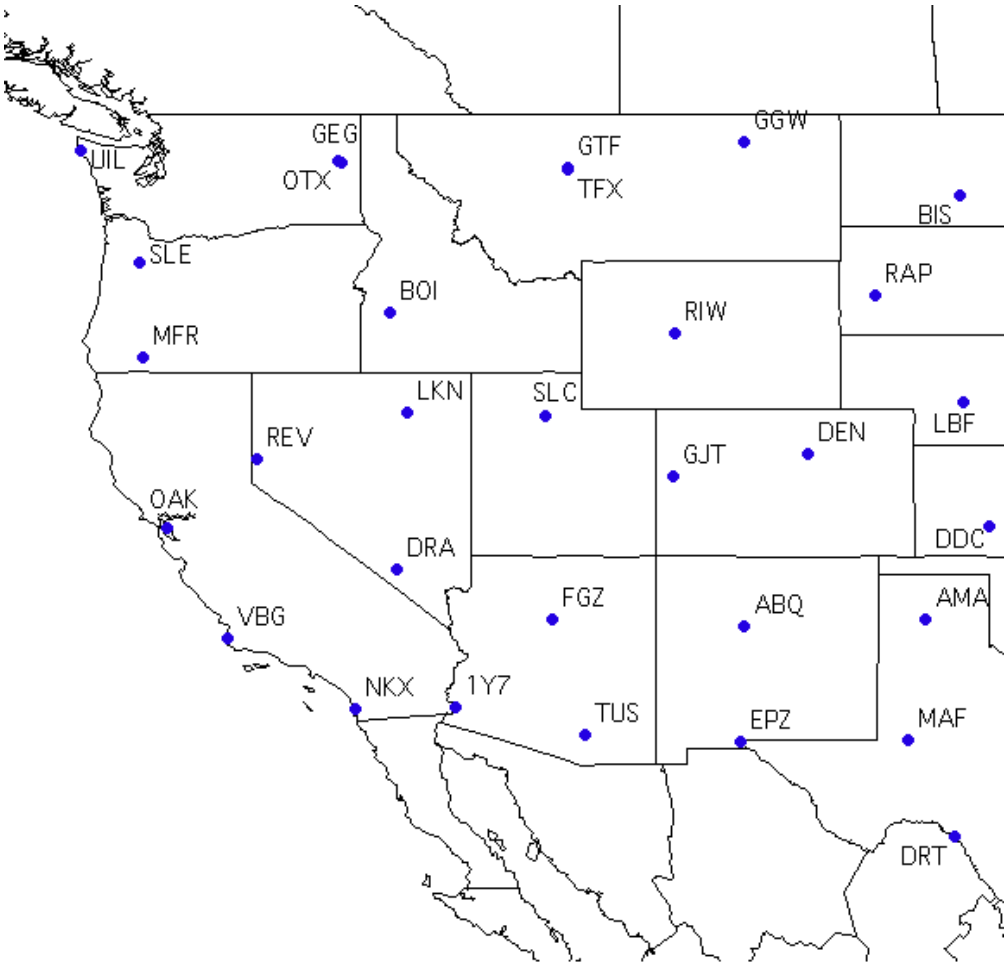

Figure 1-1 The geographical locations of the upper-air sounding stations in the western United States.

The current methodology utilized by the National Weather Service (NWS) for fire weather and smoke management forecasts described by Holzworth (1967) can be somewhat subjective. This procedure neglects humidity and does not make use of the entire atmospheric profile when determining the mixing height which can often lead to assessment error (Stull, 1988). Further, the Holzworth technique adds a *5 °C* factor to the minimum sounding surface temperature prior to determining the 12 UTC mixing height. This factor was arbitrarily determined by inspection of urban-rural differences in minimum surface temperature at many locations, and it usage accounts for the effects of some surface heating shortly after sunrise. This factor in itself can be somewhat of an overestimate (Holzworth, 1972). Due to the concerns of this technique, an alternative method that utilizes concepts described by Stull (1988, 1991) for estimating mixing layer height will be introduced and compared to the Holzworth procedure.

As previously discussed, mixing height and mean transport forecasts are currently produced from observed sounding measurements which have been the accepted data source by fire weather forecasters for a number of years (NWS, 2000). However, more recently tools used to provide assessment of these variables have been improved as derived soundings from model output are now being utilized. This can be quite advantageous as model output incorporates radiosonde data during assimilation, and accounts for temperature and moisture advection, synoptic scale lift or subsidence. Even though model information is currently being used in mixing height and mean transport forecasts, determined values are still only readily available at upper-air station locations (Figure 1-1) and forecasts rarely exceed 12 hours.

The limited availability of sounding data can inhibit planning and decision-making by fire agencies as prediction is poorly represented both spatially and temporally. This study examines using output from the 80 km grid domain (Figure 1-2) of the National Centers for Environmental Prediction's (NCEP) Eta model in providing data for spatial and temporal improvements of mixing height forecasts. The Eta model provides the necessary variables for computing mixing height and mean transport wind at 80 km resolution. The model output analyses are available twice daily (00 and 12 UTC) and contain nine corresponding forecasts that are 6 hourly out to 48 hours.

Research objectives

The first objective of this study is to address the methodology concerns of the Holzworth technique. To do this, an alternative method for computing mixing height (Stull, 1988; 1991) is introduced. In order to evaluate and compare the Stull method with the Holzworth technique, mixing height and mean transport wind values were determined twice daily (00 and 12 UTC) for the period of September 1997 through August 1999. This was performed using NCEP Eta model initialization output (80 km horizontal resolution) and sounding data from fifteen upper air stations that provided representative spatial coverage of the West (Figure 1-3). Mixing height values computed from the sounding data at the fifteen upper air stations were compared to estimates derived from the closest Eta model grid point. These calculations were performed for both the Stull and Holzworth procedures in order to evaluate the two methods and test whether the Stull technique may be preferable over Holzworth in future fire weather prediction of mixing height.

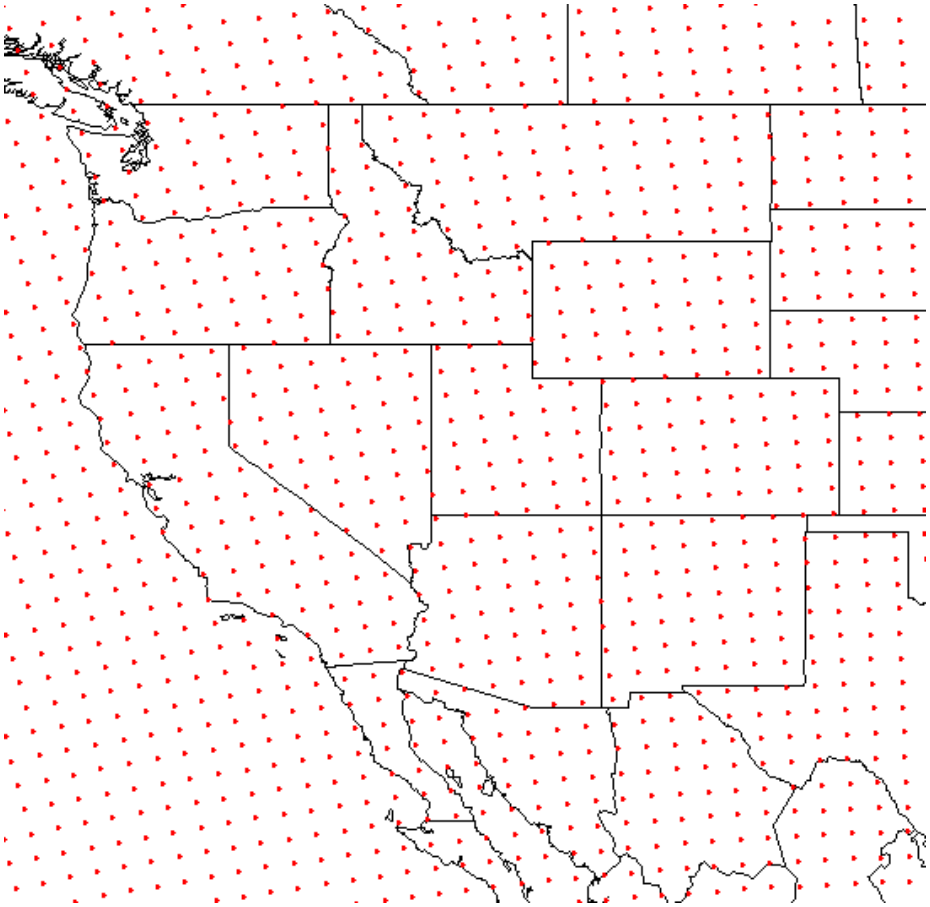

Figure 1-2 A geographic depiction of the 80 km NCEP Eta model grid points located in the western U.S.

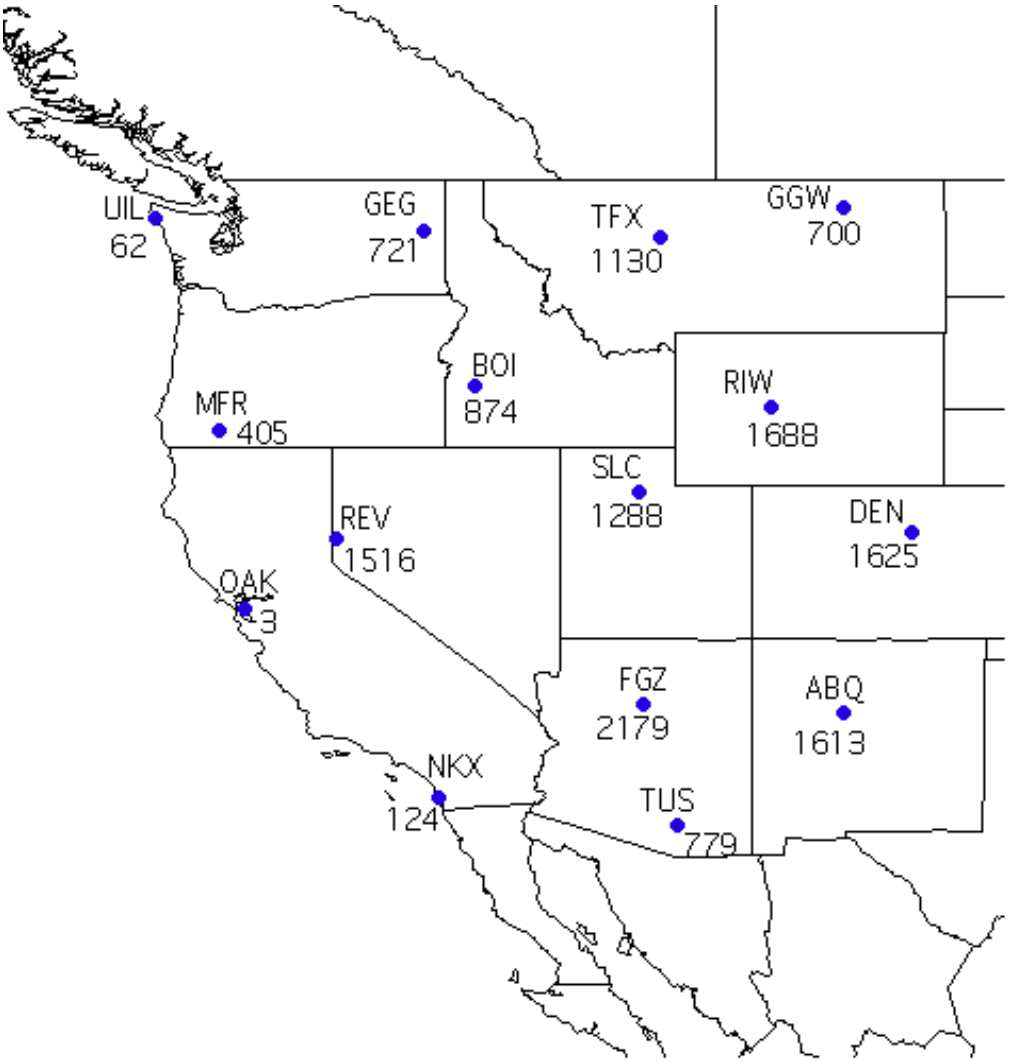

Figure 1-3 A geographical depiction of the sounding station locations used in this study and their corresponding elevations in meters.

Mixing heights determined from individual model grid points and sounding station data were also used to fulfill the second objective in this study - to examine the reliability of computing mixing height from the NCEP Eta model. This also involved comparing sounding mixing heights of the fifteen upper air stations to the closest Eta model grid point.

The third objective of this study is to address the current spatial and temporal problems of fire weather and smoke management forecasts. To do this, mixing height values were determined at all model grid points available in the western U.S. (i.e., Figure 1-2). Monthly mean spatial plots of mixing height for both 00 and 12 UTC are discussed in order to describe the advantages of using Eta model output.

Specifically, the principal objectives of this study are:

(1) To introduce an alternative method for determining mixing height described by Stull (1988, 1991) and statistically compare it to the commonly used procedure for fire weather and smoke management forecasts described by Holzworth (1967).

(2) To examine and compare mixing height differences computed from NCEP Eta model output to atmospheric sounding measurements using the Stull method.

(3) To address the poor spatial and temporal representation of mixing height and mean transport wind values produced from soundings (upper-air stations) over the western U.S. by examining the feasibility of using the NCEP Eta model grid (80 km resolution) as a data source. Model forecast output is typically

available at 6 hourly intervals out to 48 hours from 00 and 12 UTC initializations, and spatially it can provide values every 80 km (Figure 1-2).

Contents

Numerous studies performing mixing layer height and mean transport estimation have been published. Many of these articles describe a unique methodology used for assessment. Chapter 2 provides some detailed background on mixing layer structure and discusses previous techniques used for prediction.

Chapter 3 describes the details of the data sets used and provides background on the NCEP Eta model. This chapter also provides a more comprehensive review of the mixing height methodology specifically used along with an outline of procedures used for analysis.

Chapter 4 presents the analyses and results. It begins with a mixing height method comparison between the Stull and Holzworth technique where heights values were generated from NCEP Eta model output and sounding data. This is followed by a data set comparison where height values at fifteen upper air stations are compared to values computed from the closest Eta model grid point. Also in this chapter is a discussion that describes the spatial coverage that can be provided from the NCEP Eta model over the western U.S.

Chapter 5 presents a summary discussion of the results, concluding remarks, and potential future work.

CHAPTER TWO

BACKGROUND

General PBL structure and mixing layer variability

In a practical sense the planetary boundary layer[•] (PBL) structure can be separated into three major parts - the mixed layer, the residual layer, and the stable boundary layer. When clouds are present, the mixed layer is often partitioned further by distinguishing a cloud layer and a sub-cloud layer (Stull, 1988). Each of these layers experience strong diurnal variability. Figure 2-1 illustrates the typical diurnal evolution and the different layer components of the PBL over a land region. From the diagram, one can conceptually visualize how the mixing layer depth is strongly controlled by the intensity of solar heating that is present at the surface of the earth. As one may expect, the greatest depth mixed layer often occurs during the afternoon hours. After sunset, the depth of the mixing layer decreases dramatically and often times may disappear completely as surface cooling minimizes positive buoyancy and upward vertical transport of momentum allowing the stable layer to form. The mixed layer height can be defined as the altitude above ground level to which pollutants vertically disperse. The development of the mixing layer is dominantly driven by convective sources (i.e., heat transfer from a warm ground surface or radiative cooling from a cloud top), but mixing can also be enhanced from mechanical turbulence (irregular wind motion, i.e., vertical wind shear; Wallace and Hobbs, 1977; Stull, 1988).

[•] Synonyms for the planetary boundary layer (PBL): atmospheric boundary layer (ABL) or boundary layer (BL)

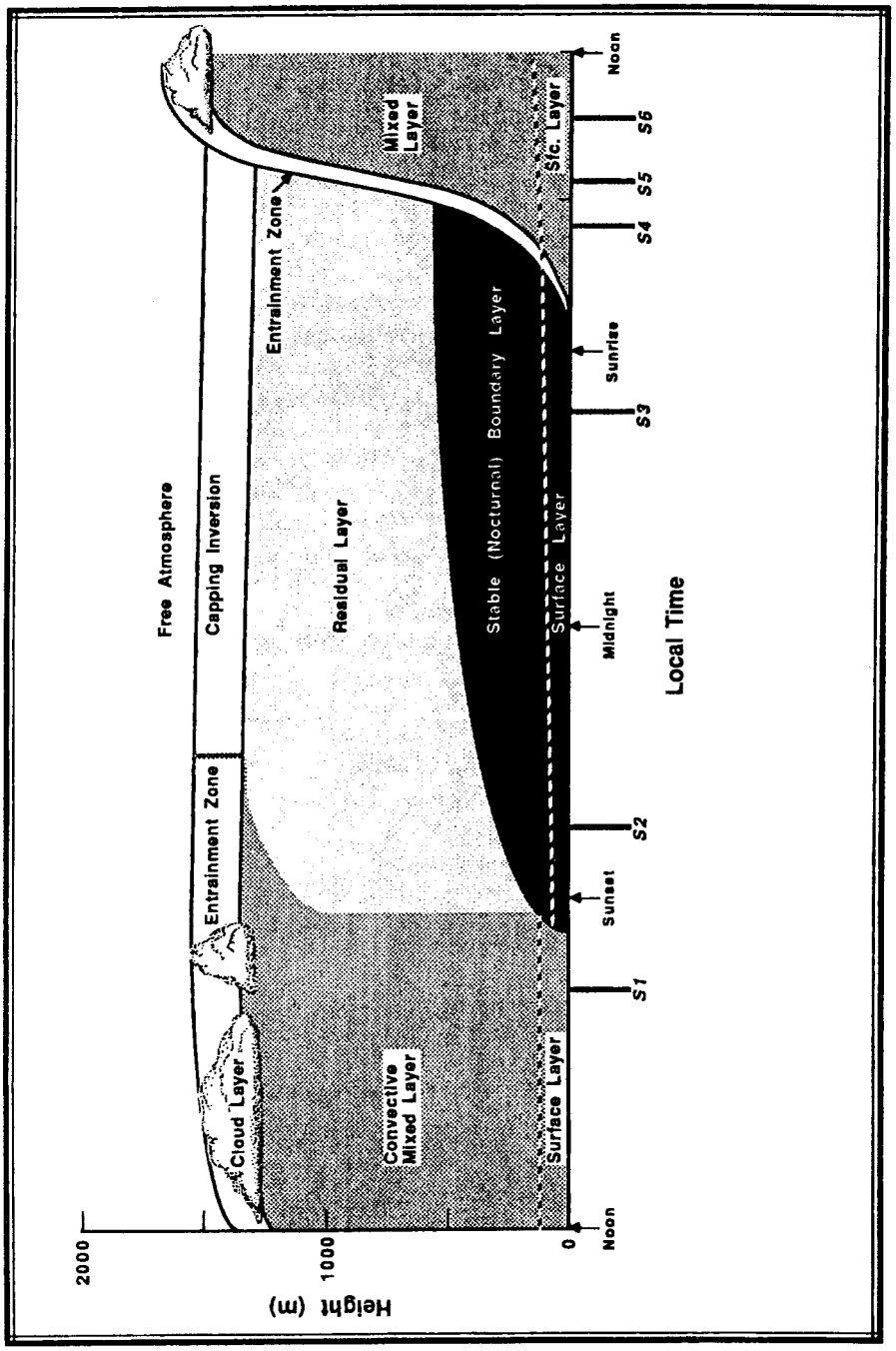

Figure 2-1 The diurnal evolution of the boundary layer detailing the sub-layer structure that typically develops during the daytime to nighttime transition. From Stull (1988).

To fully understand the diurnal variability and structure of the mixing layer, it is often helpful to separate the PBL evolution in terms of a daytime convective boundary layer and a nighttime or nocturnal boundary layer. The development of the PBL is often more pronounced during the daytime, especially over land regions, and therefore tends to receive more attentive study. However, assessment of the PBL during nighttime is also important, as vertical structure can be very different.

The convective boundary layer consists of a surface layer, mixing layer, and an entrainment zone or interfacial layer. The daytime growth of the mixed layer is controlled by the properties that develop within and near the surface layer and the entrainment zone (Figure 2-1). The surface layer, which forms just above earth's surface and is in direct contact with it, represents only about 10% of the boundary layer, but it tends to have the most dominant influence on the development of the mixing layer. As the surface of the earth is heated during the daytime, the shallow surface layer begins to form near the ground where small turbulent thermals or eddies develop. The thermals are much warmer than surrounding air that are not in direct contact with the ground and therefore become positively buoyant. The heating creates vertical instability (warmer air underlying cooler air) and thus the heated air (turbulent eddies) mix with neighboring air. With continued heating, this convection process amplifies from the surface upward extending the vertical depth of the mixing layer. To go a step further, convection sometimes occurs at the top of the mixed layer when clouds are present. Instead of warm air rising, cooler air sinks downward from the base of the clouds and creates an area of vertical instability that allows for enhanced upward vertical mixing (Stull, 1988).

During the convection process, the daytime mixed layer can also develop from entrainment which is a different type of mixing that may occur at the top of the PBL (Figure 2-1). The top of the boundary layer is often marked by a stable region or inversion (when the temperature increases with height) that can act as a lid to buoyant air (air ascending upward from the convection). This region, referred to as the entrainment zone, is described as the boundary between turbulent air from a mixed layer and non-turbulent air from the free atmosphere. This is a region where motions are treated as large-scale and neglect induced effects from the ground surface (Stull, 1988). When rising thermals reach the top of the mixed layer, they possess positive upward momentum and often penetrate through into the entrainment zone where air from the free atmosphere mixes with air from the developing mixed layer. The net effect is for the depth of the mixed layer to increase as non-turbulent air is entrained.

Beyond convection processes, the daytime mixed layer can also develop from induced mechanical turbulence (irregular wind motion which is typically the result of wind shear). This situation can occur in the vicinity of strong surface wind convergence as motion can force air vertically upward, which over time can lead to vigorous mixing (Figure 2-2). The mixed layer can also be suppressed by mechanical turbulence during the presence of strong wind convergence aloft and divergence below (subsidence), which can often act to oppose the convection process (Figure 2-2). The latter tends to be associated with the presence of synoptic high pressure systems where mixed layer growth by mechanical turbulence tends to be from orographic forcing, frontal lifting, or the presence of developing vertical motion (Stull, 1988).

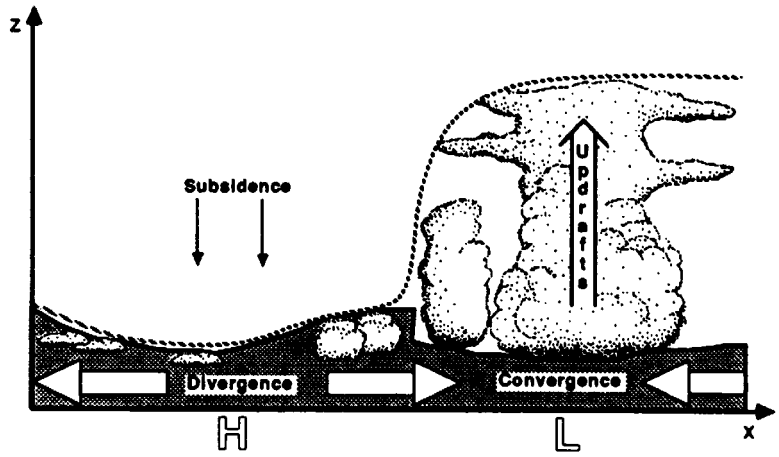

Figure 2-2 A graphical depiction of wind convergence aloft and at the surface. The left portion of the graphic indicates how a mixed layer can be suppressed due to strong wind convergence aloft. The right portion of the graphic indicates how a mixed layer can develop from strong surface wind convergence. From Stull (1988).

Similar to daytime, the nighttime or nocturnal boundary layer can be partitioned into sections in terms of a surface layer, a stable layer or inversion, and a residual layer that is often topped by an inversion (Figure 2-1). After sunset when the ground surface begins to cool, the daytime mixing layer starts to erode allowing a stable, shallow surface layer to form. As with the convective boundary layer, the surface layer forms adjacent to the ground and is the dominant influence on the development of nighttime conditions. However, the radiative cooling at the surface, unlike the daytime heating, creates a stable environment (cooler air underlying warmer air) near the ground that minimizes the upward mixing dramatically. This is the main reason for distinguishing between a nighttime and daytime mixed layer as smoke and other particulate trapping can develop due to the lack of upward vertical mixing (Figure 2-3). Above the stable layer there tends to be a residual layer containing remnants of well-mixed air characteristic of the daytime convective mixing layer. The residual layer is typically topped with a second inversion that separates the PBL from the free atmosphere (Stull, 1988).

Methods and concepts used in mixed layer estimation

Variables used for mixed layer assessment

Many practical techniques used for estimating the height of the mixing layer involve determining the vertical static stability structure for a particular sounding profile; classifying where air is unstable, stable or neutral within the profile (defined in more detail below). This involves using the assumption that the atmosphere is in hydrostatic equilibrium; the complete balance between the force of gravity and the vertical pressure

Figure 2-3 An example of poor dispersion where smoke and other particulate trapping has developed due to the lack of upward vertical mixing. From NWS (2000).

gradient force (Huschke, 1959). To perform static stability analysis, atmospheric variables such as potential temperature or virtual potential temperature are often used, as they tend to reveal a rather smooth vertical fluctuation with changes in altitude. The potential temperature (θ) is defined as the temperature a parcel of dry air would have if brought dry adiabatically to 1000 mb. Dry adiabatically refers to parcel movement along a line of constant θ, which in terms of temperature represents a lapse rate of $\frac{\partial T}{\partial Z} = -\Gamma_d$, where $-\Gamma_d$ is the dry adiabatic temperature lapse rate equal to $9.8\frac{K}{km}$, ∂T is the change in temperature in K, and ∂Z is the change in height in km. The mathematical expression for θ is given by

$$\theta = T\left(\frac{1000}{P}\right)^{\kappa},$$

where P is the pressure in mb and T is temperature in K at the initial state referenced from the (arbitrarily selected) standard pressure level of 1000 mb, and the exponent κ is a constant equal to 0.286 (Huschke, 1959).

Examining density variation is perhaps the most efficient way to assess static stability within a sounding profile. However, density is a difficult variable to measure due to its strong variability in the atmosphere. Therefore, often times static stability and the height of the mixed layer are determined using the virtual potential temperature (θ_v) given by

$$\theta_v = T_v\left(\frac{1000}{P}\right)^{\kappa},$$

where T_v is the virtual temperature in K, which is the temperature that dry air must have in order for its density to be equal to that of moist air at the same pressure. Here T_v is given by

$$T_v = T\left(\frac{r_{sat} + \varepsilon}{\varepsilon}\right)\frac{1}{\left[1 + r_l + r_{sat}\right]},$$

where T is temperature (K), r_{sat} is the saturation mixing ratio for vapor (*g/g*), r_l is mixing ratio for liquid (g/g), and ε is a constant equal to 0.622 (Stull, 1988). Since moist air is less dense (more buoyant) than dry air, the virtual temperature is always greater than the actual temperature. Unlike density, T_v is easy to compute from sounding measurements or model output, and since it accounts for the influence of vapor, which is related to changes in density, variations in T_v can be studied in place of variations in density. θ_v is therefore a popular variable for static stability and mixing height determination because it incorporates moisture through T_v. Figure 2-4 provides an example of the diurnal evolution of the PBL using an average profile of virtual potential temperature.

Lapse rate

Prior to defining atmospheric stability more specifically, it is often useful to have a good understanding of lapse rate terminology as stability and lapse rate are commonly associated improperly (Stull, 1991). When analyzing a local segment or lapse rate of virtual potential temperature $\left(\frac{\partial \theta_v}{\partial Z}\right)$ within a sounding profile, constancy is referred to

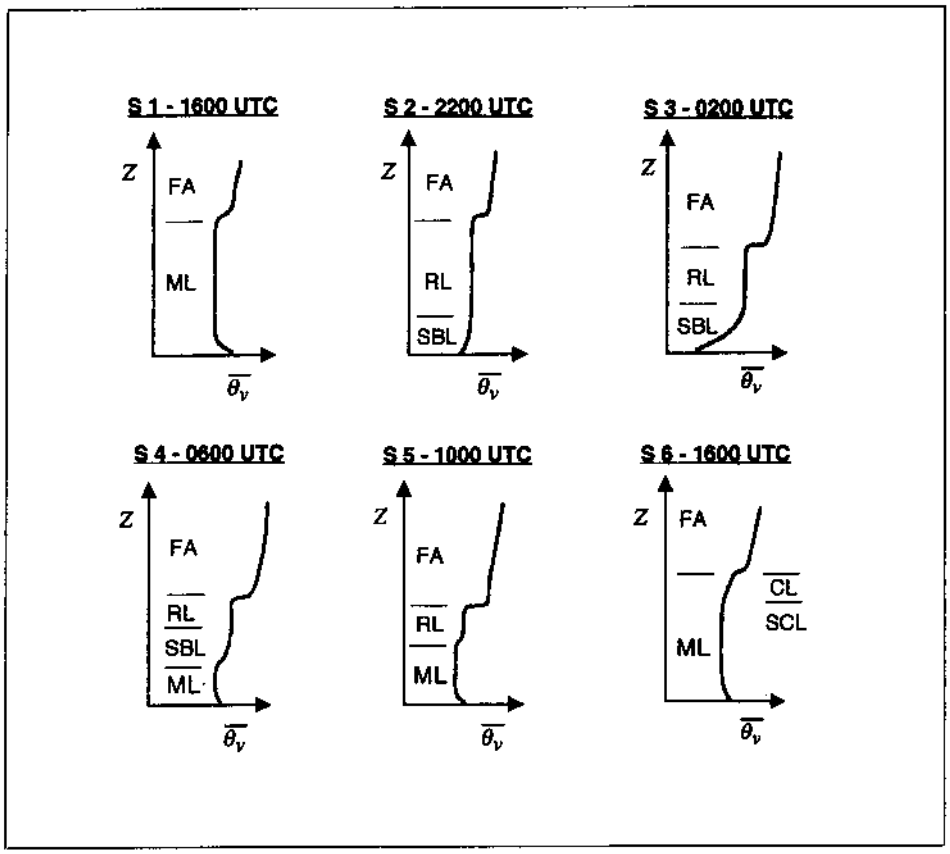

Figure 2-4 Profiles of mean virtual potential temperature showing the boundary layer evolution during a diurnal cycle. S1 (sounding one) begins the 6-hour incrementing sequence at 1600 local time and S6 (sounding six) ends at 1600 local time the following day. The abbreviations used are (ML) – mixing height, (FA) – free atmosphere, (SBL) – stable boundary layer, (RL) – residual layer, (CL) – cloud layer, and (SCL) – sub-cloud layer. From Stull (1988).

as adiabatic $\left(\frac{\partial T_v}{\partial Z} = -\Gamma_d, \ \frac{\partial \theta_v}{\partial Z} = 0\right)$. If virtual potential temperature is increasing or warming with height, the lapse rate is referred to as subadiabatic or greater than adiabatic $\left(\frac{\partial T_v}{\partial Z} > -\Gamma_d, \ \frac{\partial \theta_v}{\partial Z} > 0\right)$. Alternatively, if θ_v is decreasing or cooling with height then lapse rate is referred to as superadiabatic or less than adiabatic $\left(\frac{\partial T_v}{\partial Z} < -\Gamma_d, \ \frac{\partial \theta_v}{\partial Z} < 0\right)$. These definitions apply similarly for potential temperature. Table 2-1 quantifies the above description of local lapse rates.

Table 2-1 Traditional or local lapse rate names and definitions commonly used to determine static stability. From Stull (1991).

Local Lapse Rate			Local Static Stability
Name	$\frac{\partial \theta_n}{\partial z}$	$\frac{\partial T}{\partial z}$	
superadiabatic	< 0	$< -\Gamma_d$	unstable
adiabatic	$= 0$	$= -\Gamma_d$	neutral
subadiabatic	> 0	$> -\Gamma_d$	stable

Traditional or local static stability methods

A common method for estimating PBL structure involves determining the traditional or local static stability (e.g., Coulter, 1979; Goldman, 1980; Heffter, 1980). The procedure involves determining the local lapse rate for individual segments of a sounding, and then based on that information, a determination of the static stability is

performed. A lapse rate where virtual potential temperature is considered adiabatic often leads to the static stability classification of neutral. If virtual potential temperature is increasing or warming with height, static stability is then labeled stable. Alternatively if the virtual potential temperature is decreasing or cooling with height, static stability is classified as unstable. Table 2-1, in addition to showing local lapse rate definitions, identifies how traditional or local static stability is commonly determined. Figure 2-5 is an illustrative example of how local static stability is estimated from a sounding profile.

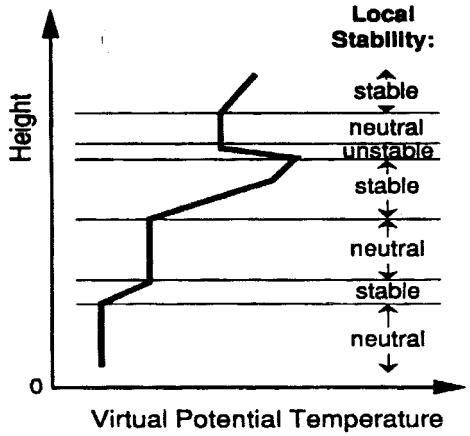

Figure 2-5 Idealized example of how local static stability is determined using a sounding profile of virtual potential temperature. From Stull (1991).

Coulter (1979) described a method of estimating the daytime mixing height using the local static stability procedure. He defined it as the altitude, once above the surface layer, at which the potential temperature first became greater than adiabatic. Figure 2-6 shows a conceptual example of the Coulter technique. Goldman (1980) established a similar method that defined the mixed layer height as the lowest level at which the vertical temperature gradient $\left(\frac{\partial T}{\partial Z}\right)$ exhibits a stable lapse rate through a significant

atmospheric layer. The identified stable layer had to occur above a surface-based, well-mixed layer that contained an unstable or neutral lapse rate. Further, the lapse rate present within the selected stable layer had to be greater than (more positive than) or equal to $\frac{-0.5°C}{100m}$, and occur through a depth of at least 100 m. Figure 2-6 provides an illustrative example of this procedure.

Another method very similar to (Goldman, 1980) that is currently used by the National Oceanic and Atmospheric Administration/Air Resources Laboratory (NOAA/ARL) was developed by (Heffter, 1980). The Heffter technique consists of analyzing θ profiles for the existence of a critical inversion, which is assumed to mark the top of the mixed layer. It is defined as the lowest inversion whose potential temperature lapse rate is equal to or larger than $5\frac{K}{km}$, and the temperature difference between the inversion base and its top must exceed 2 K (Piringer et al., 1997). Figure 2-6 provides a graphical example of how the Heffter method is applied to a sounding profile.

For years scientists have been using local lapse definitions to assess mixing layer depth. Typically during the daytime and especially over an inland station, a sounding profile, when looking from the surface upward, exhibits a superadiabatic lapse rate within the surface layer. Increasing with height, the profile tends to become adiabatic until an inversion or subadiabatic lapse rate is encountered which often marks the top of the mixed layer. For most environmental applications, the daytime surface layer and the mixed layer are often studied as one layer under the assumption that pollutants disperse readily until encountering an inversion.

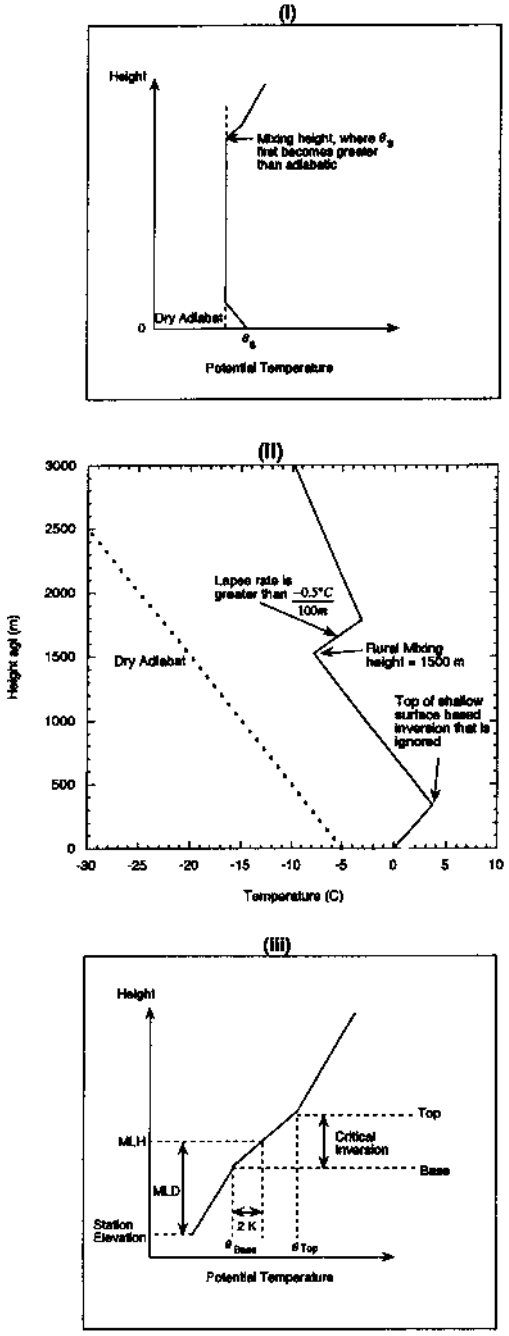

Figure 2-6 Examples of (i) the Coulter method (adapted from Coulter, 1979), (ii) the Goldman method (adapted from Goldman, 1980), and (iii) the Heffter method (adapted from Capuano and Atchison, 1984).

The three PBL assessment techniques described above use the concept of traditional static stability and the idea of local lapse rates as an initial model, but then differ when defining the base of the inversion which leads to different values of mixing layer height. These procedures are often discouraged because the methodologies only utilize ambient temperature values measured by the radiosonde and do not consider convective parcel movement in regions where buoyancy (negative or positive) is present; hence, the label "traditional or local". Further, local static stability determination has been found to be inconsistent given observation of vigorous convective mixing (Figure 2-7). Thus, a nonlocal approach of determining static stability has been suggested by Stull (1991) which involves using convective air parcel movement across finite distances.

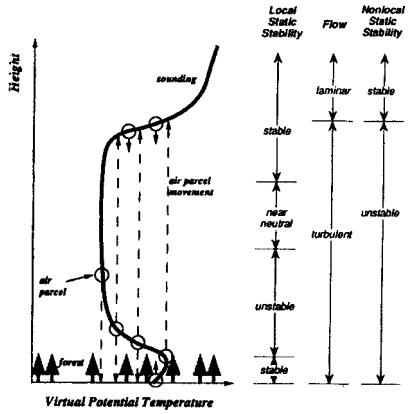

Figure 2-7 An example illustration showing the difference between local and nonlocal static stability. From Stull (1991).

Nonlocal or parcel displacement static stability methods

Using nonlocal static stability methods to estimate mixed layer depth is often preferred over traditional techniques as they incorporate convective parcel movement (i.e., Stull, 1988; 1991). Stull (1991) describes a nonlocal procedure that uses profiles of

θ_v. This methods involves displacing parcels of θ_v upward from the relative maxima and downward from the relative minima where parcel movement is based on buoyancy measured by comparing the virtual potential temperature of the parcel to the environment at the same height. Ascent or descent of the parcel is tracked until it intersects the environmental profile or becomes neutrally buoyant. Once all parcel movements have been tracked for the entire profile, the static stability is then determined for each portion of the sounding domain. Figure 2-8 provides several examples of this procedure.

The Stull technique is not currently used in operational smoke management forecasts produced by the NWS. The prevalent method to produce mixing height in smoke management forecasts (Holzworth, 1967) has been used for years by the NWS. Utilizing the 00 and 12 UTC radiosonde measurements and the assumption of the surface temperature remaining dry adiabatic (e.g. constant potential temperature) through a well-mixed layer, Holzworth established a procedure for estimating a morning and afternoon mixing height. The morning mixing height is defined as the level above ground at which the dry adiabatic ascent of the morning minimum surface temperature plus 5°C intersects the vertical temperature profile measured at 1200 UTC (Figure 2-9). The afternoon mixing height is based on the level above ground at which the adiabatic ascent of the maximum surface temperature intersects the 0000 UTC temperature profile (Figure 2-9). This latter method is often applied to obtain a daily forecast of the afternoon mixing height utilizing the daily forecast maximum surface temperature and 1200 UTC sounding.

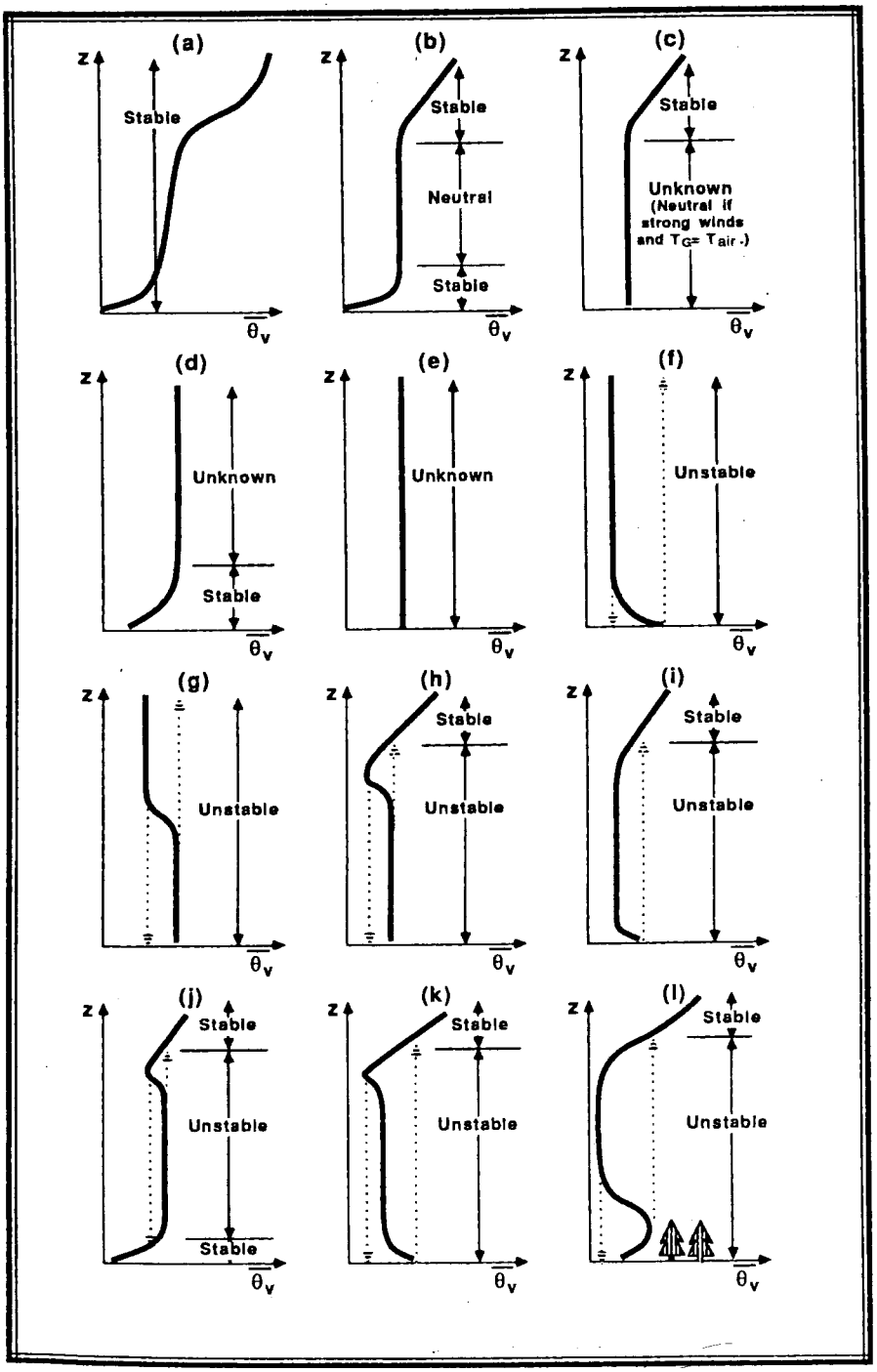

Figure 2-8 Examples of determining nonlocal static stability using the methodology discussed by Stull (1988, 1991). From Stull (1988).

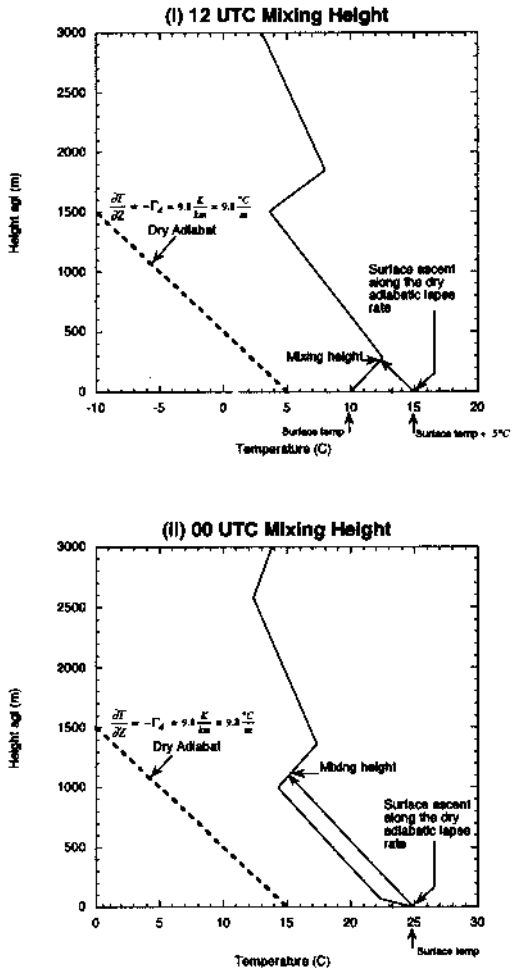

Figure 2-9 Holzworth method of determining (i) the 12 UTC or morning mixing height and (ii) the 00 UTC or afternoon mixing height.

There are a number of distinguishing concepts in methodology that exist when comparing the Stull procedure to that of Holzworth. For example, the Holzworth procedure incorporates the basic idea of parcel movement. However, it does not track parcels downward (parcels that are negatively buoyant), and once the surface parcel intersects the sounding profile during adiabatic ascent, the rest of the profile is neglected. Further, similar to most methods, the Holzworth technique uses potential temperature which in a dry environment can be a good approximation, but if moisture is present, this usage can lead to error in mixing height determination (Stull, 1988).

Figure 2-10 is an idealized example of how mixing height is determined for both the Stull and Holzworth procedures, and is quite evident as to how significantly different the computations can be. Note Holzworth uses θ and Stull uses θ_v which is one reason why mixing height values can be different as values of θ are typically less than values of θ_v. However, height difference in this case is more importantly a result of the Stull method incorporating the entire sounding, whereas the Holzworth technique stops after the surface parcel intersects the ambient profile for the first time.

Using remote sensing techniques

Some other methods used for estimating mixing height that are not examined in this study are those which involve remote ground-based observing systems (e.g. wind profiler, sodar, and lidar). Profilers utilize microwave pulse signals to vertically probe the atmosphere. The return patterns from these signals can be used to interpret atmospheric temperature and wind which in turn can be used to determine mixing layer

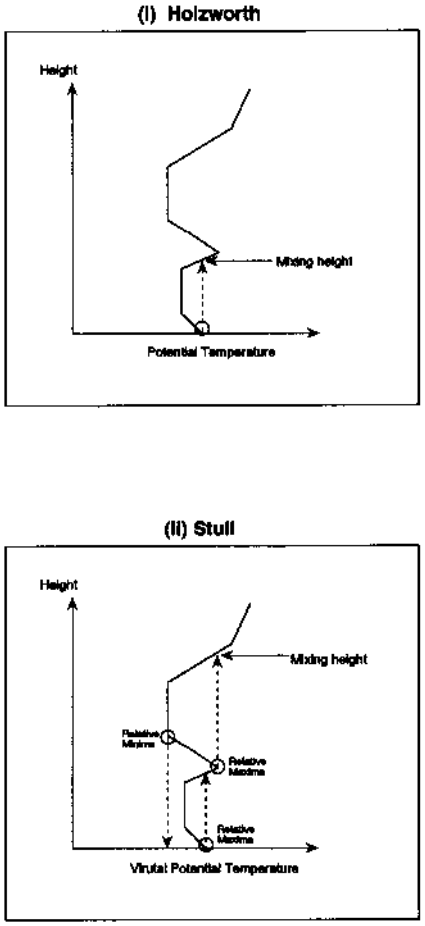

Figure 2-10 Idealized examples of mixing height computation for (i) the Holzworth method (1967) and (ii) Stull method (1988, 1991) using the same 00 UTC sounding. Note Holzworth uses θ and Stull uses θ_v.

height (e.g., Marsik et al., 1995). During fair conditions, the boundary layer is often more humid than the free atmosphere allowing for an interpretable boundary or interface to be present in the return signal. This signal pattern is then often used to estimate height of the mixed layer (Stull, 1988). Caution should be used during signal assessment as ground clutter such as buildings, insects, and vegetation can sometimes create interpretation problems (Marsik et al., 1995). Further, the existence of clouds and precipitation can often affect return signal patterns due to additional pulse scattering that is difficult to examine (Fairfall, 1991).

Sodar is very similar to the wind profiler in that its return signal can be used to interpret temperature variation and wind if it has a Doppler capability. However, it differs from profilers by transmitting acoustic waves. The return signal from the sodar is often used to locate elevated inversions that almost always mark the top of the mixed layer. Unfortunately, sound is attenuated so rapidly in the atmosphere that it is difficult to detect higher than 1 km. Since mixed layers can grow above 1 km, especially in the afternoon, sodar is typically only useful for nighttime detection of the mixing height (Stull, 1988).

Lidar, a laser light-transmitting instrument, is another remote sensing tool used estimate the top of the mixed layer. The light signal is scattered when encountering air molecules, cloud droplets and aerosols through a chosen vertical depth above the earth's surface. Since the source of many aerosols exist near the ground or within the boundary layer, the return signal tends to be quite high for the entire depth of the PBL and much lower in the free atmosphere. This instrument is consequently seeing the boundary layer

air as opposed to looking for a gradient at the top of it. Lidar signal interpretation can be a problem when clouds or precipitation exist in the viewing area because the light beam can become severely attenuated which can make return patterns impossible to examine.

Using the bulk Richardson Number

Sometimes wind estimates attained from wind profilers can be useful in determining boundary layer stability through the use of the bulk Richardson number (R_i). The mathematical expression for R_i is given by

$$R_i = \left(\frac{g}{T}\right)\left[\left(\frac{d\theta}{dz}\right)\left(\frac{z}{u}\right)^2\right],$$

where g is gravitational acceleration in ms^{-2}, T is surface temperature in K, $\frac{\partial\theta}{\partial z}$ is vertical change in potential temperature with height where θ has units of K and z is in meters, and u is mean wind speed in ms^{-1} with the layer of interest given by a geometric height z (Caiazza et al. 1992). A vertical profile of R_i values can reveal a structural pattern that can be used to estimate the depth of turbulence. Both temperature variation and wind are incorporated in the R_i calculation and therefore, it provides a vertical description of both static and dynamic (motion) stability. Values of R_i less than zero correspond to an unstable situation with $\frac{\partial\theta}{\partial z} < 0$. Values of R_i greater than zero are associated with a stable environment $\left(\frac{\partial\theta}{\partial z} > 0\right)$. For neutral stability, $\frac{\partial\theta}{\partial z} = 0$, and R_i values tend to approach zero. Using the bulk Richardson number can be alternative method to estimate the mixing height as a profile of values can be obtained.

Using meteorological pre-processors

Many environmental scientists use dispersion models to track or forecast pollution episodes. These guidance tools require a reliable depiction of the PBL parameters as input, and therefore an estimation of mixing height is needed. In order to determine the boundary layer variables used in dispersion models, researchers often develop or use a pre-existing meteorological pre-processor. These models provide three-dimensional mass-adjusted wind fields and scaling parameters (like friction velocity u_*, Monin-Obukhov length L, Coriolis force f, and mixing height h; Lena and Desiato, 1999). There are several mixing height algorithms employed in many different pre-processors that use a variation of u_*, L, and f to compute mixing height. Data sources include but are not limited to radiosonde measurements, wind profilers, sodar, and lidar. Some of the most popular pre-processors are CALMET (Lena and Desiato, 1999), OML (Olesen and Brown, 1987), and HPDM (Hanna and Chang, 1993).

Mixing height techniques used in this study

This second half of this chapter provided a review of previous methodology applicable to mixing layer height estimation. However, the technique utilized in this study involves the theory described by Stull (1988, 1991). It is compared to Holzworth (1967) and analyzed in detail to provide NWS fire weather forecasters and air quality modelers with an alternative mixing height technique that will be valuable for smoke management assessment.

CHAPTER THREE

DATA AND METHODS

Atmospheric sounding data and Eta model initialization output were the two data sets used to generate mixing heights and mean transport wind in this study. Both were available twice daily (00 and 12 UTC) from September 1997 through August 1999. This time range was selected because of the convenient availability of Eta model output and model physics consistency.

The first half of this chapter will focus on data description, data preparation, and relevant background history of the Eta model. The second half will provide a detailed description of the Stull and Holzworth mixing height methods followed by a discussion of the analysis procedures used in this study.

Data

Variables used for mixing height and transport wind assessment

Depending on the method, profiles of potential temperature (θ) or virtual potential temperature (θ_v) were used to determine the mixing height. As previously discussed in chapter two, θ is defined as the temperature a parcel of dry air would have if brought dry adiabatically to 1000 mb. Dry adiabatically refers to parcel movement along a line of constant θ. At this point, it may be helpful to state that θ is mathematically defined by

$$\theta = T\left(\frac{1000}{P}\right)^{\kappa},$$

where P is the pressure in mb, T is temperature in K at the initial state referenced from the (arbitrarily selected) standard pressure level of 1000 mb, and the exponent κ is a constant equal to 0.286 (Huschke, 1959). θ_v is defined the same as θ, only it is calculated using virtual temperature (T_v) instead of actual temperature (T) to account for moisture. Therefore, it is greater than θ sometimes by as much as 4 K (Stull, 1988). Using profiles of θ (Holzworth method) and θ_v (Stull method), mixing height values were computed above ground level by subtracting surface elevation (sounding or Eta in units of meters) from a referenced geopotential height (z) value, the height in meters of above mean sea level. Profiles of zonal (u) and meridional (v) wind components were then averaged through the depth of the determined mixed layer and used to compute mean transport wind speed (ms^{-1}) and direction (degrees). u and v wind components were also referenced above ground level by subtracting surface elevation from geopotential height.

Sounding measurements

The sounding data used in this study were provided by the Western Regional Climate Center (WRCC). Measurements from fifteen upper-air stations located in the western U.S. were used in the analysis. Each location was purposely selected to account for distinct differences in climate and elevation, and to provide representative spatial coverage of the West (Figure 1-3).

From the operational radiosonde measurements, variables for determining mixing height and mean transport wind are available directly (geopotential height, wind speed and

direction) or by computation (virtual potential temperature and potential temperature) on mandatory (m) and significant (s) pressure levels (Table 3-1). Sounding data sets are commonly used when estimating the depth of the mixed layer as they were one of the first data sources readily available (Holzworth, 1967) and can be quite operationally convenient (NWS, 2000). Almost all research studies (e.g., Coulter, 1979; Baxter, 1990; Beyrich, 1997; Marsik et al., 1995; Ulke and Mazzeo, 1998; Berman et al., 1999) that involve analyses of mixing height from an alternative data source (e.g., sodar, lidar, wind profiler) commonly compare computational results to sounding estimates. Using radiosonde data for comparative purposes is especially useful in this study because the Eta model incorporates sounding data during assimilation (an algorithm used to sort through model input data and select a best fit prior to initialization; Nelson, 1999).

Though sounding data are often used and convenient for mixing height estimation, the vertical resolution available can be quite coarse, especially for stations located at high elevation (Table 3-1). Like other measurements that are generated operationally, error checking and quality control for inaccuracies and missing data were performed on the data set prior to its use in this study. For example, error checking involved confirming whether or not temperature values were realistic as sometimes a value of potential temperature would show up as 900 K. In the case of missing data, a certain number of levels (significant or mandatory) containing all variables were required to be present within two selected layers for the sounding profile to be usable. These layers were chosen strategically so that the majority of the boundary layer would be accounted for; the first layer being from the ground to 700 mb and the second from 700

Table 3-1 Example output of a sounding profile (Flagstaff, AZ) showing how data are distributed on significant (s) and mandatory (m) levels. This also shows how a station at high elevation can have a limited number of levels between the surface and 500 mb.

Station: 72376 (FGZ)
Time: 97090412

Typ	Prs mb	Ht m	Theta K	Temp C	DewPt C	RH %	Dir deg	Spd kt
G	791	2179	303.8	11.0	10.5	97	300	3
s	784	2254	307.6	13.8	7.8	67		
s	774	2363	313.1	17.8	8.8	56		
w		2438					130	14
w		2742					165	13
m	700	3213	315.5	11.8	4.8	62	180	17
w		3656					190	22
s	643	3917	315.8	5.2	4.0	92		
w		4266					185	21
s	611	4332	315.8	1.2	0.4	94		
s	572	4861	318.4	-1.7	-4.7	80		
w		4875					185	19
s	555	5101	319.1	-3.5	-4.5	93		
s	530	5464	320.7	-5.7	-8.4	81		
w		5484					230	16
m	500	5920	322.9	-8.3	-9.1	94	225	19
w		6094					215	21
s	476	6300	324.5	-10.7	-11.3	95		
s	463	6513	327.3	-10.5	-18.5	52		
s	434	7007	328.8	-14.1	-26.1	36		
w		7617					245	18
m	400	7620	331.9	-17.7	-26.7	45	245	18
s	385	7905	332.4	-20.1	-29.1	45		
w		7922					245	18
s	367	8259	335.6	-21.1	-34.1	30		
w		8836					220	27
w		9141					225	26
m	300	9720	339.7	-32.3	-43.3	33	235	27
w		9750					240	29
w		10664					240	32
m	250	10970	343.1	-42.3	-52.3	33	240	29
w		11578					250	33
m	200	12440	347.6	-53.7	-61.7	37	240	32

mb to 500 mb. The necessary number of levels that were required within these the two layers, in order for the profile to be classified usable, were determined arbitrarily through data inspection while taking into account station elevation. Table 3-2 lists the necessary number of levels required per station. From Table 3-2, it is noticeable that fewer levels were required for stations at higher elevation (e.g., Flagstaff, Arizona – FGZ). This was more common for the layer that extended from the surface to 700 mb, as the higher the station elevation, the closer the ground surface was to the 700 mb level.

NCEP Eta model output

The Eta model output archive used was provided by the National Weather Service Cooperative Program for Operational Meteorology, Education and Training (COMET) located in Boulder, Colorado. Similar to radiosonde measurements, the Eta output acquired was twice daily (00 and 12 UTC) and only model initializations were used (not forecasts). This allowed for a direct comparison and analysis between the observed soundings and the model output.

The NCEP Eta numerical forecast model has been one of the premier operational, short-range guidance models for the atmospheric sciences community since its implementation in June 1993 (Nutter and Manobianco, 1999). The model receives its name "Eta" because it utilizes the Eta vertical coordinate (η) defined by Mesinger (1984). Since its inception, numerous code changes have been applied to the Eta in order to improve its model physics, its vertical and horizontal resolution scale, and its data assimilation package. These continuous efforts by NCEP to make the Eta the most useful forecast model have prompted atmospheric scientists to extend the use of its output toward more tailored applications (e.g., mixing height estimation.

Table 3-2 Station listing showing the number of levels necessary for the sounding data to be classified usable.

Station id	Elevation (m)	# of levels from the Surface to 700 mb	# of levels from the 700 mb to 500 mb	# of levels required total
OAK	3	5	3	8
UIL	62	5	3	8
NKX	124	5	3	8
MFR	405	5	3	8
GGW	700	5	3	8
GEG	721	4	3	7
TUS	779	4	3	7
BOI	874	4	3	7
TFX	1130	4	3	7
SLC	1288	4	3	7
REV	1516	4	3	7
DEN	1608	3	3	6
ABQ	1613	3	3	6
RIW	1688	3	3	6
FGZ	2179	2	4	6

The original version of the NCEP Eta model (referred to as the "Early" Eta) was implemented in June 1993 and had a horizontal resolution of 80 km with 38 vertical layers (Figure 3-1). In August 1995, NCEP began running a mesoscale version of the Eta model (referred to as the Meso Eta or Eta-29) in addition to the 80 km run which had a horizontal resolution of 29 km and 50 vertical layers (Figure 3-2). In October 1995, NCEP modified the horizontal resolution original or "Early" Eta from 80 km to 48 km while also applying changes to the cloud prediction scheme and creating a data assimilation package used to produce the initial analyses (Nutter and Manobianco, 1999). Changes applied to the Eta from August 1995 until August 1997 encompassed a rather large handful of alterations to the model's physics package while those performed from August 1997 through August 1999 were modifications that had a greater effect on model resolution (Table 3-3). The main reason for selecting the two-year time period of September 1997 through August 1999 is because most of the code alterations performed dealt with resolution and topography adjustment rather than changes to model physics (Table 3-3).

Eta output is typically available in terms of grid numbers which are representative of the horizontal resolution (e.g., grid 211 – 80 km, grid 212 – 40km). Grid 211 was chosen for this study because it was consistently available at 80 km and feasible to obtain. Even though the changes previously discussed here describe significant alterations in horizontal resolution, output was always made available at 80 km. For example, the model run performed by NCEP may have initially been at 48 km; however,

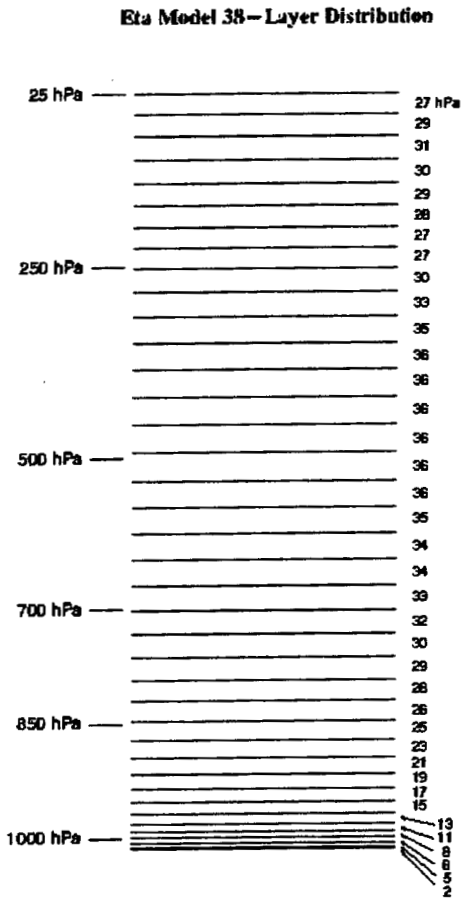

Figure 3-1 The distribution of the 38 layers in the Eta-48. The pressure values on the left axis indicates the layers' position with respect to the standard atmosphere, while the numbers on the right axis give an approximate pressure depth of each layer. From Rogers and Coauthors (1997).

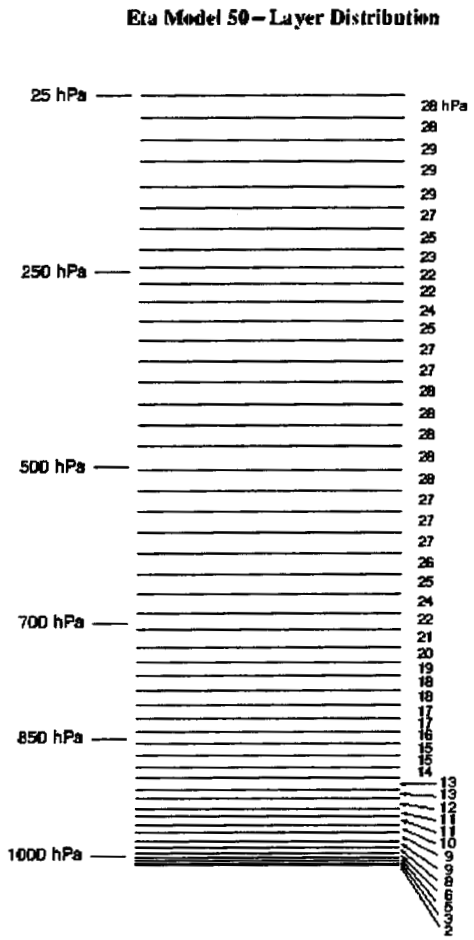

Figure 3-2 Same as Figure 3-2 except for 50 layers in the Eta-29. From Rogers and Coauthors (1997).

Table 3-3 Major code changes applied to NCEP Eta model from October 1995 through August 1999. From Rogers and Coauthors (1997) and EMC (2000).

Date	NCEP Eta Code Changes
October 1995	- horizontal resolution of "Early" Eta increased from 80 km to 48 km (Eta-48) - explicit cloud microphysical scheme was added
January 1996	- "Early" Eta (now also Eta-48) code was upgraded to match that of Eta-29 - new land-surface scheme developed to provide soil moisture and temperature
February 1997	- a bundle of changes were performed on the model physics that include the addition of a form-drag scheme, changes to the radiation scheme, changes to the snow melt physics and bare soil evaporation
August 1997	- Major code change was implemented to remove an error in the computation of the depth of the PBL
February 1998	- the grid point interpolation scheme was changed to incorporate a 3-D system which performed variable calculations for the entire grid simultaneously instead of computing individual grid points values independently - the Eta-48 resolution was increased from 48 km and 38 vertical layers to 32 km and 45 vertical layers (referred to as the Eta-32); most of the layers added were done so to better resolve low-level mesoscale structure and therefore most of the levels added were below 700 mb
November 1998	- modifications were performed to remove all smoothing of fields where discontinuities or sharp gradients were likely to be present (e.g., topography)

the grid made readily available for analysis purposes (i.e., grid 211) was post-processed to an 80 km resolution (Figure 1-2).

Prior to using model output for research and analysis, it is useful to have an understanding of its data initialization procedure. The Eta model, similar to other models, uses an assimilation package which determines the best fit of both observational data and model first-guest forecasts (Nelson, 1999). The model first guess is generated by Eta Data Assimilation System (EDAS) which continuously cycles producing new and incorporating previous model forecasts. Before model output is made available for analysis purposes, first guess values for a particular model run are formulated and then compared to observational data (e.g., atmospheric sounding measurements). This involves using a 3-dimensional variation analysis technique (3DVAR) that interpolates the observational data and previous forecasted model output to the locations of the newly forecasted grid values. Modification is then performed for each newly generated first-guess value in order to find the best-fit forecast value at each model grid point (Staudenmaier, 1996b). The 3DVAR-interpolation procedure replaced the earlier used optimum interpolation (OI) technique in February 1998 (Table 3-3).

Even though the 3DVAR procedure has shown improvement in forecasts and is a reasonable assimilation method, terrain resolution problems still create biases in model derived variables. These biases are particularly concentrated in the lower pressure levels (e.g., 1000 and 900 mb levels) and with the 2 m above ground variables (e.g., model surface temperature), especially over complex terrain such as the western U.S. Biases develop due to large differences in elevation between the model surface and true ground.

Usually the Eta's surface is well above the true ground in complex terrain areas which makes incorporating measured observational data that is located below the model surface quite difficult. In order to account for this problem during assimilation, downward extrapolation is performed from the mid-point of lowest model surface to the elevation of the observed measurement. This distance sometimes becomes too large and makes for unrealistic extrapolation. Therefore, to make the assimilation process easier, the downward extrapolation process is limited to 25 mb. If observational data is more than 25 mb below the model terrain, those values are simply not used and variables derived below model terrain are determined only by interpolated first guess forecast values (Staudenmaier, 1996b, Figures 3-3 and 3-4; Table 3-4).

Table 3-4 Average depth of data not used from the lower portion of the radiosonde in the Eta assimilation process. Adapted from Staudenmaier (1996b).

Station id	**Average Depth Of Data Lossed (mb)**
OAK	18
UIL	14
MFR	109
GGW	29
GEG	4
TUS	60
BOI	55
SLC	50
REV	36
RIW	104
FGZ	0

Figure 3-3 Map of the western U.S. showing those areas (shaded) likely to have surface observations included in the Eta data assimilation process. From Staudenmaier (1996b).

Figure 3-4 Map of the western U.S. showing those areas (shaded) most likely to have surface observations not used in the Eta data assimilation process as they would be 25 mb below model terrain. From Staudenmaier (1996b).

Similar to the sounding data, the Eta output required considerable manipulation in order for it to be usable for the mixing height estimation. General Meteorological Package (GEMPAK) software was used to compute and extract all necessary variables (θ_v, θ, z, u and v winds) into a format useful for analysis. Geopotential height and wind components were readily available on pressure levels at each model grid point where potential temperatures (θ and θ_v) were calculated using available temperature and mixing ratio. Each of the variables were extracted using a prewritten GEMPAK algorithm that derives the location of each model grid point from the 80 km Eta grid to a row columnar text format.

Prior to the data extraction, it was desirable to interpolate these variables from pressure to sigma (σ) coordinate surfaces. Sigma is given by

$$\sigma = \frac{p}{p_s}$$

where p is pressure at the level of interest in mb and p_s is the model surface pressure in mb. Sigma is a non-dimensional coordinate where pressure at a particular level is normalized by the model surface pressure allowing all surfaces to be above ground level. This is particularly convenient for analyses over complex terrain (e.g., western U.S.). The model sigma surfaces used here were interpolated using available pressure levels located at or above model terrain. The vertical interpolation performed was linear (average value between two pressure levels) and where possible quadratic (averaging values from four surrounding grid points on a given level, S. Chiswell, Unidata Support, 2000, pers. comm.). Sigma surfaces in the model are computed so that a greater number of levels define the boundary layer. Levels range from .9950 to .8000 in increments of

.005 in the lower atmosphere and then from .8000 to .4500 in increments of .05 aloft (47 levels total) where .995 signifies the sigma level closest to the surface.

Even though variables computed on the lowest sigma level can be used as an estimate of surface conditions, a more approximate value was needed (a value more representative of surface conditions). This is especially true for the potential temperature values used in mixing height calculations, as heights are so dependent on the initial surface temperature. In order to obtain a representative surface temperature the 2 m above ground surface was used.

Although previous literature describes the existence of the 2 m biases in the Eta output (i.e., McNulty and Cairns, 1999 and Staudenmaier, 1996b), θ, θ_v, and z variables were extracted at all model grid points on the 2 m and sigma surfaces. The 2 m surface was used in order to have some estimate of surface temperature that could be usable for the mixing height procedures examined in this study. Unlike the potential temperatures, u and v wind components were only used on available sigma surfaces to allow the majority of the potential low-level model bias to be focused on 2 m potential temperatures. Figure 3-5 is a grid point example of a θ_v profile where the 2 m and the sigma coordinates surfaces used for determining mixing height are indicated.

Methods

As previously mentioned, part of the objective of this study is to examine two mixing height methods. One is the prevalent technique (Holzworth, 1967) used by NWS fire weather forecasters and air quality modelers, and the other is an alternative procedure

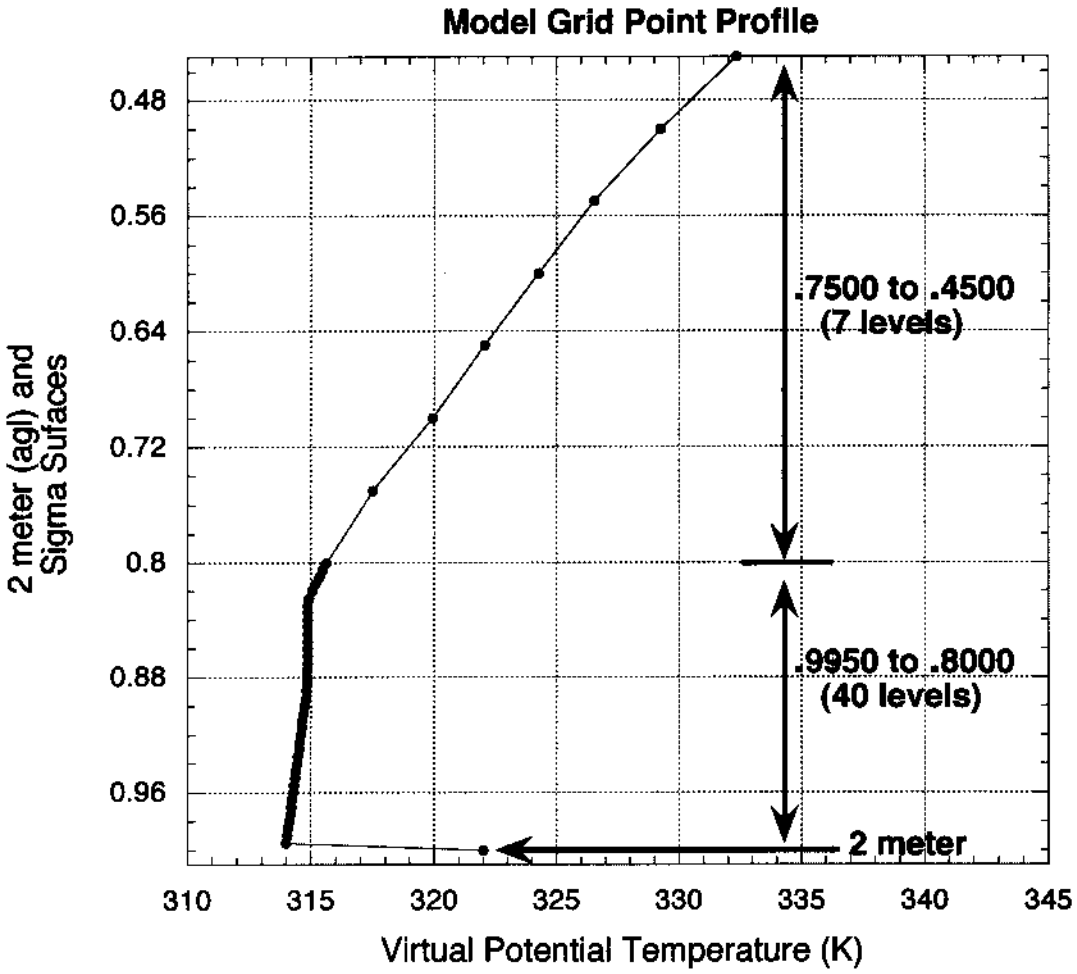

Figure 3-5 An example grid point profile of θ_v from the Eta showing how the 2 meter and sigma surfaces are distributed with height. The large difference between the 2 m point and .995 sigma points is due to the interpolation method used to obtain a 2 m value.

(Stull, 1988; 1991) that is noticeably more thorough in mixing height estimation. This section provides a detailed description of these two techniques and summarizes the procedures used to perform the analyses.

Holzworth mixing height procedure

The current method used to produce mixing height in smoke management forecasts (Holzworth, 1967) has been used for years by the NWS. The top of the mixed layer is computed by examining parcel movement of the θ surface value. Surface parcel ascent is performed based on the positive parcel buoyancy available and using the dry adiabatic assumption (i.e., constant θ) through a well-mixed layer. Parcel buoyancy for this technique is measured by comparing the potential temperature of the surface parcel to the environment at the same height. Using these concepts, the 12 UTC mixing height is defined as the level above ground at which the dry adiabatic ascent of the sounding surface temperature plus 5°C intersects the vertical temperature profile measured at 12 UTC (Figure 3-6). The $T+5℃$ factor was determined arbitrarily by Holzworth (1967) from analyzing urban-rural temperature differences and was applied to account for the heating that occurred shortly after sunrise. The afternoon mixing height is based on the level above ground at which the adiabatic ascent of the 00 UTC sounding surface temperature intersects the 00 UTC temperature profile (Figure 3-6). This latter method is often applied to obtain a daily forecast of the afternoon mixing height utilizing the daily occurred with the ambient profile from surface forecast maximum surface temperature and 12 UTC sounding. Once intersection has parcel ascent, no other analysis is

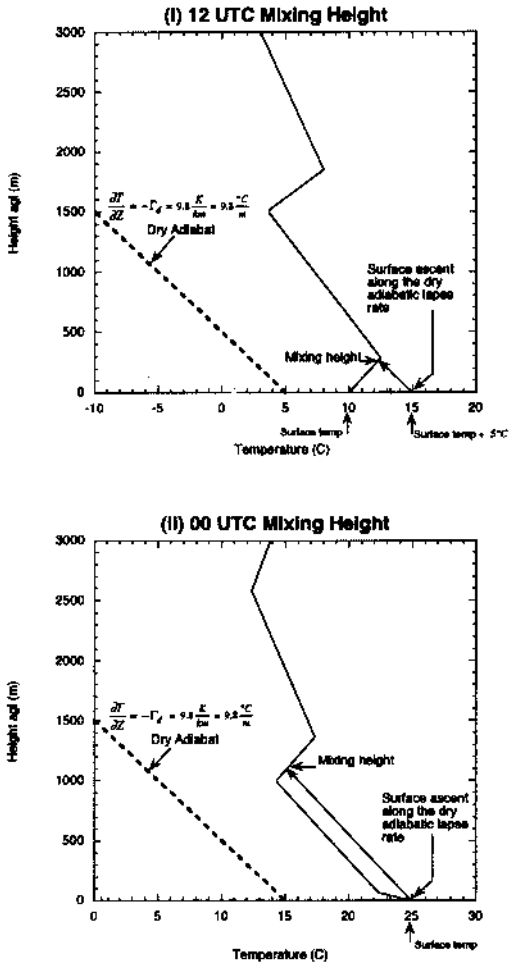

Figure 3-6 Graphical depiction of Holzworth method for determining (i) the 12 UTC or morning mixing height and (ii) the 00 UTC or afternoon mixing height.

performed, and therefore only a portion of the sounding profile is used for mixed layer estimation.

Stull mixing height procedure

This method described by Stull (1988, 1991) involves examining nonlocal stability by displacing parcels of θ_v upward from the relative maxima and downward from the relative minima where parcel movement is based on buoyancy measured by comparing the θ_v of the parcel to the environment at the same height. Ascent or descent of the parcel is tracked until it intersects the environmental profile or becomes neutrally buoyant. Once the parcel movements have been tracked, the static stability portions of the sounding domain are then determined in the following order:

1) Unstable: those regions where the parcel can move under its own buoyancy. If a subregion is buoyantly traversed by one air parcel, and a different air parcel traverses a subregion that partially overlaps the first subregion, then the entire region formed is classified as unstable (Figure 2-8 profile (l)).
2) Stable: portions of the sounding with a subadiabatic lapse rate that are not unstable (Figure 2-8 lower portion of profile (b)).
3) Neutral: regions with an adiabatic lapse rate that are not unstable (Figure 2-8 middle portion of profile (b)).
4) Unknown: regions at the top or bottom of the sounding profile that are apparently stable or neutral but do not end at the ground (Figure 2-8 mid to upper portion of profile (d)).

Figure 2-8 provides several examples of how to determine the nonlocal static stability. Once the nonlocal static stability is known for the entire profile, then mixing height can be determined (Figure 3-7).

Correction procedure applied to the Eta output

From inspection of the observed and computed variables at the 2 m model surface, and due to the assimilation issues described above, a correction was applied to the derived Eta 2 m θ and θ_v. These variables are supposed to be representative of 2 meters above the true ground surface. However, they are actually 2 meters above the Eta model terrain which, as previously discussed, can be quite different than 2 meters above the true terrain, especially over the western U.S. Table 3-5 lists the median difference values in elevation between the sounding surface and the Eta ground (Eta minus sounding). Corrections were performed on the potential temperature values instead of the variables used to calculate them (i.e., temperature, mixing ratio, and pressure) because θ and θ_v typically have a smooth vertical gradient.

The procedure used to correct the Eta 2 m θ and θ_v involved applying monthly mean differences (sounding surface minus the Eta 2 m) to the daily differences that existed within a particular month. For example, suppose the daily difference in θ_v was 5 K (the sounding value would be warmer by 5 K), and the monthly mean difference in θ_v was 4 K. Then 4 K would be added to the daily 2 m temperature value from the Eta. Each day for the time period analyzed was examined in this manner and the correction methodology was only applied if the Eta 2 m value could be brought closer to that of the

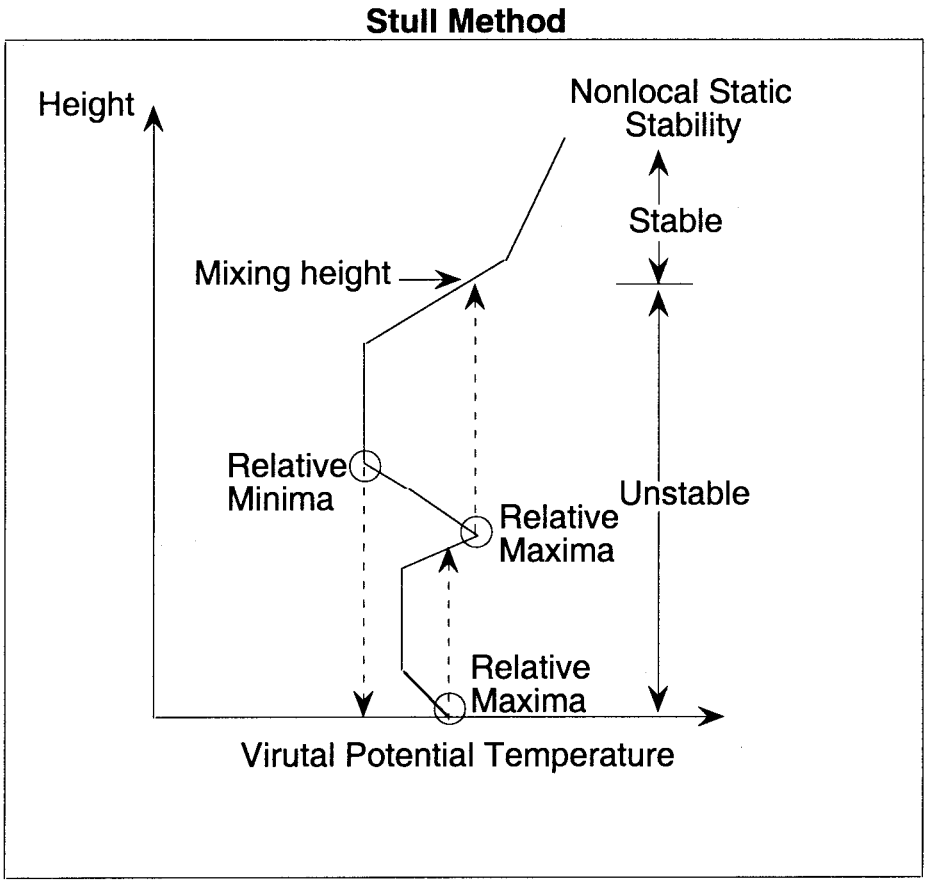

Figure 3-7 Graphical depiction of Stull method for determining mixing height once nonlocal static stability is assessed for the entire profile.

Table 3-5 Median elevation differences between the Eta terrain surface and the sounding surface (Eta minus sounding). Model resolution changed three times during the time period of this study that affected model elevation. Period 1 was 9/1/97 - 2/9/98, period 2 was 2/10/98 - 11/9/98, and period 3 was 11/10/98 – 8/31/99.

Station id	Period 1 (m)	Period 2 (m)	Period 3 (m)
REV	142.7	90.7	202.2
GGW	139.25	91.87	25.42
NKX	115.41	116.06	-123.39
FGZ	-240.1	-326.5	74.2
OAK	56.506	37.701	134.27
BOI	724.9	550	435.7
TUS	259.6	207.1	304.8
DEN	810.1	716.9	395.4
UIL	16.42	11.062	290.66
GEG	-20.36	-92.66	-11.92
MFR	1014.7	926.3	870.3
TFX	207.6	138.7	-10.2
SLC	712.1	745.8	753.9
RIW	531.2	409.1	10.3
ABQ	644.4	496	272.4

sounding surface value; otherwise, the original Eta temperature was used. Further, if the applied corrections resulted in θ being greater than θ_v (θ_v is always greater than θ because humidity is used in its calculation), but the sounding data indicated otherwise, the original Eta temperature values were retained. These corrections also were performed separately for 12 and 00 UTC. For the case of θ at 12 UTC (Holzworth method), the original value was determined using $T + 5°C$ for both the sounding surface and Eta 2 m and then it was corrected where possible.

Mixing height and transport wind procedure

When determining mixing heights from the sounding data using the Stull method, z and θ_v were examined on isobaric surfaces that extended from the ground surface up to 200 mb. A FORTRAN computer algorithm was designed to incorporate the parcel ascent

and descent procedures described earlier under the Stull method. Similarly, mixing heights for the Holzworth technique were determined using a FORTRAN algorithm which incorporated the theory described above.

It should be mentioned that the wind data used to compute mean transport for both the Stull and Holzworth methods, in the case sounding estimates, were from the Eta output. This was done because wind measurements from radiosondes can often times be unreasonably coarse and therefore undesirable to use. Wind data from Eta output on the other hand is available on all 47 sigma levels making these much more suitable for computation of mean values.

Similar computer code was used to calculate mixing height from the Eta output. However, variables were based on sigma coordinate surfaces instead of pressure. This was done to ensure levels would be above ground level and to sharpen the structural resolution of the lower boundary layer.

Analysis procedures

The analysis for this study, of which the results are presented in chapter four, can be described in terms of three primary objectives:

1) Method comparison
    - Examine time series plots of mixing height differences between Stull and Holzworth separately for 00 and 12 UTC using both data sets
    - Establish physical reasons for height differences separately for 00 and 12 UTC
    - Examine the effect of the mixing height differences between Stull and Holzworth on the mean transport wind speed and direction

2) Data set comparison (Stull method only)
   - Examine time series plots of mixing heights differences between the sounding data and the Eta model output (Eta minus sounding) for each of the fifteen site locations separately for 00 and 12 UTC
   - Assess differences using physical reasoning
3) Spatial analysis of mixing height computed from the Eta output
   - Generate mean monthly plots of mixing height for the entire western U.S. separately for 00 and 12 UTC
   - Present a discussion of the spatial advantages of using Eta output for generating mixing height

These analysis procedures will be used to describe the overall differences between the Holzworth and Stull methods in hopes of suggesting future usage of the Stull technique operationally. Following the method comparison, the reliability of using the Eta model output to produce mixing height forecasts will be examined by comparing individual model grid points to co-located upper air sounding stations. This evaluation will lead into a discussion that describes the spatial advantages of using Eta model output to produce mixing height forecasts, as large geographical coverage of values can be made available operationally along with extended prediction.

CHAPTER FOUR

RESULTS

Mixing height method comparison

In order to compare the Stull and Holzworth mixing height methods, time series plots of mixing height difference (Stull minus Holzworth) for the fifteen upper-air stations were used for both 00 and 12 UTC. Using the time series graphics, an initial generalized assessment of mixing height differences was examined for many climatologically unique point locations throughout the western U.S. This comparative analysis was performed separately for 12 UTC (morning) and 00 UTC (afternoon). Once a general perspective of differences in mixing height methodology was formulated from the time series plots, individual physical examples of mixing height differences were counted and categorized. These categories were developed based on recurring patterns that were observed in the sounding profile structures of θ and θ_v. As a result, three unique groups of differences were developed for the 00 UTC data and two for 12 UTC. These individual groups were analyzed to provide a more detailed physical explanation as to why the Stull and Holzworth methods can generate different mixing height results.

00 UTC mixing heights

Figures 4-1a through 4-1e provide illustrations of the mixing height difference values (Stull minus Holzworth) at 00 UTC for the two-year period for both sounding data and Eta output. Three stations, grouped roughly by their elevation and localized topography, are shown in each Figure. It is noticeable that mixing height values can be spatially inconsistent depending on the methodology used. For example, height

differences seem to be slightly more pronounced at inland locations (i.e., Flagstaff, AZ – FGZ; Figure 4-1c) than at coastal sites (Figure 4-1a), especially during the warmer months. This corresponds well to the general notion of coastal environments being more stable compared to inland locations because of the consistent marine influence which often acts to regulate afternoon solar heating. Inland locations across the West, especially high desert areas (i.e., Salt Lake City, UT – SLC, Figure 4-1e) during the summer months, are climatologically more unstable environments because of the strong afternoon solar heating that occurs at the ground surface. In general, greater surface heating implies more vertical instability, however this alone does not completely identify why the two methods indicate larger differences in mixing height during the warm season. The method differences seem to be more related to how well the structural profiles of θ and θ_v compare, as the incorporation of moisture by θ_v often allows for important distinctions to exist between the two variables (described in more detail below).

In terms of elevation and overall surrounding topography in relation to method differences, only a general interpretation can be made. For example, similar height difference patterns exist at Boise (BOI) and Tucson (TUS; i.e., Figure 4-1d). These sites are similar in elevation and topography as they both have mountains to the north and east, and more flat, arid terrain to the south and west. Another example would be Glasgow (GGW) and Great Falls (TFX; i.e., Figure 4-1b) which are slightly different in elevation, but are both located in the high-plains east of the Rocky Mountains.

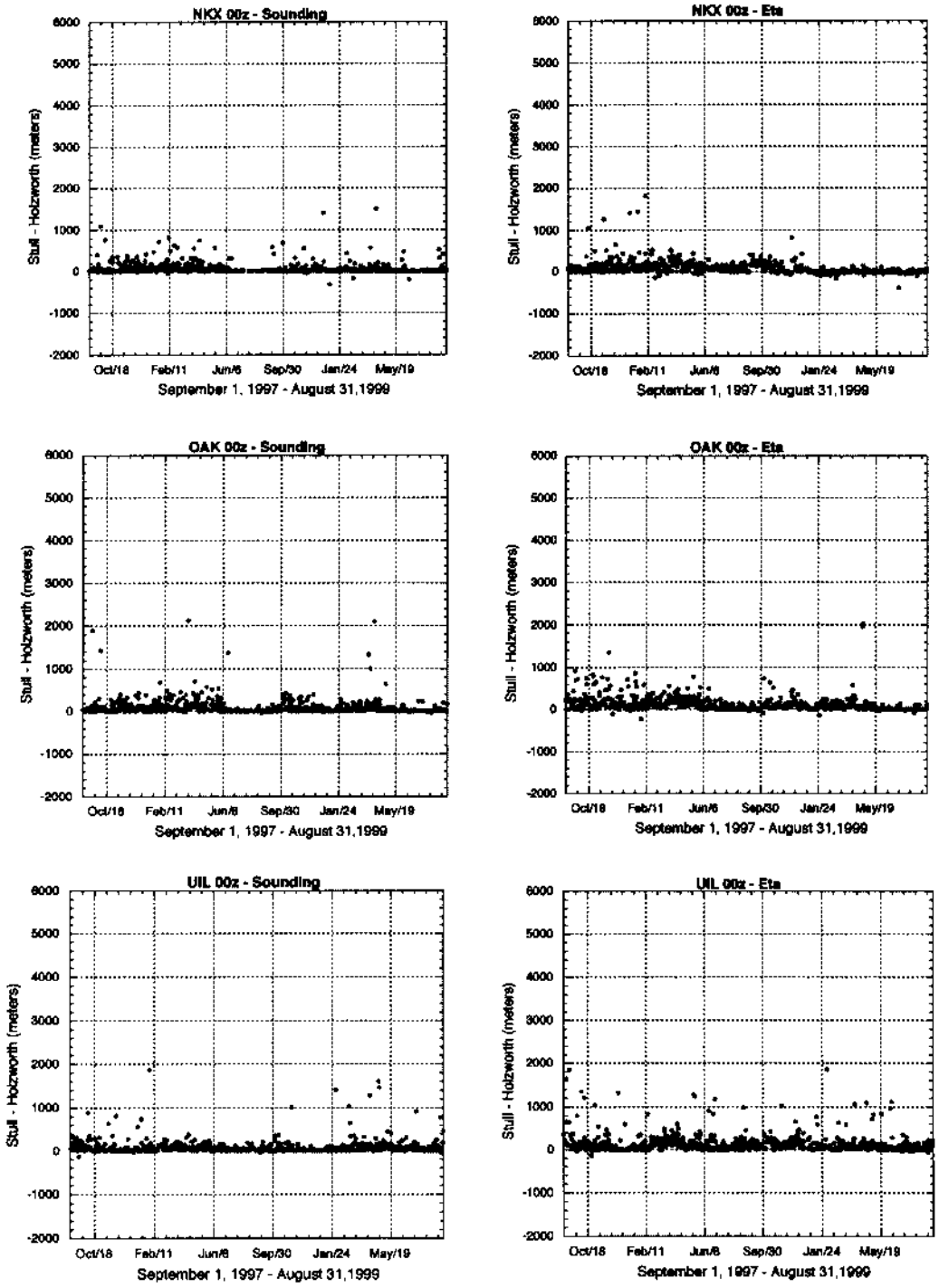

Figure 4-1a 00 UTC time series plots of mixing height differences (Stull – Holzworth) in meters computed using the sounding data (left) and the Eta output (right) for Miramar, CA (NKX), Oakland, CA (OAK), and Quillayute, WA (UIL).

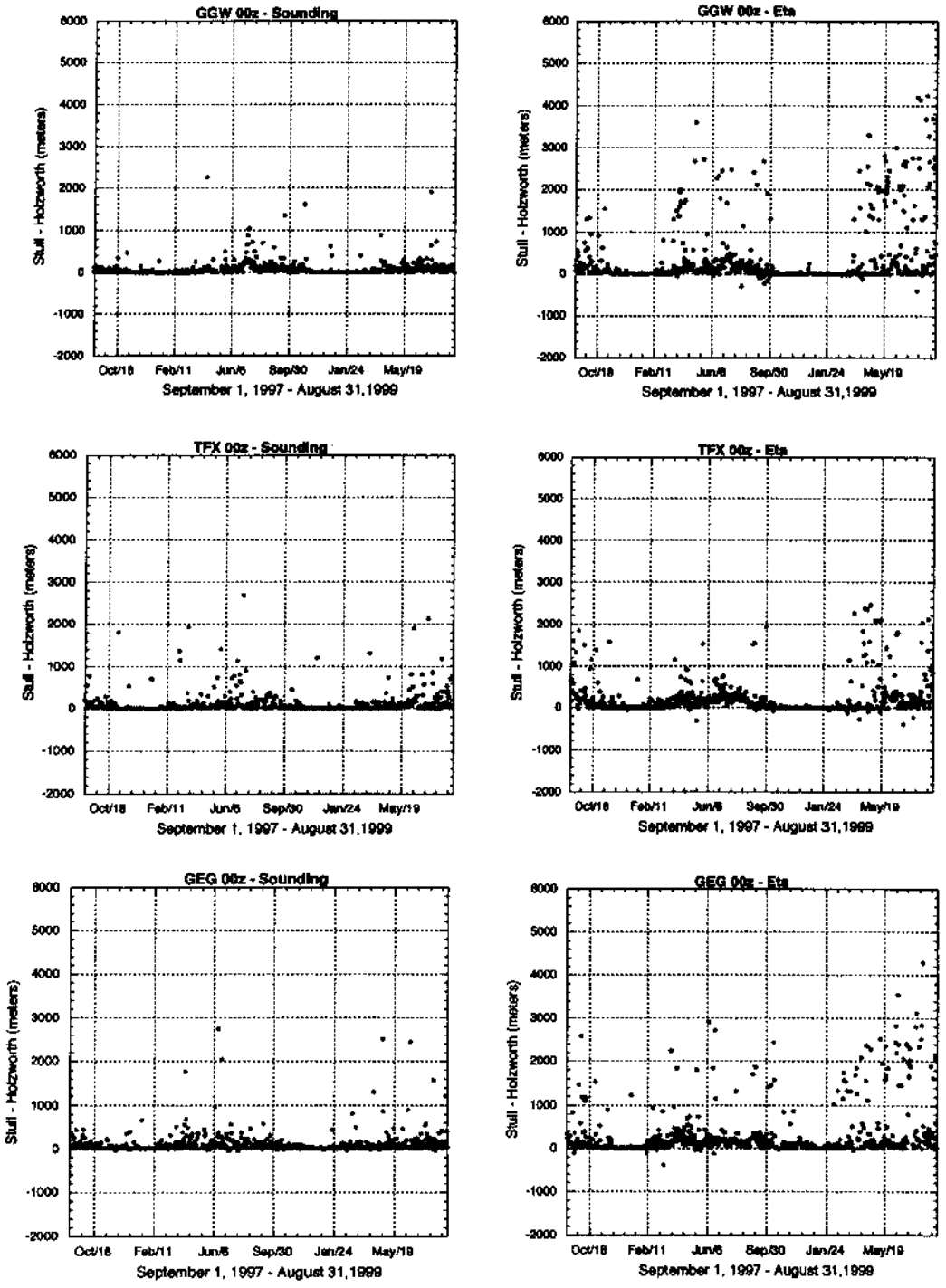

Figure 4-1b Same as Figure 4-1a illustrating Glasgow, MT (GGW), Great Falls, MT (TFX), and Spokane, WA (GEG).

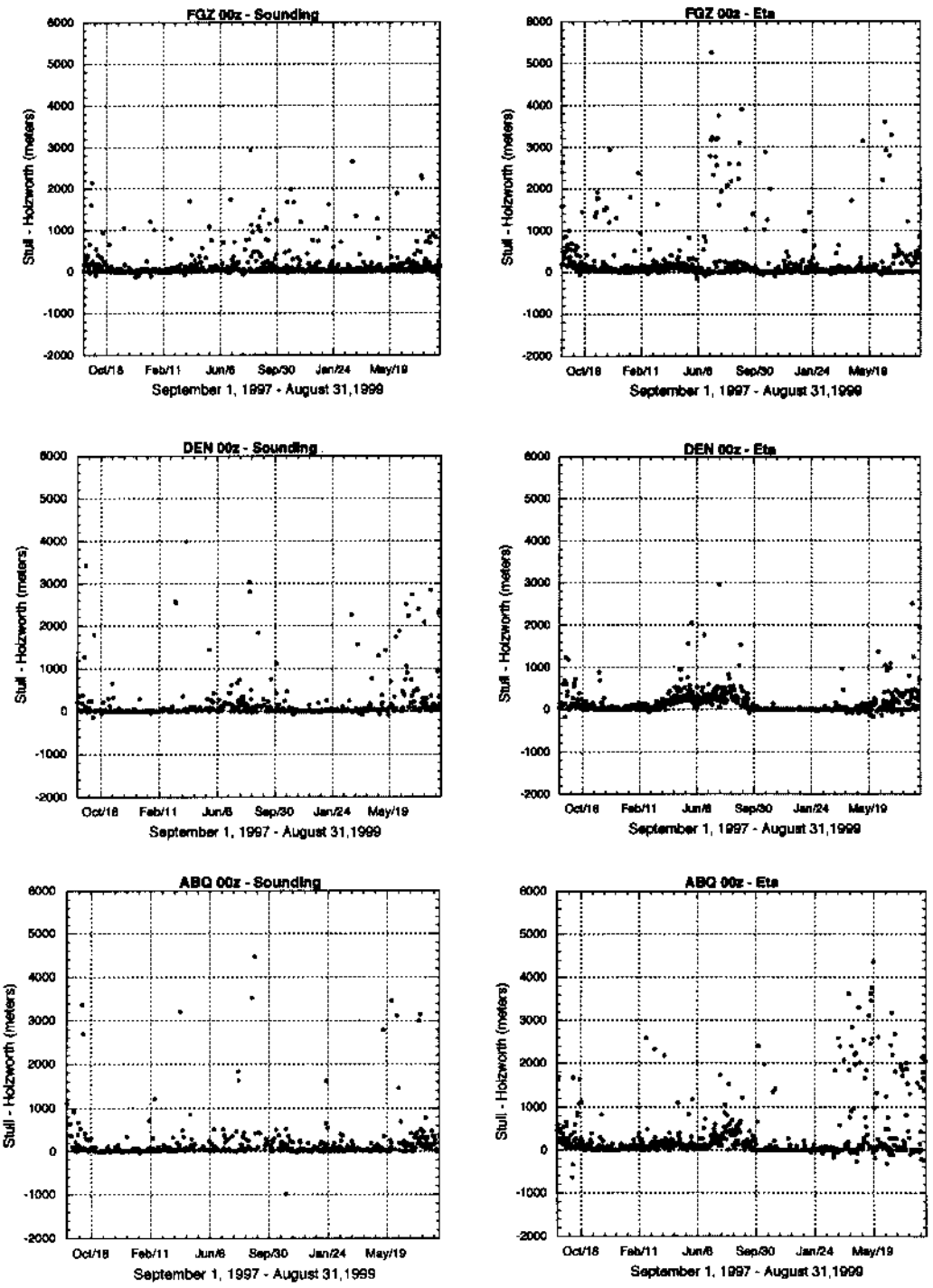

Figure 4-1c Same as Figure 4-1a illustrating Flagstaff, AZ (FGZ), Denver, CO (DEN), and Albuquerque, NM (ABQ).

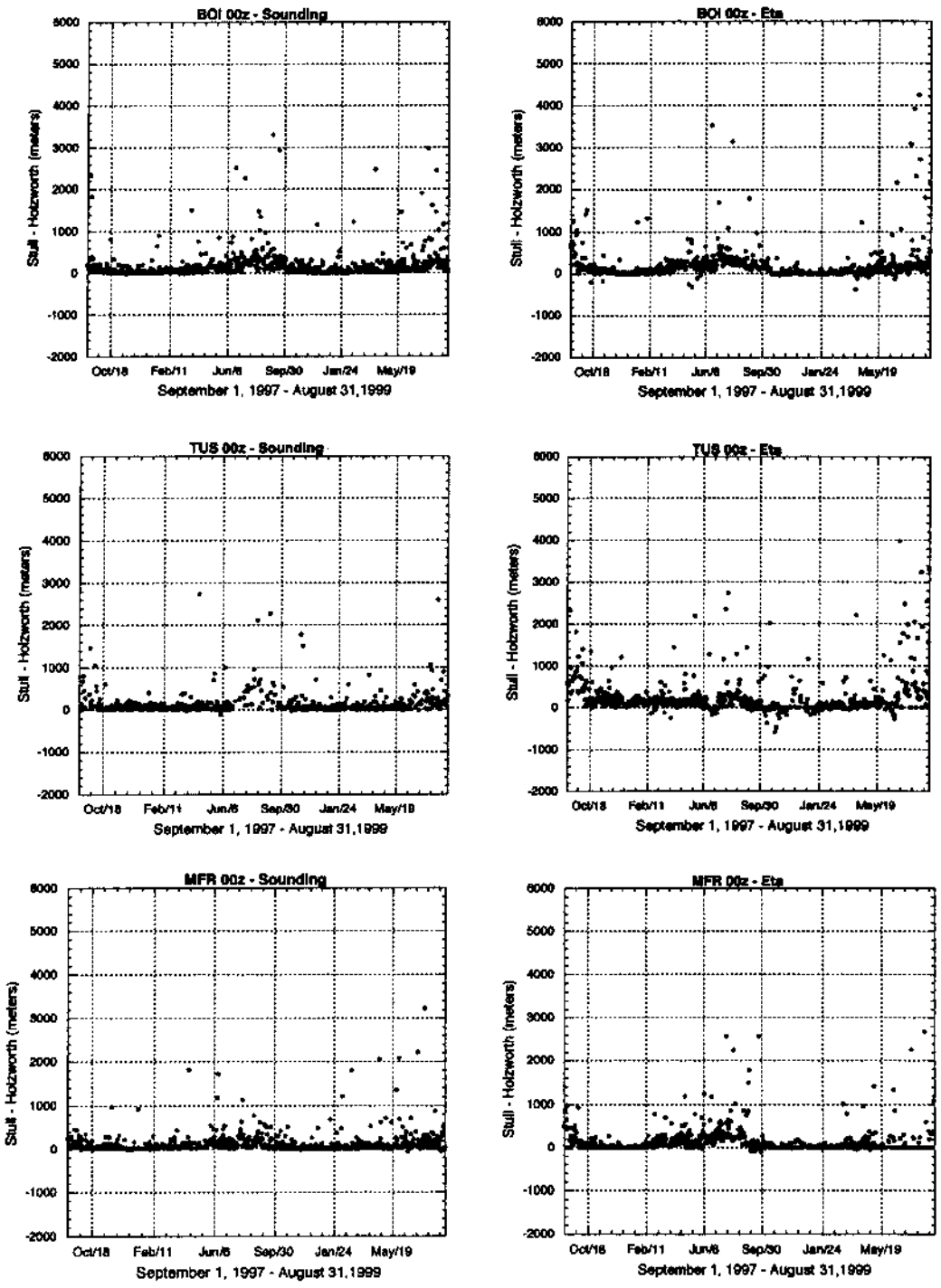

Figure 4-1d Same as Figure 4-1a illustrating Boise, ID (BOI), Tucson, AZ (TUS), and Medford, OR (MFR).

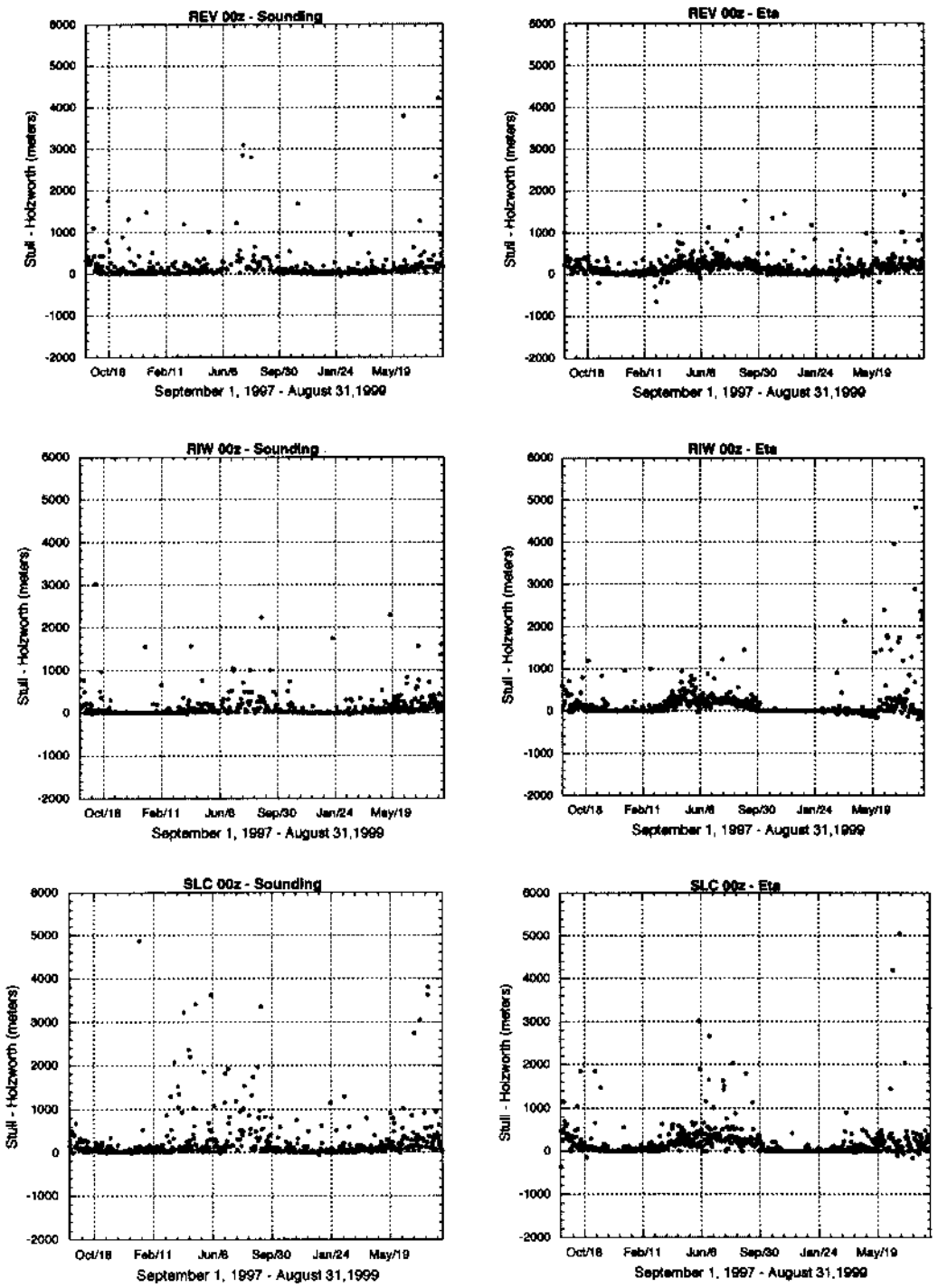

Figure 4-1e Same as Figure 4-1a illustrating Reno, NV (REV), Riverton, WY (RIW), and Salt Lake City, UT (SLC).

Since only two years of data were available for this study, the time series graphics could only provide a generalized depiction of the differences that exist in mixing height methodology. In order to quantify the interpretation, a more physical approach of examining methodology difference was undertaken. This involved analyzing sounding profile structure for recurring patterns. Three distinct patterns were observed where height differences were significant based on a threshold value of 500 meters. This value is somewhat subjective, but is well representative for the afternoon as 12 UTC mixing heights are frequently observed to be less than 100 meters when computed from either the Stull or Holzworth method. Therefore, height differences of 500 meters or greater are substantial when comparing values determined from the two distinct methodologies, regardless of time of day.

Using the 500 m threshold value, considerable difference in mixing height values at 00 UTC were counted and grouped into three categories based on the recurring pattern observed in the sounding profile. These categories are separated for discussion by case 1, case 2, and case 3.

Case 1

The Stull method involves examining the stability for the entire sounding profile (all positive and negatively buoyant parcels are adiabatically tracked) prior to computing the mixing height, whereas the Holzworth technique only uses a portion of the profile (only the adiabatic ascent of the surface parcel is tracked). This sometimes allows for computed mixing height values to be greater when using the Stull method as a significant unstable layer can be elevated and may go undetected if the Holzworth technique is used.

Figure 4-2 shows two profile plots of θ and θ_v measured at Salt Lake City, UT in early September 1998 where parcel movement is performed to indicate the mixing height values determined from the Stull and Holzworth methods. The θ_v profile (ii) is a good example of how an elevated unstable layer can exist and a higher mixing height value is then computed using the Stull method. The θ profile (i) is a good example of how the Holzworth technique could be a disadvantage in this case because the procedure only involves examining the lower portion of the sounding.

Case 2

The Stull method uses θ_v where the Holzworth technique uses θ, and by the definition of θ_v presented in Chapter 2, values are typically greater (warmer) than values of θ due to the incorporation of moisture. This can cause mixing height differences to be large, especially when moisture is plentiful at the surface, as lifted θ_v surface parcels are then warmer initially, sometimes by as much as 4 K. A slightly warmer surface parcel can allow further adiabatic ascent particularly when the ambient profile is superadiabatic near the surface, and thus a larger mixing height value is computed using the Stull method.

Figure 4-3 shows three profile plots of mixing ratio, θ_v, and θ measured at Denver, CO in early July 1999 where parcel movement is performed to indicate the mixing height values determined from the Stull and Holzworth methods. The mixing ratio profile (iii) exemplifies a sharp vertical moisture gradient that decreases from the ground upward dramatically. This, along with a warm surface temperature, can allow the θ_v profile (ii) to be superadiabatic near the surface, more so than the θ profile (i). This is a good example

of how a higher mixing height value can be computed using the Stull method simply because θ_v is used and not θ.

Case 3

During rare instances, greater mixing height values are determined using the Holzworth technique. This tends to occur when small θ_v inversions are present just above the surface. These stable regions develop from the presence of a large moisture gradient and reasonably warm temperatures at low levels. An inversion in θ is also noticeable, but it is generated from the warm temperatures alone, and as a result it may not be quite as sharp (temperature warming with height is more gradual) as the θ_v inversion. These cases are often associated with subadiabatic lapse rate near the surface. Therefore, if ascent is performed using a θ surface parcel, the ambient θ profile may not be intersected as quickly due the presence of a weaker inversion.

Figure 4-4 shows three profile plots of mixing ratio, θ_v and θ measured at Albuquerque, NM in early November 1998 where parcel movement is performed to indicate the mixing height values determined from the Stull and Holzworth methods. The mixing ratio profile (iii) exemplifies a sharp vertical moisture gradient that substantially increases from the ground upward. This, along with a reasonable warm surface temperature, can allow the θ_v profile (ii) to be slightly subadiabatic near the surface, more so than the θ profile (i). This is a good example of how a higher mixing height value can be computed using the Holzworth technique simply because moisture is not incorporated into the method.

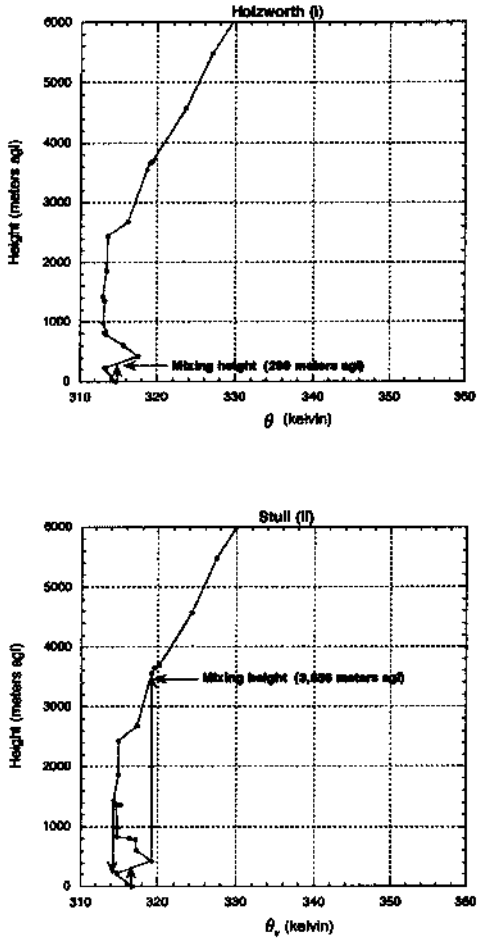

Figure 4-2 Profile examples of mixing height determination using the Holzworth method (i) and the Stull method (ii). (i) shows the adiabatic ascent of the θ surface parcel only and (ii) shows the adiabatic ascent of the relative maxima and minima of θ_v.

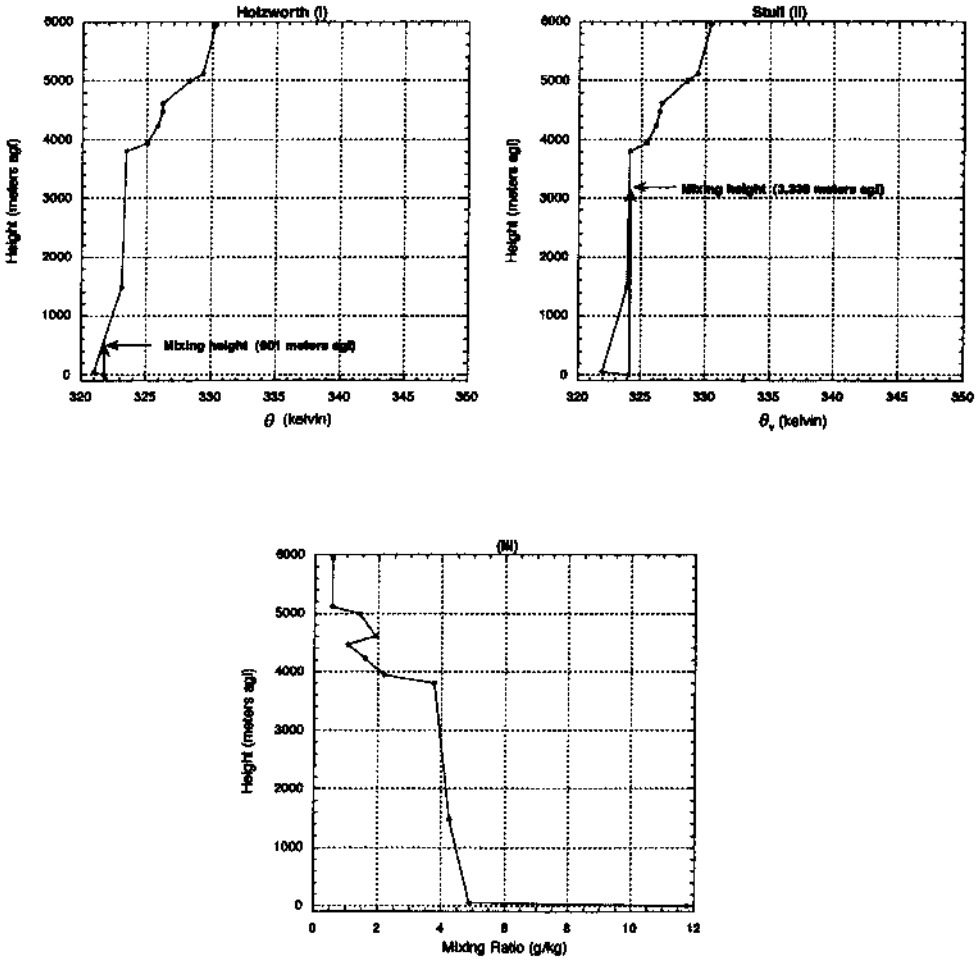

Figure 4-3 Profile examples of mixing height determination for the Holzworth method (i), the Stull method (ii), and mixing ratio (iii). (i) shows the adiabatic ascent of the θ surface parcel only and (ii) shows the adiabatic ascent of the relative maxima and minima in θ_v. (iii) shows a dramatic decrease in mixing ratio near the surface.

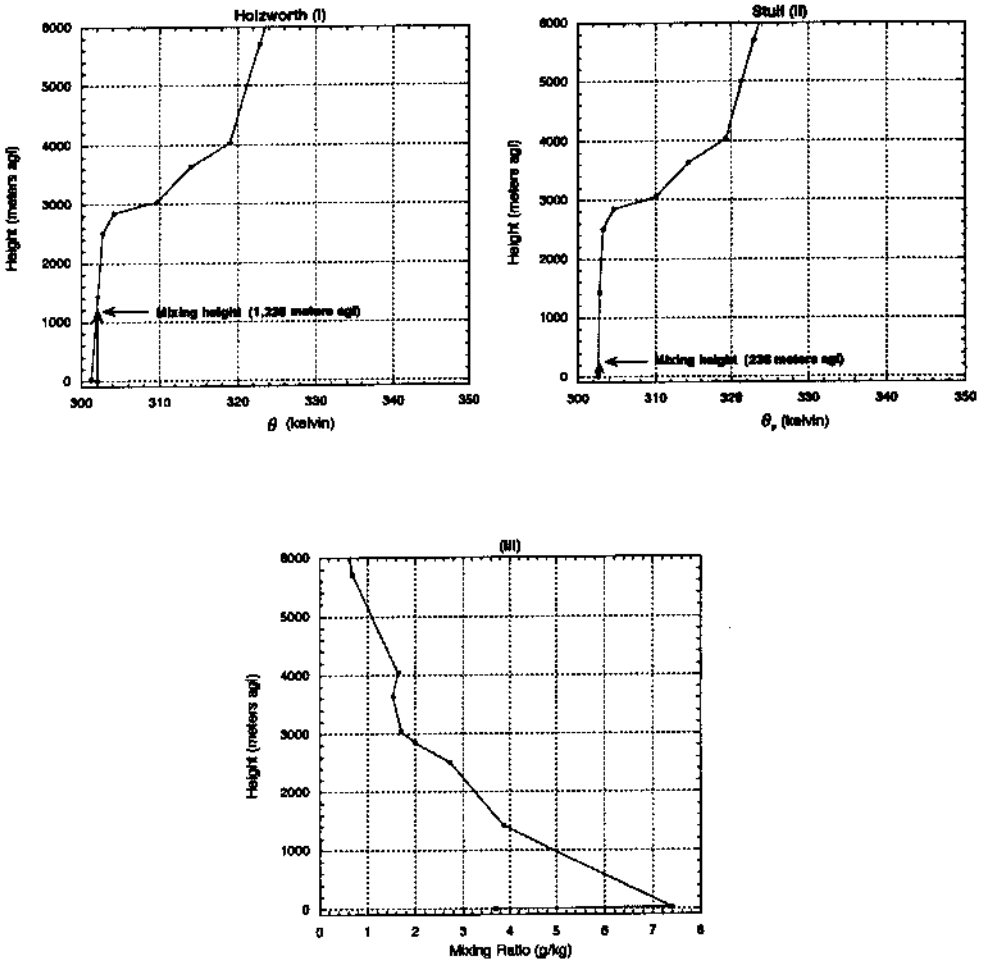

Figure 4-4 Same as 4-3 only (iii) shows a dramatic increase in mixing ratio near the surface.

Table 4-1 is listing of the percent occurrence for the sounding data of the three individual case groups for 00 UTC just discussed. Overall, the percentages for each case are not that different for the Stull and Holzworth methods. When differences do occur, almost always the Stull method estimates a large mixing height value, as indicated from the case 3 percentages that mainly give a value of zero. The only exception is Albuquerque (ABQ), which perhaps had more instances where the θ_v profile was slightly subadiabatic near the ground surface indicating the presence of a sharp vertical moisture gradient that substantially increased from the ground upward (i.e., case 3). It is also interesting to note that all the coastal stations show a slightly larger percentage for case 2 than case 1. Case 2 is when the Stull method produces greater height values due to the presence of a large moisture gradient at the surface (sharp decrease with height), thus allowing the surface θ_v to be significantly greater than θ, sometimes by as much as 4 K. Case 1 indicates that the Stull method has a higher mixing height value due to elevated instability that exists within sounding profile, and thus suggests that tracking only the ascent of the surface parcel (i.e., Holzworth method) is not sufficient to accurately define the top of the mixed layer. It seems reasonable to have moisture intrusions at low-levels for Quillayute (UIL), Miramar (NKX) and, Oakland (OAK) since their elevations are all fairly close to sea level, and they are under consistent marine influence.

In regard to the similarities in elevation and topography in Table 4-1, there appears to be an interpretable pattern in the percentages between case 1 and case 2. Boise (BOI) and Tucson (TUS) both show a higher percentage for case 1 than case 2, and are similar in elevation and topography as previously discussed. An example of case 2

showing a higher percentage than case 1 can be observed for Denver (DEN) and Albuquerque (ABQ). Both of these stations are similar in elevation, but different in topography; DEN is located on high-plains just east of the Rockies and ABQ is in a river valley setting just west of the Sandia Mountains. Another interesting example where case 1 and case 2 indicate similar percentage values is for Great Falls (TFX) and Glasgow (GGW). Though these two sites are somewhat different in elevation, their topography is quite similar, as they both are located in the high-plains of Montana.

Table 4-1 Percent occurrence of the three individual case groupings where each case describes a physical process that can explain why the mixing height values computed from the Stull method can be significantly different than those determined from the Holzworth technique for 00 UTC.

Station id	**Elevation (m)**	**Stull > Holzworth Case 1 %**	**Stull > Holzworth Case 2 %**	**Holzworth > Stull Case 3 %**
UIL	62	0.3	2.7	0.0
NKX	124	1.0	1.6	0.0
OAK	3	0.9	1.1	0.0
GEG	721	1.7	1.7	0.0
TFX	1130	3.2	3.4	0.0
GGW	700	1.4	1.2	0.0
MFR	405	2.1	3.0	0.0
BOI	874	6.1	2.2	0.0
TUS	779	5.0	1.5	0.0
REV	1516	4.8	1.9	0.0
SLC	1288	7.5	5.5	0.0
RIW	1688	4.3	2.2	0.0
DEN	1608	3.4	5.5	0.0
ABQ	1613	2.8	4.2	0.2
FGZ	2179	3.9	5.7	0.0

Based on the discussion of the 00 UTC individual case percentages, it seems that local topography and elevation have a fairly significant influence on the development of the daytime mixed layer for inland locations. The marine influence seems to be more

important at coastal stations as it often regulates the amount of surface heating. As far as which is more controlling on the development of the daytime mixed layer, elevation or localized topography, at inland locations it is unclear. Therefore, a more in depth study would have to be performed in order to quantify these findings, as greater knowledge of localized mesoscale processes is needed for further explanation (i.e., differential heating).

12 UTC mixing heights

Figures 4-5a through 4-5e provide illustrations of the mixing height difference values (Stull minus Holzworth) at 12 UTC for the two-year period for both sounding data and Eta output. Three stations, grouped roughly by elevation and topography, are shown in each figure. At first glance, the height differences seem difficult to assess as there are times when values are fairly close to zero (indicating good agreement in methodology), and there are times when values are far from zero (indicating poor agreement in methodology). This general pattern is quite consistent for all fifteen sites. However, for the instances where height differences are large in magnitude, much larger mixing height values are computed from the Holzworth procedure. These differences highlight the usage of the $T+5\,^{\circ}C$ concept that is typically applied to the Holzworth method at 12 UTC. This consistent estimation of much larger mixing height values at 12 UTC was also found by Goldman (1980), and was described to be unrealistic when compared to observation. From Figures 4-5a through 4-5e, the Stull method produces higher height values only a handful of times, which is most likely due to the occurrence of elevated instability.

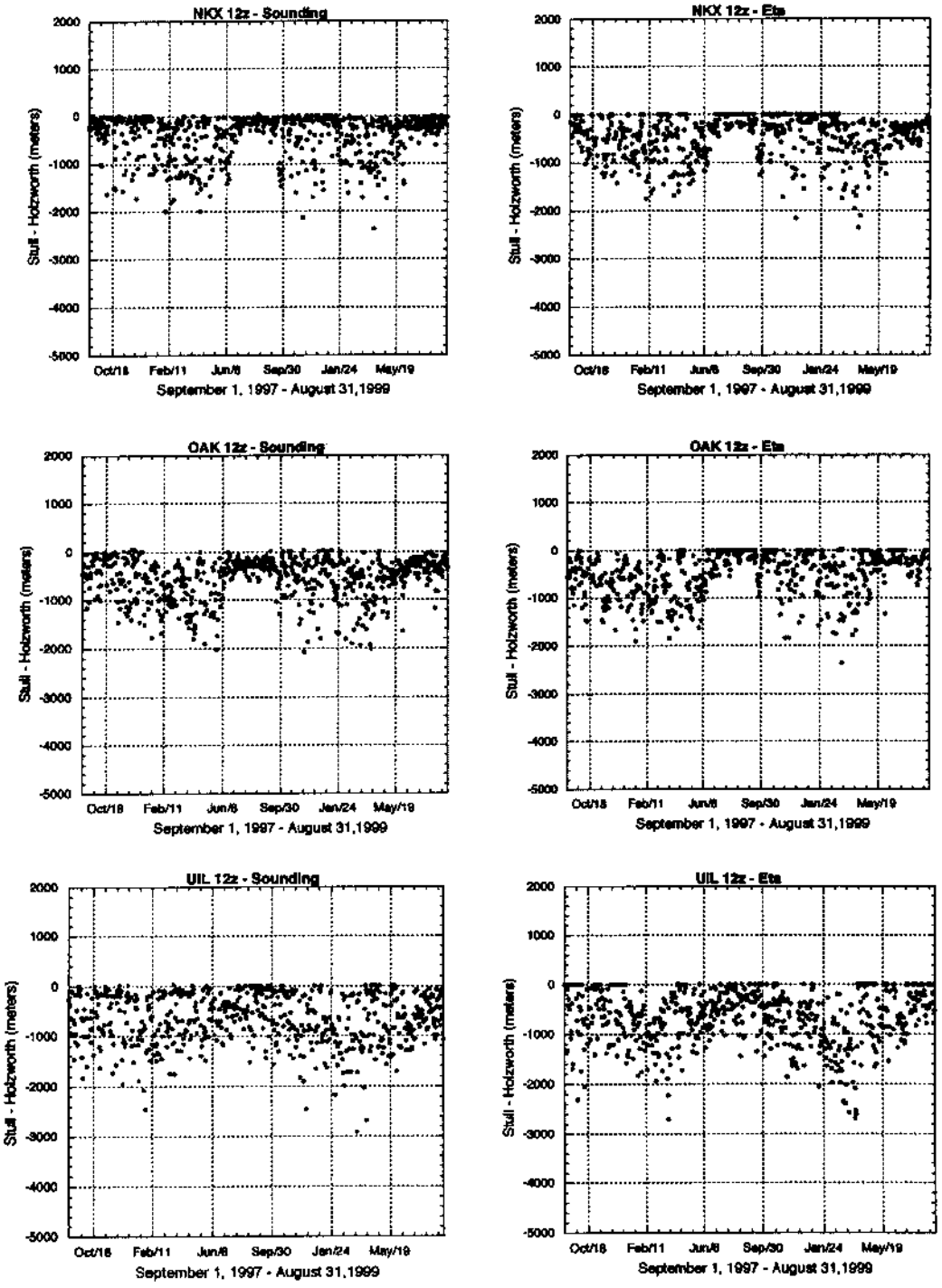

Figure 4-5a 12 UTC time series plots of mixing height differences (Stull – Holzworth) in meters computed using the sounding data (left) and the Eta output (right) for Miramar, CA (NKX), Oakland, CA (OAK), and Quillayute, WA (UIL).

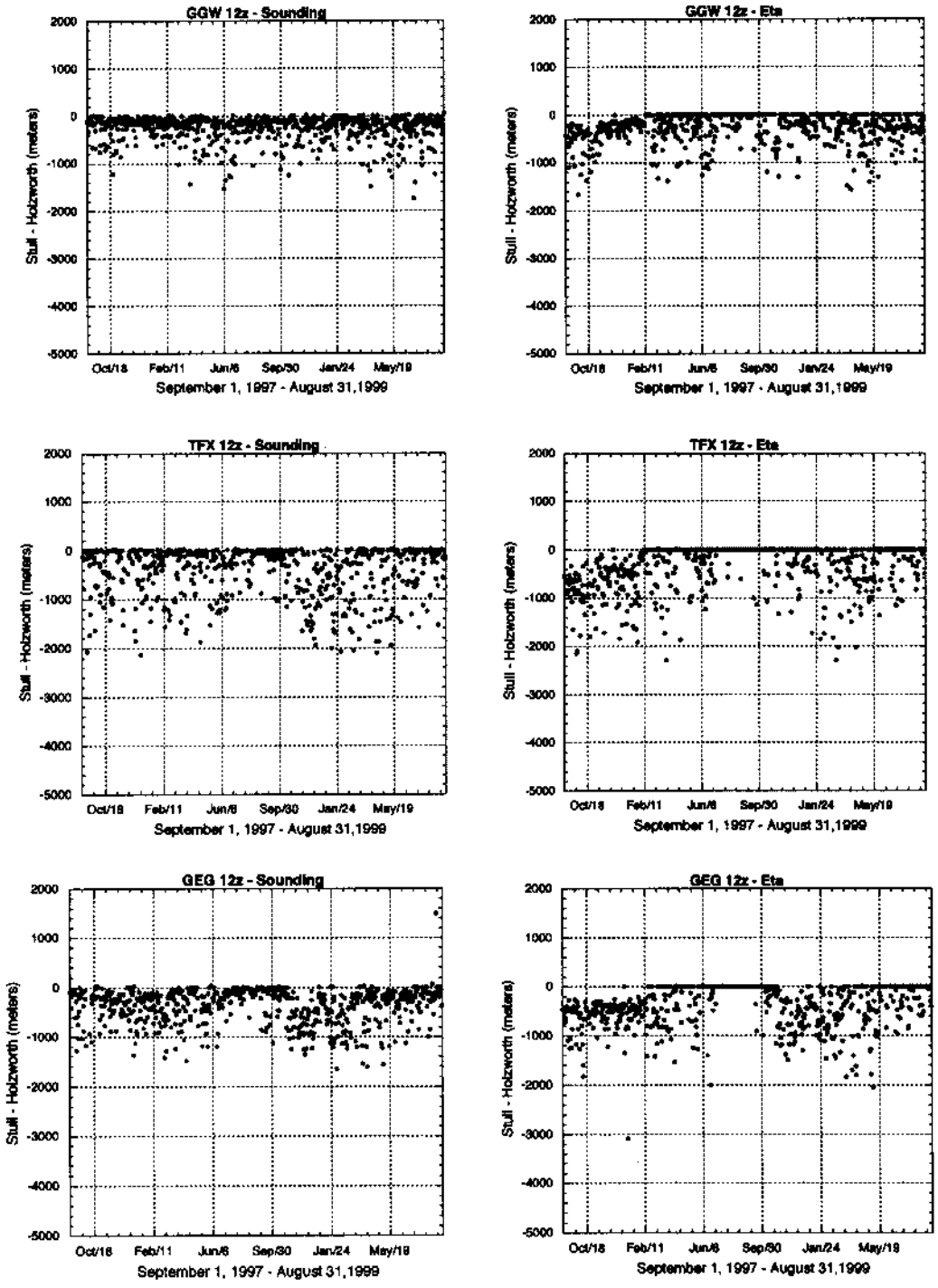

Figure 4-5b Same as Figure 4-5a illustrating Glasgow, MT (GGW), Great Falls, MT (TFX), and Spokane, WA (GEG).

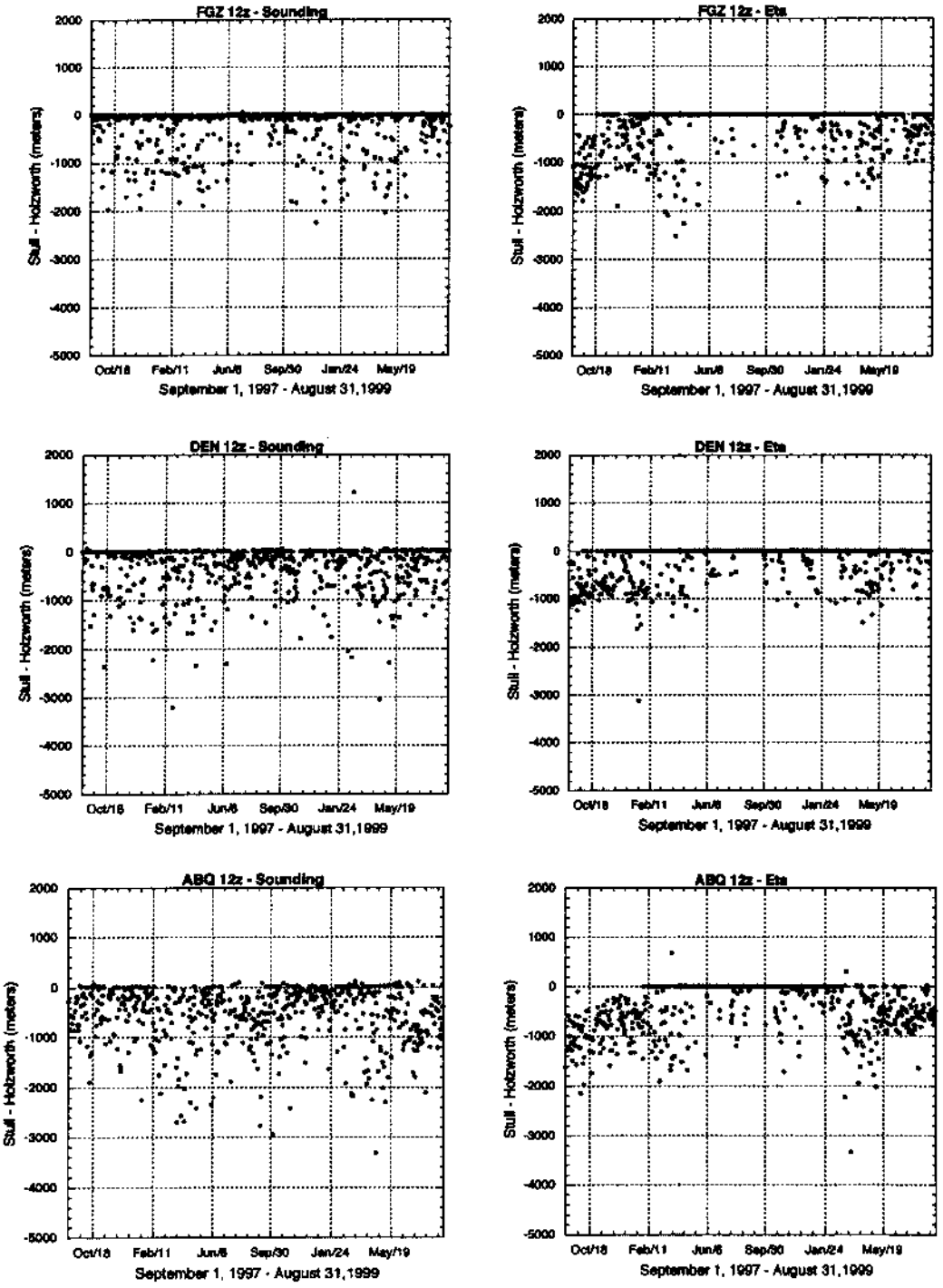

Figure 4-5c Same as Figure 4-5a illustrating Flagstaff, AZ (FGZ), Denver, CO (DEN), and Albuquerque, NM (ABQ).

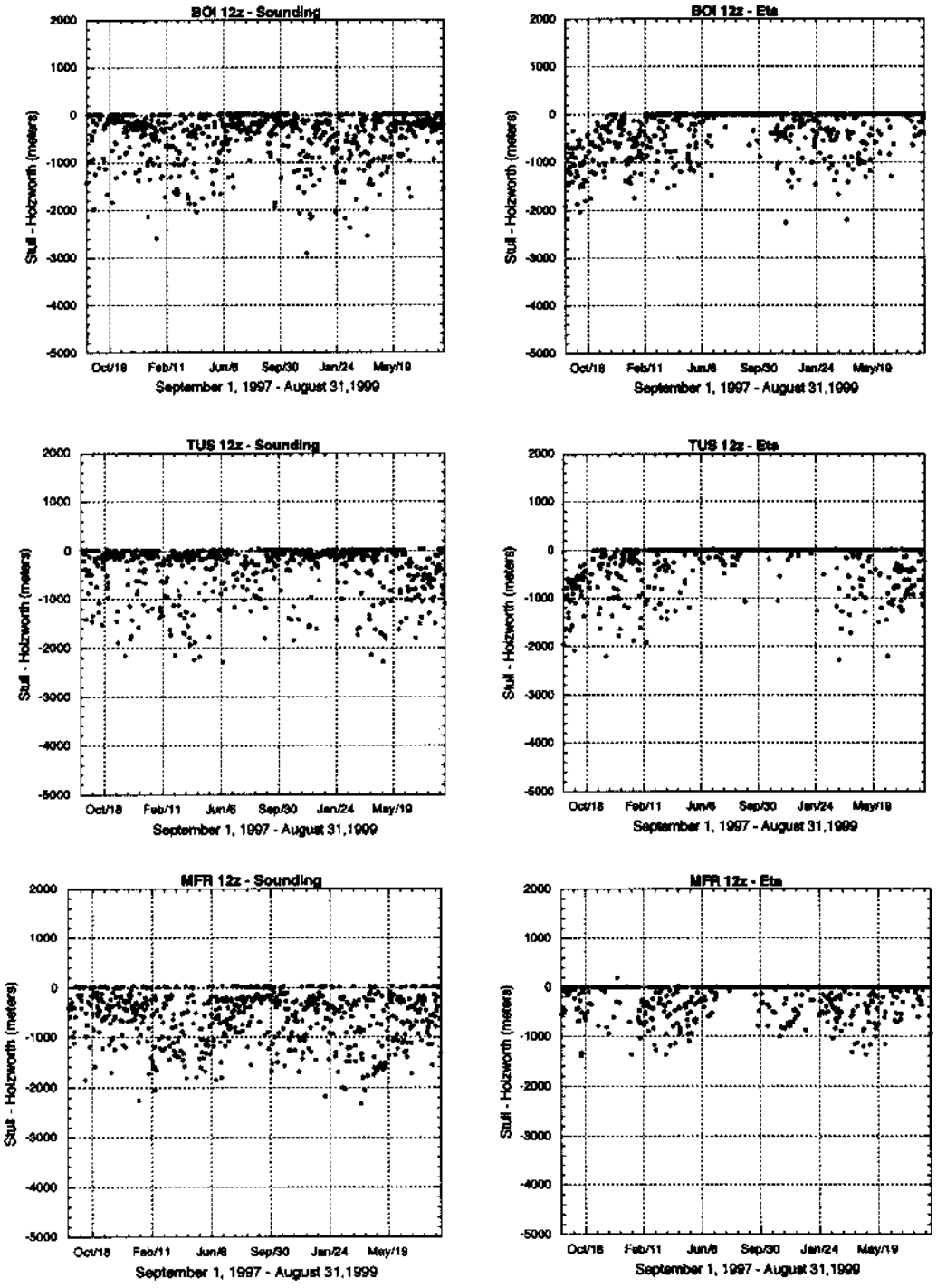

Figure 4-5d Same as Figure 4-5a illustrating Boise, ID (BOI), Tucson, AZ (TUS), and Medford, OR (MFR).

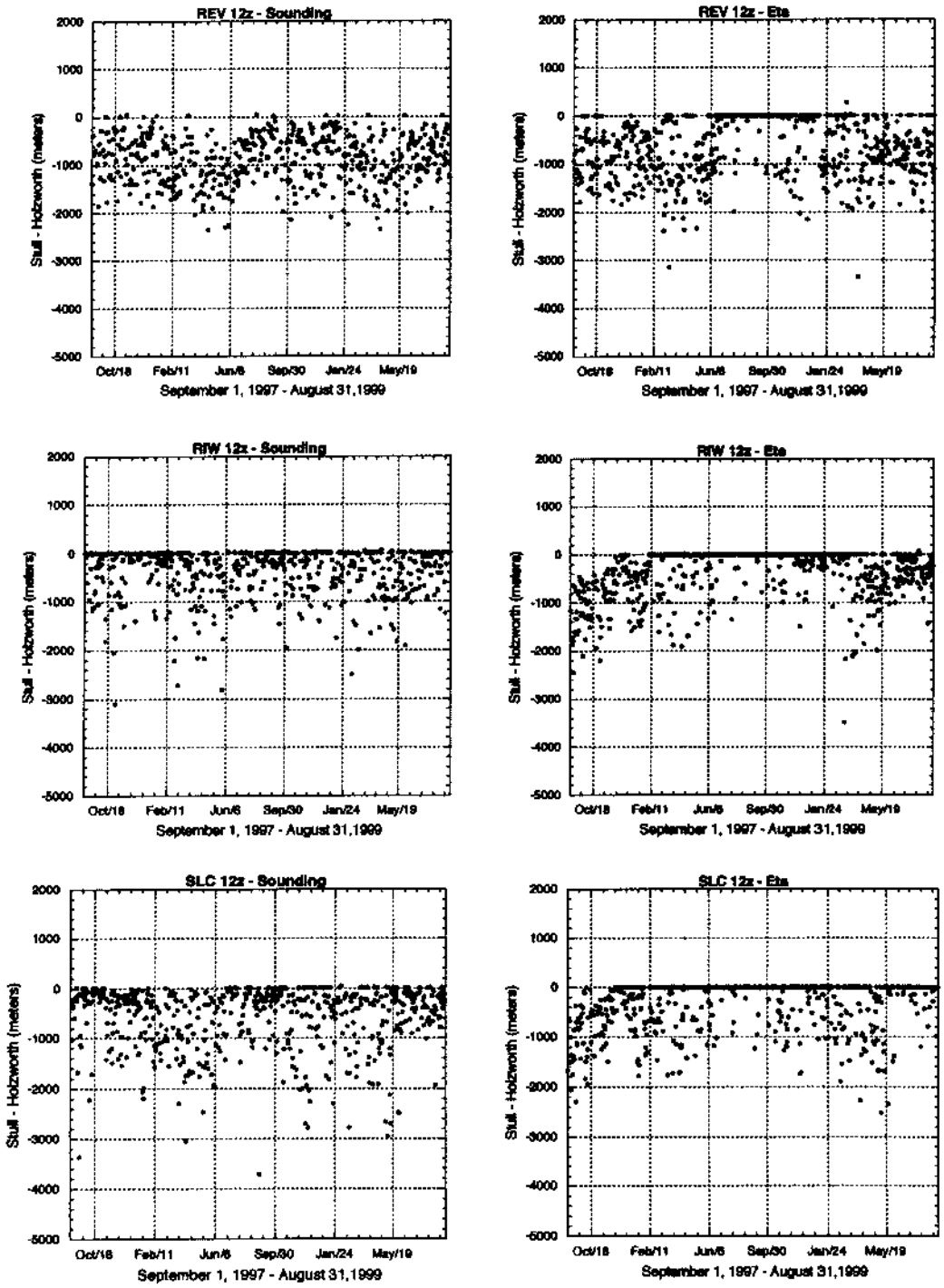

Figure 4-5e Same as Figure 4-5a illustrating Reno, NV (REV), Riverton, WY (RIW), and Salt Lake City, UT (SLC).

There is a hint of seasonal behavior in the height differences shown in Figures 4-5a through 4-5e for a majority of the sites. During the warmer months, height difference values are less pronounced (less negative) which indicates that the Holzworth method is producing height values similar to that of Stull. This may be related to the occurrence of warmer surface temperatures at 12 UTC during the summer months. Morning moisture levels are also typically higher near the surface due to overnight radiational cooling. Though this occurs year round, it can be more extreme during the warm season, especially in dry climates. The combination of warmer temperatures and greater moisture presence at 12 UTC allows θ_v surface parcels to be larger than the θ surface parcels. However, the use of $T+5\,^{\circ}C$ to compute θ at low levels is almost equivalent to adding 5 K to θ, and therefore surface θ and θ_v can become closer in value during warmer times of the year.

In terms of elevation and overall surrounding topography in relation to method differences, only generalizations can be made. Distinguishable patterns are more difficult to extract from the 12 UTC time series plots, as all stations show a fairly consistent pattern of the Holzworth procedure producing a much greater mixing height value. However, as with 00 UTC, there are indications of similarities in height differences at the coastal stations (i.e., Figure 4-5a), between TUS and BOI (i.e., Figure 4-5d), between DEN and ABQ (i.e., Figure 4-5c), and for the Montana sites of GGW and TFX (i.e., Figure 4-5b). Other locations also appear to show good height difference comparability that was not as obvious in the 00 UTC time series plots. This seems to be closely related to the occurrence of low mixing height values produced from the Stull method at 12

UTC. Typically, 12 UTC height values computed from the Stull method are below 300 meters above ground level (agl), and when height differences are analyzed, they tend to be largely negative because the Holzworth procedure generates height values that are usually 500 meters or greater. The *T+5 ℃* concept used in the Holzworth procedure is the main reason for these large differences in mixing height at 12 UTC. Therefore, since mixing heights computed from the Stull method are commonly not large to begin with, subtracting the Holzworth determined height values, which are rather large compared to Stull estimates, tends to generate height differences that are highly negative at 12 UTC.

In order to quantify these time series generalizations, individual 12 UTC cases were grouped to determine why mixing height values are significantly different based upon the methodology. Differences in mixing height values exceeding 500 m were counted and grouped into two categories based on the recurring pattern observed in the sounding profile. These categories are separated for discussion by case 1and case 2.

Case 1

This first category is exactly the same as 00 UTC in that the Stull method involves examining the stability for the entire sounding profile prior to computing the mixing height, whereas the Holzworth technique only uses a portion of the profile. As with 00 UTC, this sometimes allows computed mixing height values to be greater when using the Stull method because a significant unstable layer can be elevated and may go undetected if the Holzworth technique is used.

Figure 4-6 shows two profile plots of θ_v and θ measured at Spokane, WA in mid-April 1999 where parcel movement is performed to indicate the mixing height values determined from the Stull and Holzworth methods. The detection of elevated instability

is not nearly as noticeable at 12 UTC because the *T+5 ℃* concept allows the Holzworth method to produce mixing height values that are much larger than those generated by Stull. Therefore, the detection of elevated stability does not contribute to large height differences as it can do for 00 UTC.

Case 2

At 12 UTC greater mixing height values are almost always determined using the Holzworth technique of *T+5 ℃* to compute the θ surface parcel. This allows the θ surface parcel to be greater than that of the θ_v surface parcel, which is quite unrealistic at lower levels.

Figure 4-7 shows two profile plots of θ_v and θ measured at Miramar, CA in early May 1999 where parcel movement is performed to indicate the mixing height values determined from the Stull and Holzworth methods. This is a good example of how a higher mixing height value can be computed using the Holzworth technique simply because θ is computed using *T+5 ℃* at the surface.

Table 4-2 provides a listing of the percent occurrence for the sounding data of the two individual case groups for 12 UTC just discussed. It is quite clear that the Holzworth method almost always produces a much higher mixing height value, as indicated from the case 2 percentages. Interpretation of percentages by elevation and surrounding topography is extremely difficult given the dominance of the Holzworth method (i.e., *T+5 ℃*). A good example of how the Holzworth method produces an overestimate of mixing height can be examined for the Reno (REV) percentage for case 1 (i.e., 82.8 %). Temperature inversions are very common at REV during all times of the year, and often

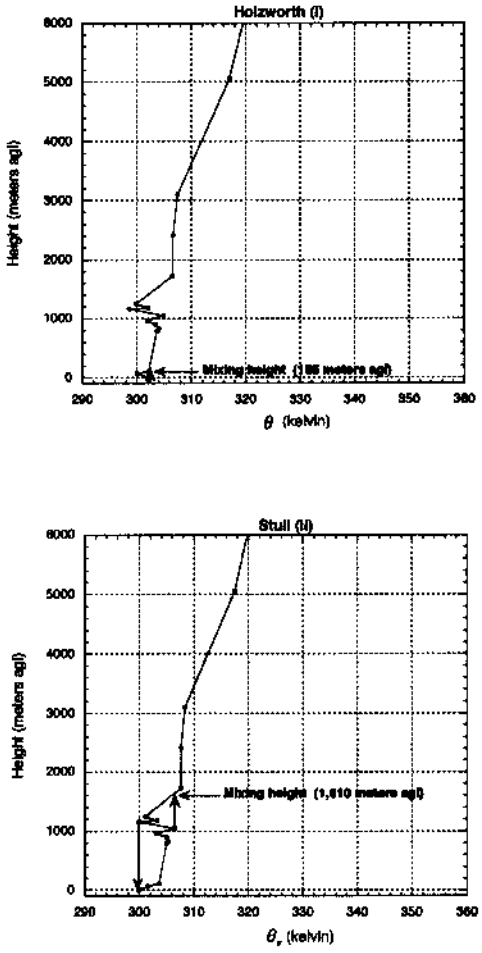

Figure 4-6 Profile examples of mixing height determination for the Holzworth method (i) and the Stull method (ii) at 12 UTC. (i) shows the adiabatic ascent of the θ surface parcel only and (ii) shows the adiabatic ascent of the relative θ_v maxima and minima. Here the Stull method indicates a higher mixing height value due the presence of elevated instability.

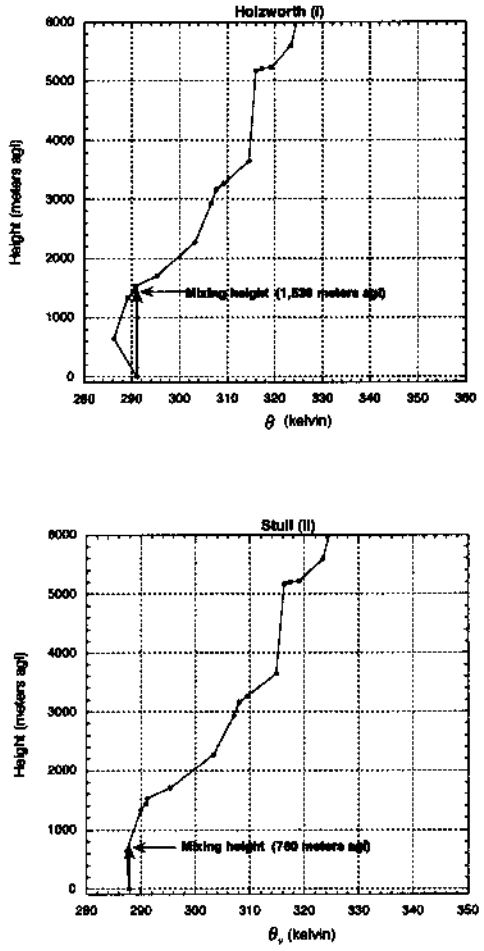

Figure 4-7 Same as 4-6 only a higher mixing height value is compute using the Holzworth method which is typical at 12 UTC due to the *T+5 ℃* concept.

Table 4-2 Percent occurrence of the three individual case groupings where each case describes a physical process that can explain why the mixing height values computed from the Stull method can be significantly different than those determined from the Holzworth technique for 12 UTC.

Station id	Elevation (m)	Holzworth > Stull Case 1 %	Stull > Holzworth Case 2 %
UIL	62	64.8	0
NKX	124	39.0	0
OAK	3	58.5	0
GEG	721	40.3	0.2
TFX	1130	39.1	0
GGW	700	26.3	0
MFR	405	56.9	0
BOI	874	42.1	0
TUS	779	33.7	0
REV	1516	82.8	0
SLC	1288	48.0	0.2
RIW	1688	36.3	0
ABQ	1613	52.4	0
DEN	1608	32.3	0.2
FGZ	2179	23.3	0

they are quite sharp and confined below 500 meters. The launch location for the REV radiosonde is approximately 500 meters above the valley wherein the city of Reno, NV lies. Therefore, the sounding surface temperature is almost always measured above the inversion top, and thus it is already warmer than the temperature at the valley surface prior to application of $T+5\,^{\circ}C$. It is highly plausible that the 12 UTC θ surface parcel used in the Holzworth method (determined using $T+5\,^{\circ}C$) at REV can produce a drastic overestimate of the mixing height.

REV is only one example, and as far as the other stations are concerned, the sounding launch location may not be an issue, but the usage of $T+5\,^{\circ}C$ may be also causing the 12 UTC θ surface parcel at these other stations to be too warm initially. This may explain why the case 1 percentages in Table 4-2 are so large, which again, suggests

mixing height values are often much greater when computed by the Holzworth technique than those determined by the Stull method at 12 UTC.

Mean transport wind

Mean transport wind speed and direction are an average computed through the depth of the determined mixed layer. These values are important for fire weather and smoke management forecasts as the dispersion and trajectory of resultant fire smoke can strongly impact health and visibility. Since the top of the mixed layer specifies the upper limit to which speed and direction values are incorporated into mean computation of transport wind, any misrepresentation of mixing height can affect the accuracy of mean transport wind calculations. Therefore, mean transport wind determined for both the Stull and Holzworth methods was examined for both 00 and 12 UTC.

When analyzing differences in wind speed and direction computed at 00 UTC, it is quite clear that there were hardly any differences when comparing Stull estimates to that of Holzworth for all stations. Due to such strong similarly at all stations, one station was selected as an example. Figure 4-8 is a time series graphic of mean transport wind speed for REV at 00 UTC where values plotted were selected based on the occurrence of significant mixing height differences. From Figure 4-8, it is clear that speed differences never exceed 5 ms^{-1} which suggests that mixing height differences at 00 UTC do not strongly affect mean transport wind speed. Wind direction is not shown here because differences were even less distinct than wind speed for all stations.

A similar examination was performed for the wind speed and direction at 12 UTC. These differences also indicate very strong similarities at each station. However,

wind speed differences were much more variable at 12 UTC in association with significant differences in mixing height.

Figure 4-9 is a time series plot of differences in mean transport wind speed for REV at 12 UTC where values plotted were also selected based on the occurrence of significant mixing height differences. The wind speed differences are directly related to the mixing height differences shown for 12 UTC at REV (i.e., Figure 4-5e) as the Holzworth method almost always estimated a larger height value. Thus, wind speed values are also consistently larger than those computed from the Stull method. Figure 4-9 suggests there is some misrepresentation of mean transport wind depending on the method used for height assessment. Speculation can also be made that the Holzworth technique may be inaccurately computing mean transport at 12 UTC as a result of the $T+5\,^{\circ}C$ concept used to determine the mixing height.

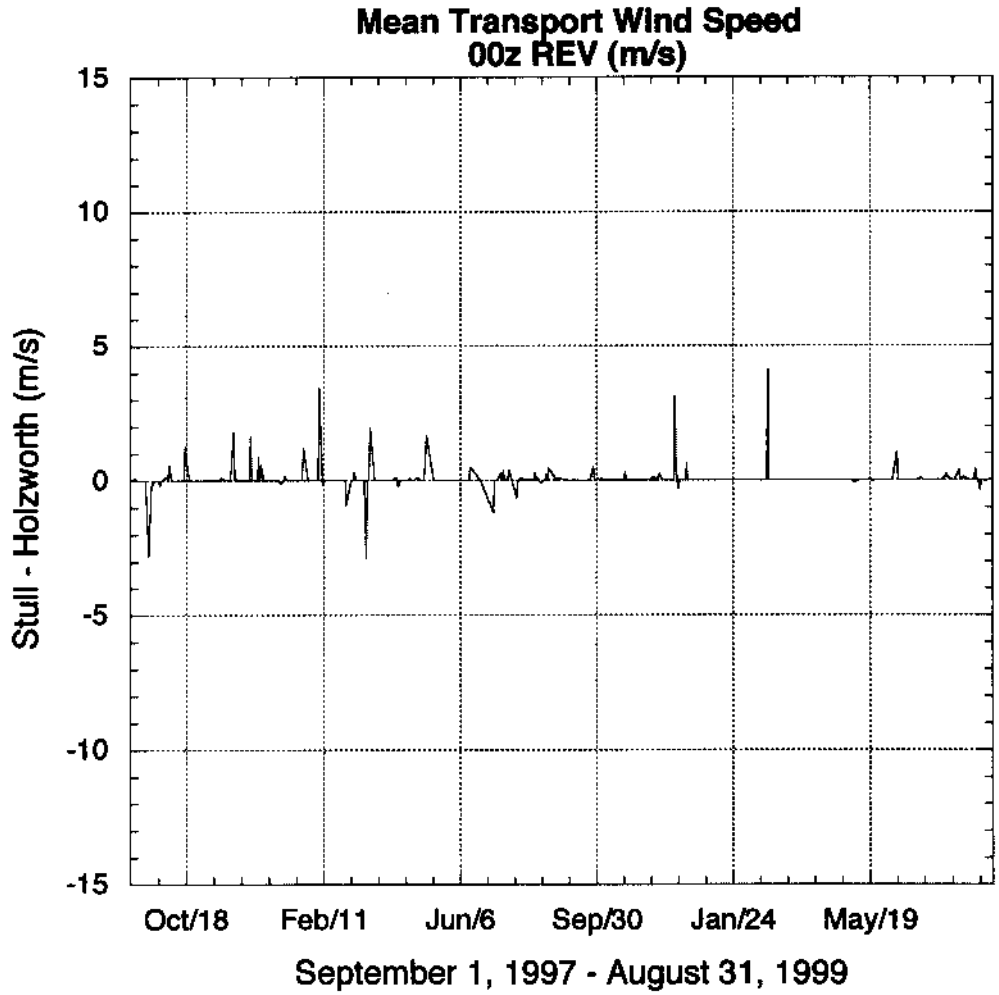

Figure 4-8 00 UTC time series plot of mean transport wind speed (ms^{-1}) for Reno, NV (REV) where speed values plotted are when significant mixing height differences have occurred.

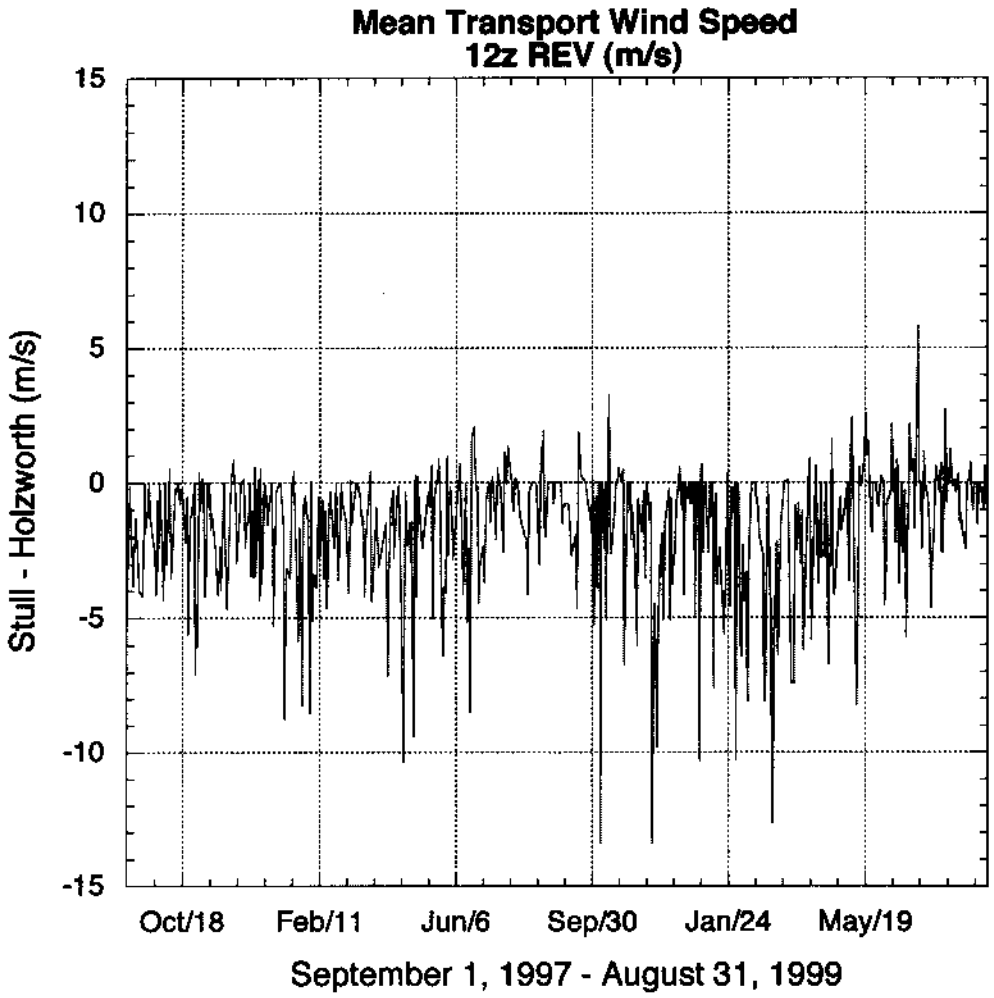

Figure 4-9 Same as 4-8 only for 12 UTC. There are also a greater number of values plotted here than at 00 UTC because there were more occurrences of significant mixing height difference at 12 UTC.

Comparison of Eta output to sounding data

Results of corrections applied to the Eta output

As discussed in Chapter 3, the corrections applied to the 2 m θ and θ_v were necessary to provide for a more accurate estimate of initial surface conditions because the mixing height methods examined in this study are greatly dependent on surface parcel temperature. Figure 4-10 is an example of the 2 m correction applied to θ (00 and 12 UTC) for the month of August. For 00 UTC (top two plots), it can be seen that the correction improved 2 m θ values by reducing the variance about the 45-degree diagonal line. Initially, the Eta indicated a slightly larger variance and an over prediction of θ. An improvement in 2 m θ was also achieved as a result of the correction at 12 UTC (bottom two plots, Figure 4-10). The original Eta values showed a drastic under prediction of the 2 m θ. After the correction was applied, a more uniform scatter occurred around the 45-degree line, thus removing much of the initial Eta bias. Monthly mean corrections of θ for the fifteen stations used are shown in the Appendix for both 00 UTC (Table A) and 12 UTC (Table B).

Figure 4-11 is an August example of how the corrections applied to the 2 m θ affected the mixing height values generated using the Holzworth method. For both 00 (top two plots) and 12 UTC (bottom two plots), the corrections applied to θ did not necessarily improve the mixing height values. At 00 UTC, original values were uniformly scattered about the 45-degree line. Once the correction was applied, the height values became slightly under predicted. At 12 UTC, original Eta values show a clear under prediction of the height, whereas the correction led to Eta over predicting the majority of the height values.

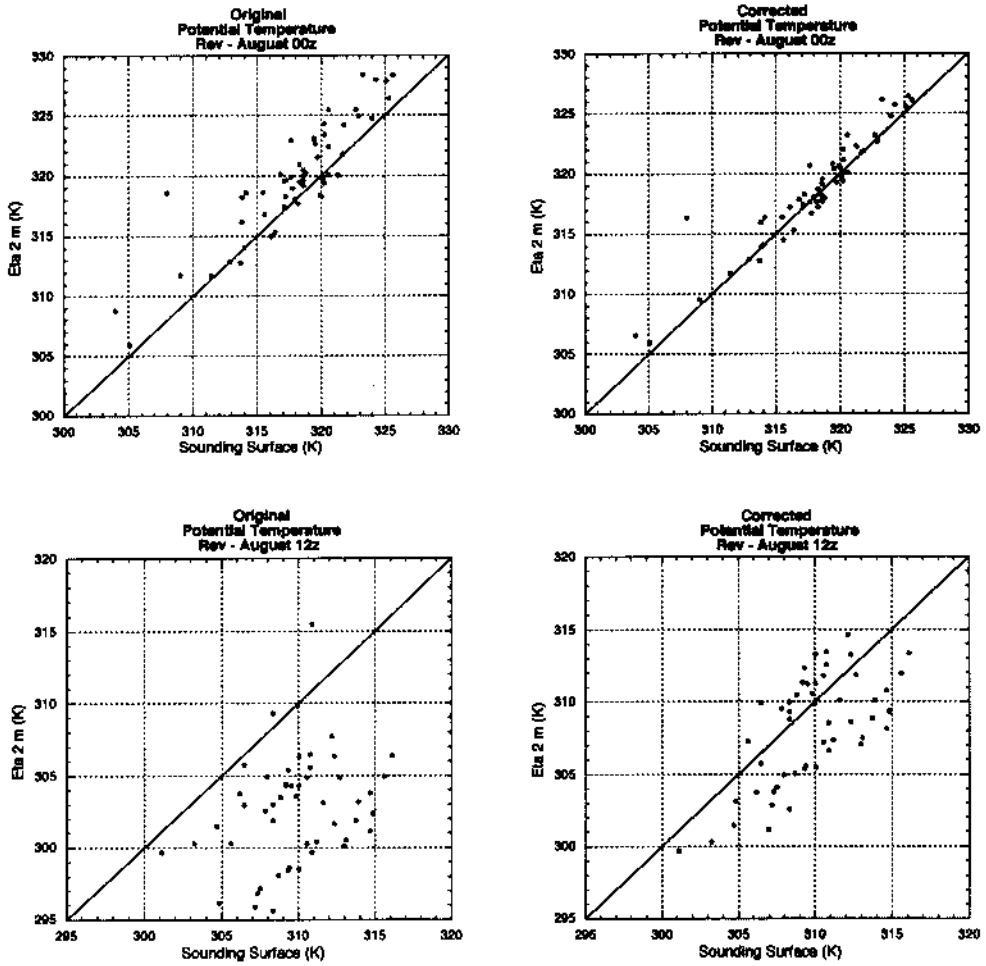

Figure 4-10 Scatter plots of 2 m Eta versus sounding surface using original and corrected values of θ for August 1998-99 at 00 UTC (top) and 12 (bottom) UTC. θ is computed and corrected for using T + 5°C at 12 UTC.

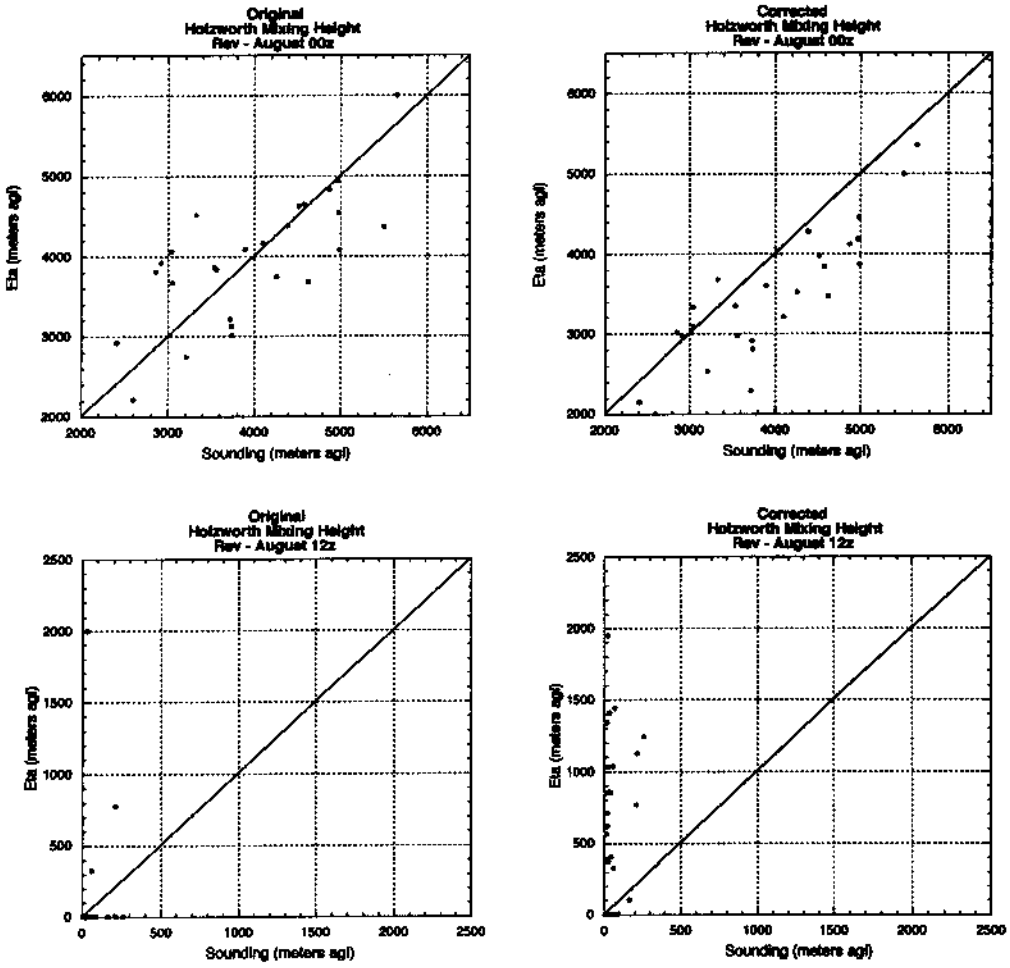

Figure 4-11 Scatter plots of the original and corrected values of mixing height for August 1998-99 at both 00 (top) and 12 (bottom) UTC computed from the Holzworth method.

Similar results were found when correcting the θ_v. Figure 4-12 is an example of the 2 m correction applied to θ_v (00 and 12 UTC) for the month of August. For 00 UTC (top two plots), it can be seen that the correction improved θ_v values by reducing the variance around the 45-degree diagonal line, whereas initially the Eta values had a larger variance and were a slight over prediction in θ_v. At 12 UTC (bottom two plots, Figure 4-12), the original Eta showed a large under prediction of the 2 m θ_v. The correction produced a more uniform scatter about the 45-degree line, thus removing some of the initial Eta bias. Monthly mean corrections of θ_v for the fifteen stations used are shown in the Appendix for both 00 UTC (Table A) and 12 UTC (Table B).

Slightly different results were obtained in the corrections applied to the mixing height values generated using the Stull method than those computed from the Holzworth method. Figure 4-13 is an example of how the corrections applied to the 2 m θ_v affected the mixing height values in August generated using Stull technique. For both 00 (top two plots) and 12 UTC (bottom two plots), the corrections applied to the 2 m θ_v did not necessarily improve the mixing height values from the Eta, but the results were somewhat better than those seen in the correction of the Holzworth mixing height values. At 00 UTC, the initial scatter about the 45-degree diagonal indicated slight over prediction by the Eta, whereas the correction showed overall reduced variance though height values were slightly under predicted. At 12 UTC, the correction shows the Eta under predicting the majority of the height values, whereas the correction still shows a large under prediction with some of values now being over predicted.

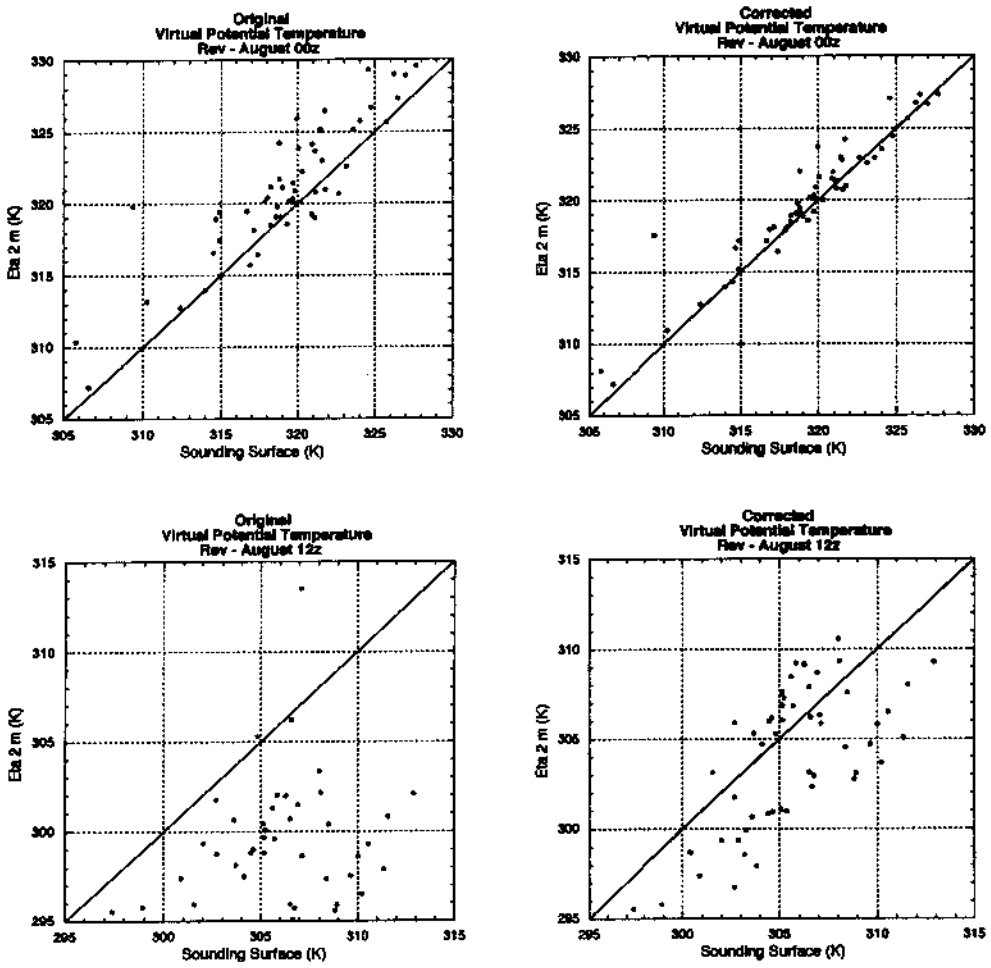

Figure 4-12 Scatter plots of 2 m Eta versus sounding surface using original and corrected values of θ_v for August 1998-99 at 00 UTC (top) and 12 (bottom) UTC.

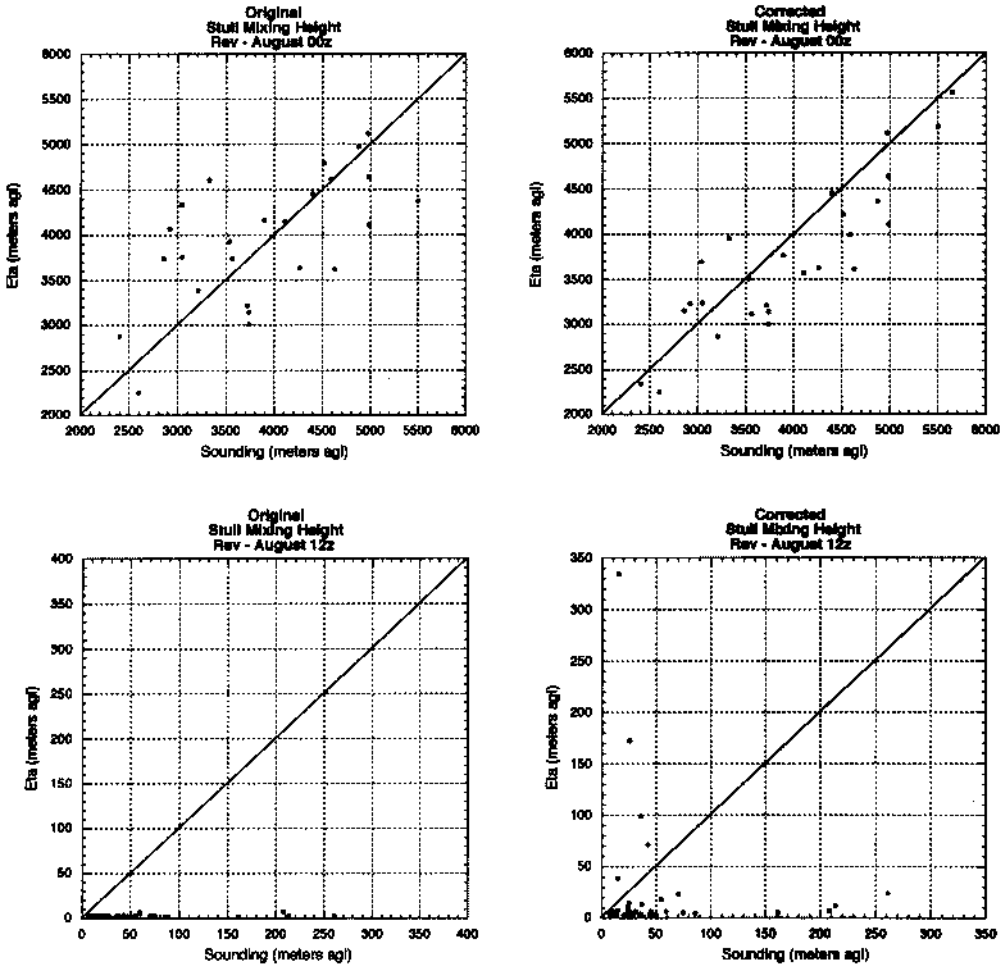

Figure 4-13 Scatter plots of the original and corrected values of mixing height for August 1998-99 at both 00 (top) and 12 (bottom) UTC computed from the Stull method.

From Figures 4-10 through 4-13, it is evident that the corrections applied to θ and θ_v did not always cause the Eta mixing height values to become closer to that of the sounding height values, especially at 12 UTC. This is because the Eta's structural profile, not just the 2 m, can show differences when compared to the sounding. This tends to be most prominent in the lower levels (Tables 4-3a and 4-3b) as the Eta's ground surface is typically several meters above the true terrain.

Mixing height comparison (Eta versus sounding)

Mixing heights generated from the Eta were compared to those computed from the sounding for both 00 and 12 UTC using the Stull method. Height differences (Eta minus sounding) at 00 UTC (Figures 4-14a through 4-14e) are more pronounced at inland locations, whereas coastal site height differences are more consistently close to zero. This pattern was also described earlier when examining mixing height differences between the Stull and Holzworth methods. Another interesting generalization is that mixing heights tend to be larger when sounding data is used for estimation at all stations, except coastal locations. However, this tendency seems to change from spring to summer and then again from summer to fall. This overall pattern may be related to the Eta biases. Perhaps there is a seasonal transition of how closely related the Eta structure is to the sounding structure going from the cool season to the warm season and vice versa. For example, during the cool season the Eta predicts a θ_v profile that is generally cooler than the sounding, and during the warm season the Eta predicts a θ_v profile that is generally warmer than the sounding. This pattern is clearly noticeable when comparing monthly mean sounding and Eta θ_v surface values at inland locations where coastal site values are

consistently close with no seasonal transition. A monthly mean time series plot of sounding surface and Eta 2 m θ_v for Albuquerque (ABQ; Figure 4-15a) shows how the Eta 2m θ_v compares to the sounding when the warm to cool season transition clearly occurs. A similar plot of monthly mean plot of sounding surface and Eta 2 m θ_v at Quillayute (UIL; Figure 4-15b) does not show the same indication of a warm to cool season transition.

Table 4-3a Mean vertical structure at standard pressure levels for April 1998-99 at 00 UTC for Reno, NV.

Level (mb)	**Sounding Height amsl (m)**	**Eta Height amsl (m)**	**Sounding θ_v (K)**	**Eta θ_v (K)**	**θ_v Differences Eta - Sounding (K)**
850	1545.67	1547.19	304.32	301.25	-3.08
750	2524.00	2523.75	298.16	297.92	-0.24
700	3046.39	3045.65	297.06	297.24	0.17
650	3506.50	3512.11	288.07	288.70	0.64
500	5593.46	5595.78	305.65	305.80	0.15
400	7209.62	7215.20	311.59	312.06	0.47
300	9172.50	9180.17	321.58	322.13	0.55
250	10372.14	10381.50	329.32	329.81	0.50
200	11802.22	11816.36	343.00	343.71	0.71

Table 4-3b Same as Table 4-3a listing 12 UTC.

Level (mb)	**Sounding Height amsl (m)**	**Eta Height amsl (m)**	**Sounding θ_v (K)**	**Eta θ_v (K)**	**θ_v Differences Eta – Sounding (K)**
850	1551.33	1547.41	296.43	296.49	0.06
750	2488.11	2487.93	294.53	294.61	0.09
700	3034.00	3032.17	296.44	296.73	0.30
650	3609.67	3610.27	298.01	298.19	0.18
500	5590.00	5591.77	306.18	306.39	0.21
400	7182.07	7185.40	311.58	311.71	0.12
300	9169.66	9175.61	322.09	322.03	-0.06
250	10357.10	10363.02	328.43	329.09	0.67
200	11794.07	11802.74	343.71	344.55	0.84

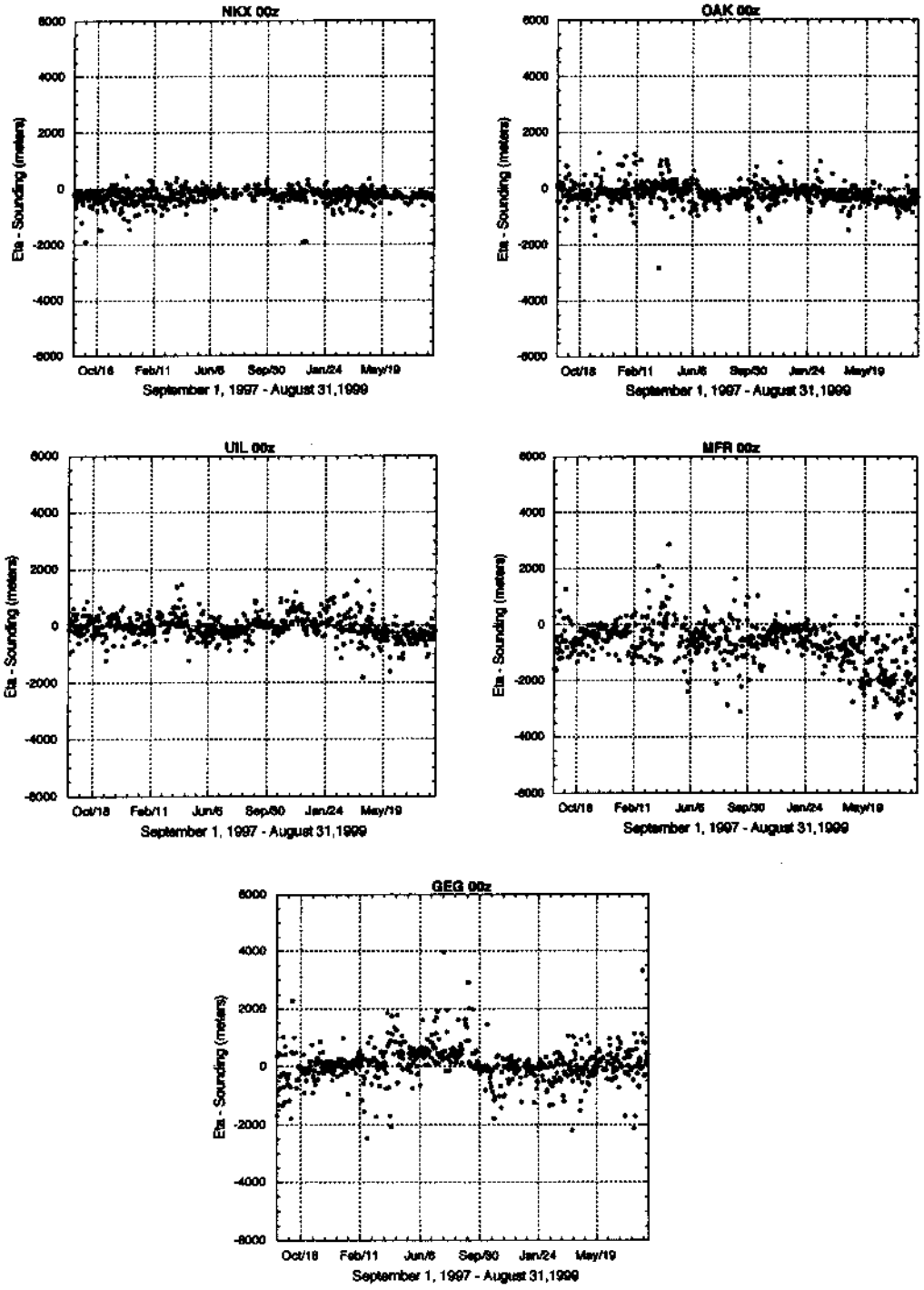

Figure 4-14a 00 UTC time series plots of mixing height differences (Eta - Sounding) for Miramar, CA (NKX), Oakland, CA (OAK), and Quillayute, WA (UIL), Medford, OR (MFR), and Spokane, WA (GEG).

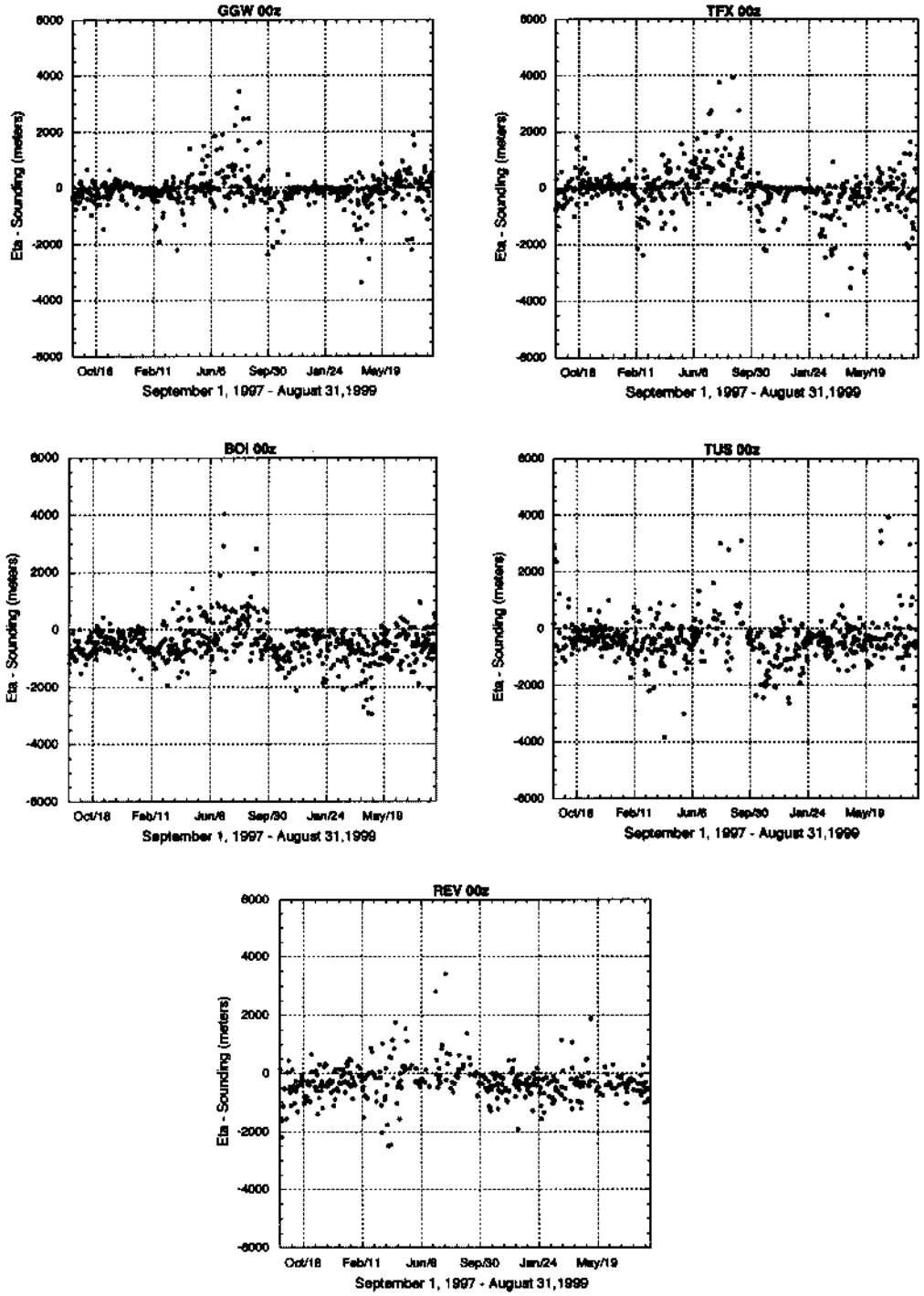

Figure 4-14b Same as 4-14a illustrating Glasgow, MT (GGW), Great Falls, MT (TFX), Boise ID (BOI), Tucson, AZ (TUS), and Reno, NV (REV).

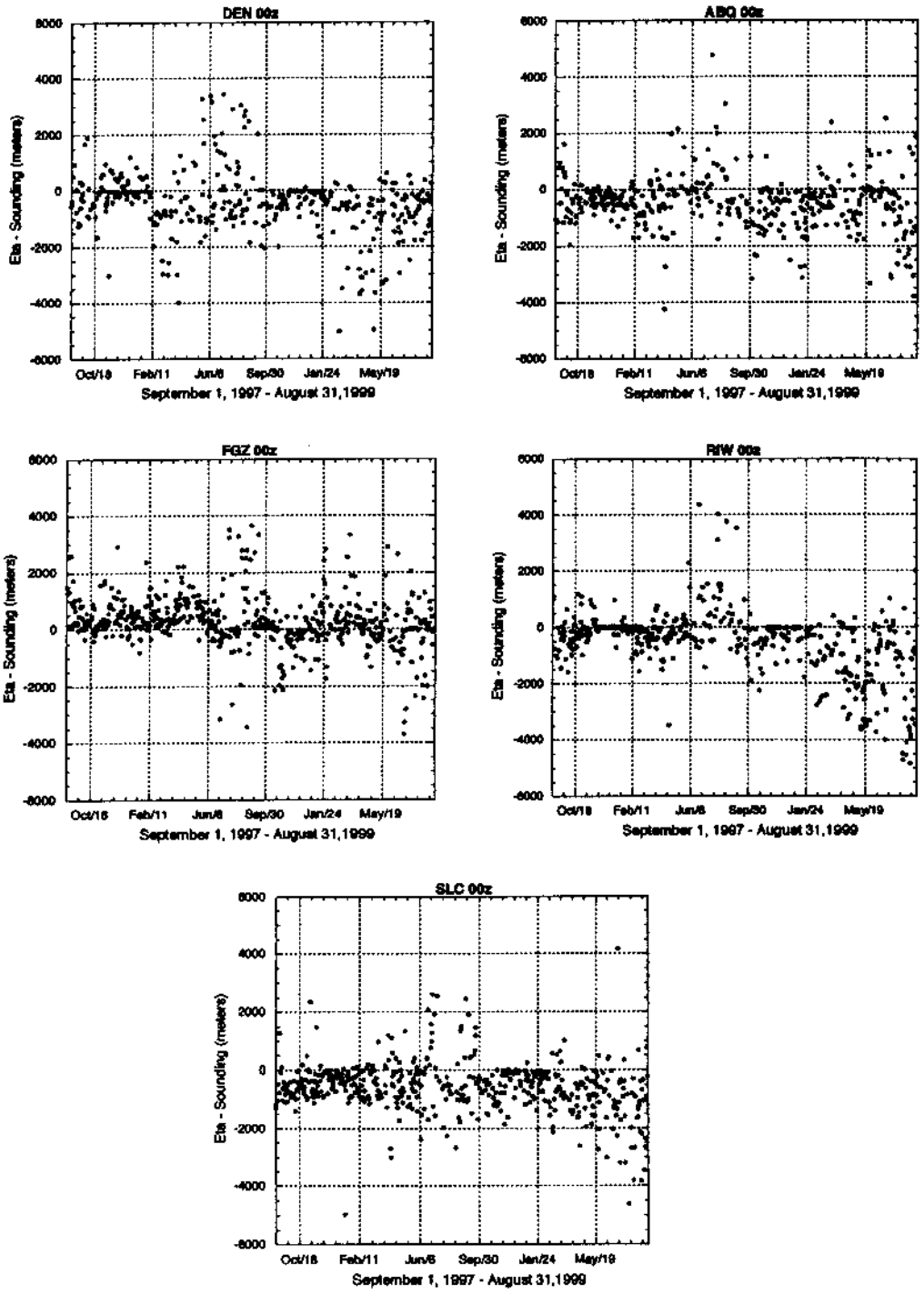

Figure 4-14c Same as 4-14a illustrating Denver, CO (DEN), Albuquerque, NM (ABQ), Flagstaff, AZ (FGZ), Riverton, WY (RIW), and Salt Lake City (SLC).

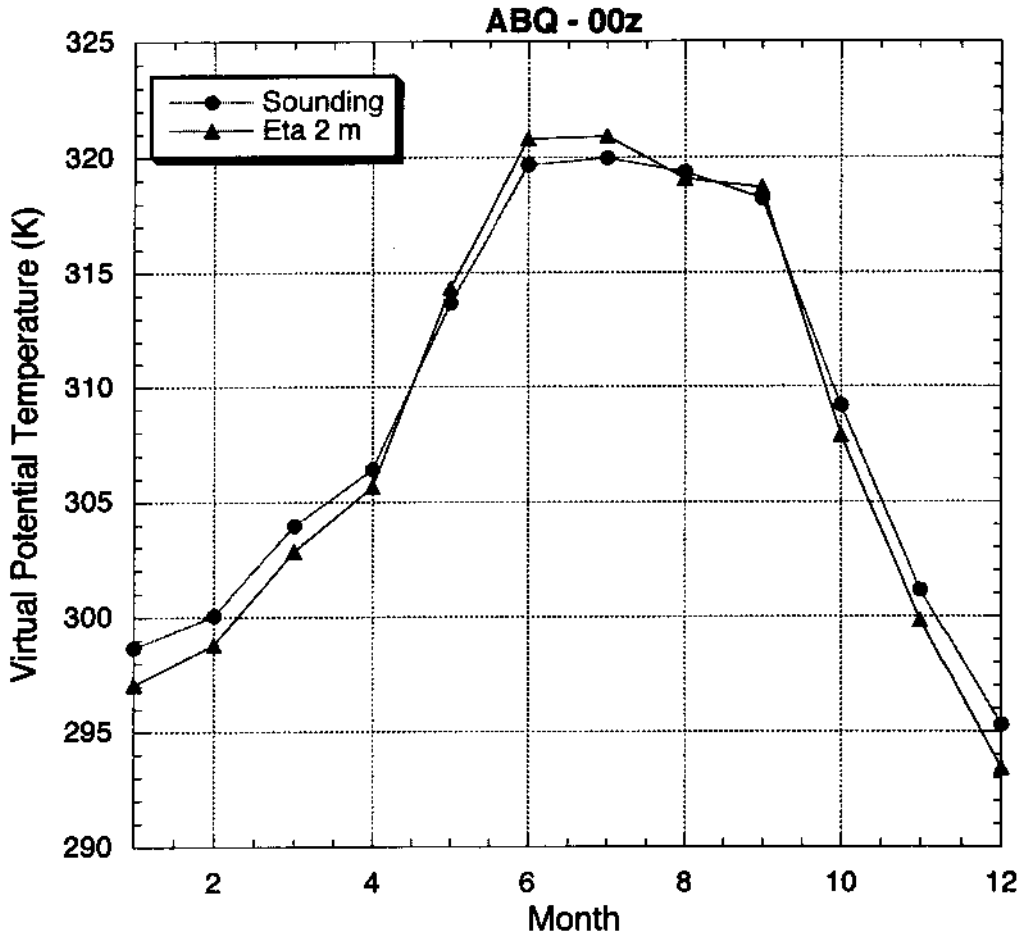

Figure 4-15a A 00 UTC monthly mean time series plot of sounding surface and Eta 2 m θ_v for Albuquerque, NM (ABQ). This shows the cool to warm seasonal transition of the Eta 2m. The first occurrence is April followed by a second transition in August.

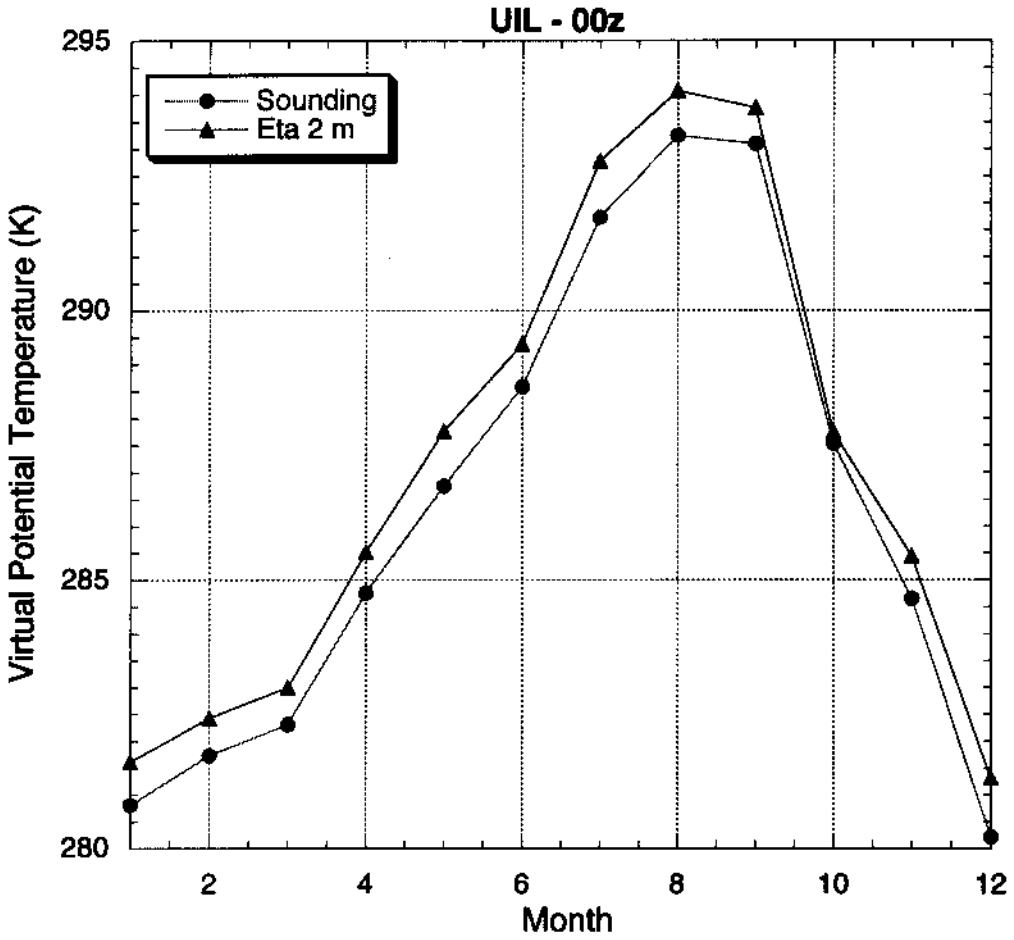

Figure 4-15b A 00 UTC monthly mean time series plot of sounding surface and Eta 2 m θ_v for Quillayute, WA (UIL). This does not indicate a seasonal transition in the Eta 2m.

Height differences (Eta minus sounding) at 12 UTC (Figures 4-16a through 4-16e) are more pronounced at coastal locations, whereas inland site height differences are more consistently close to zero. This is opposite to the 00 UTC general pattern. However, similar to the 00 UTC, the seasonal transition that seems to reflect the Eta biases is seen. In this case though, the tendency is noticeable for coastal locations, whereas at inland locations the transition may not occur. The seasonal change at 12 UTC also occurs from spring to summer and then again from summer to fall. A monthly mean time series plot of sounding surface and Eta 2 m θ_v for Miramar (NKX; Figure 4-17a) shows how the Eta 2m θ_v compares to the sounding when the warm to cool season transition for coastal locations is clearly indicated. A similar monthly mean plot of sounding surface and Eta 2 m θ_v for Flagstaff (FGZ; Figure 4-17b) shows no indication of a warm to cool season transition for an inland location.

Mixing height differences, for both 00 and 12 UTC, seem to also correspond to how well the Eta predicts the vertical structure of θ_v. Surface differences between the sounding and Eta is important, but the quality of the entire profile generated from the Eta is also a major contributor. Figure 4-18a shows profile examples of mixing height estimation for both the Eta and sounding for 00 UTC. The top two plots indicate how well the sounding (left) and Eta (right) θ_v profiles can compare as their structure is almost identical within the first 5000 meters, and the mixing height values are within one meter. On the other hand, the bottom two plots indicate a poor comparison of the sounding and Eta θ_v profiles as the structure is different between 400 and 2500 meters. However, it is

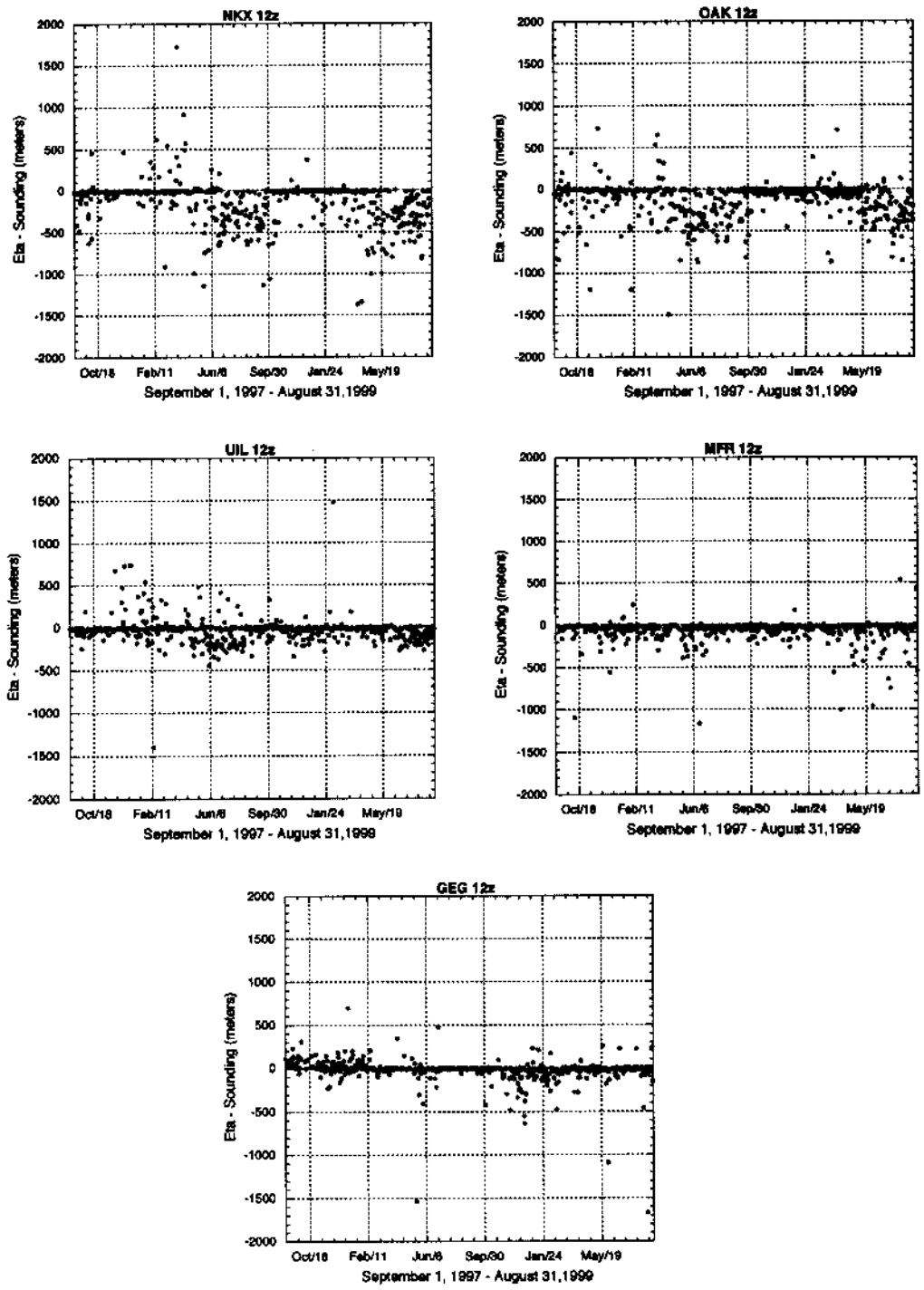

Figure 4-16a 12 UTC time series plots of mixing height differences (Eta - Sounding) for Miramar, CA (NKX), Oakland, CA (OAK), and Quillayute, WA (UIL), Medford, OR (MFR), and Spokane, WA (GEG).

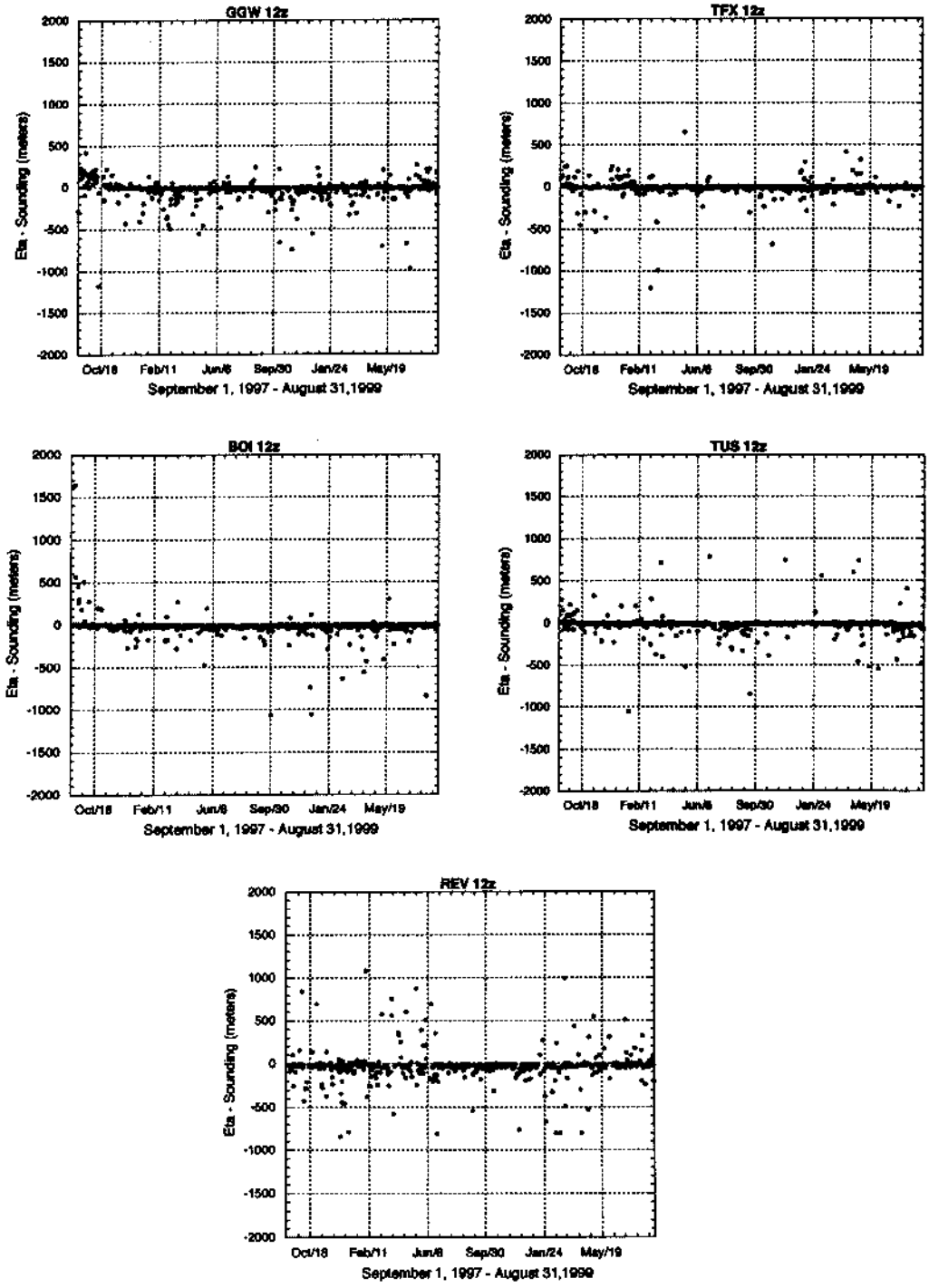

Figure 4-16b Same as 4-16a illustrating Glasgow, MT (GGW), Great Falls, MT (TFX), Boise ID (BOI), Tucson, AZ (TUS), and Reno, NV (REV).

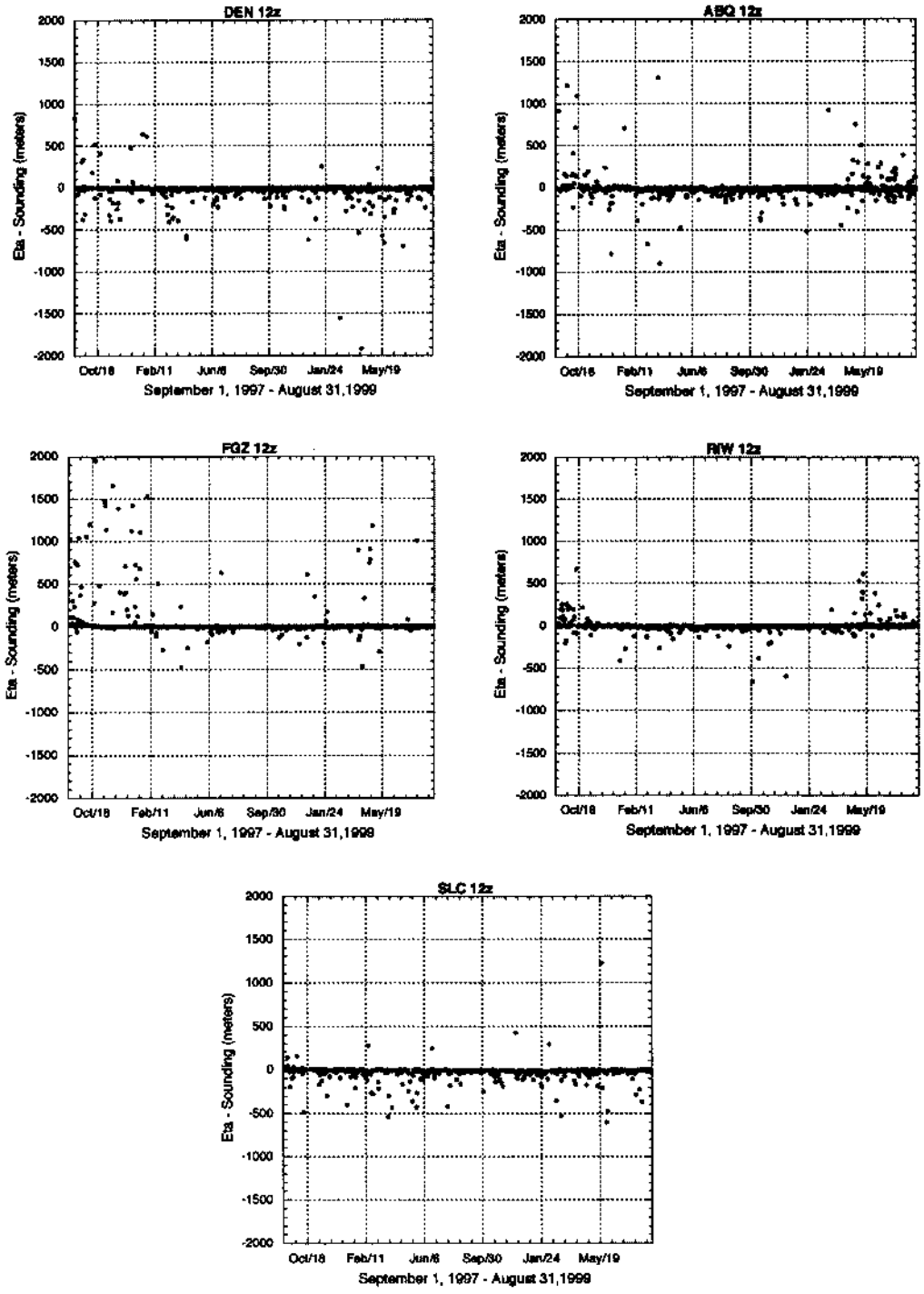

Figure 4-16c Same as 4-16a illustrating Denver, CO (DEN), Albuquerque, NM (ABQ), Flagstaff, AZ (FGZ), Riverton, WY (RIW), and Salt Lake City (SLC).

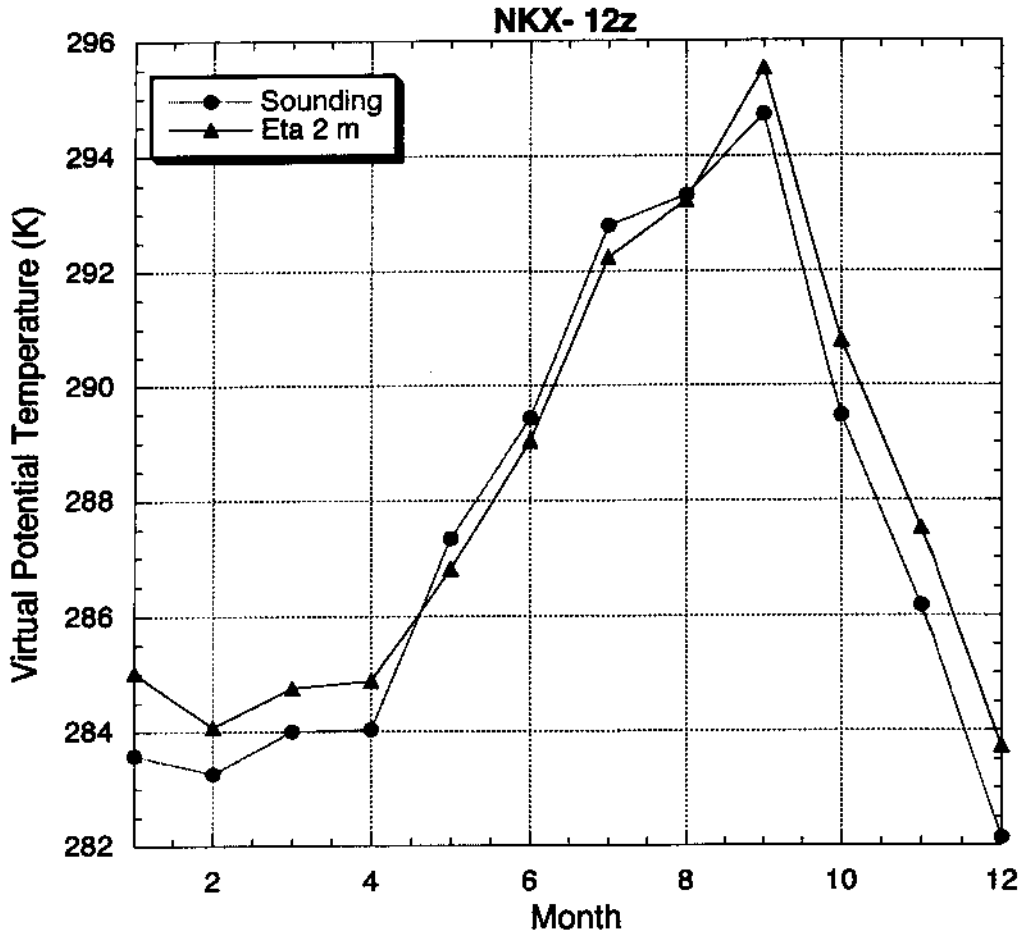

Figure 4-17a A 12 UTC monthly mean time series plot of sounding surface and Eta 2 m θ_v for Miramar, CA (NKX). This shows the warm to cool seasonal transition of the Eta 2m. The first occurrence is April followed by a second transition in August.

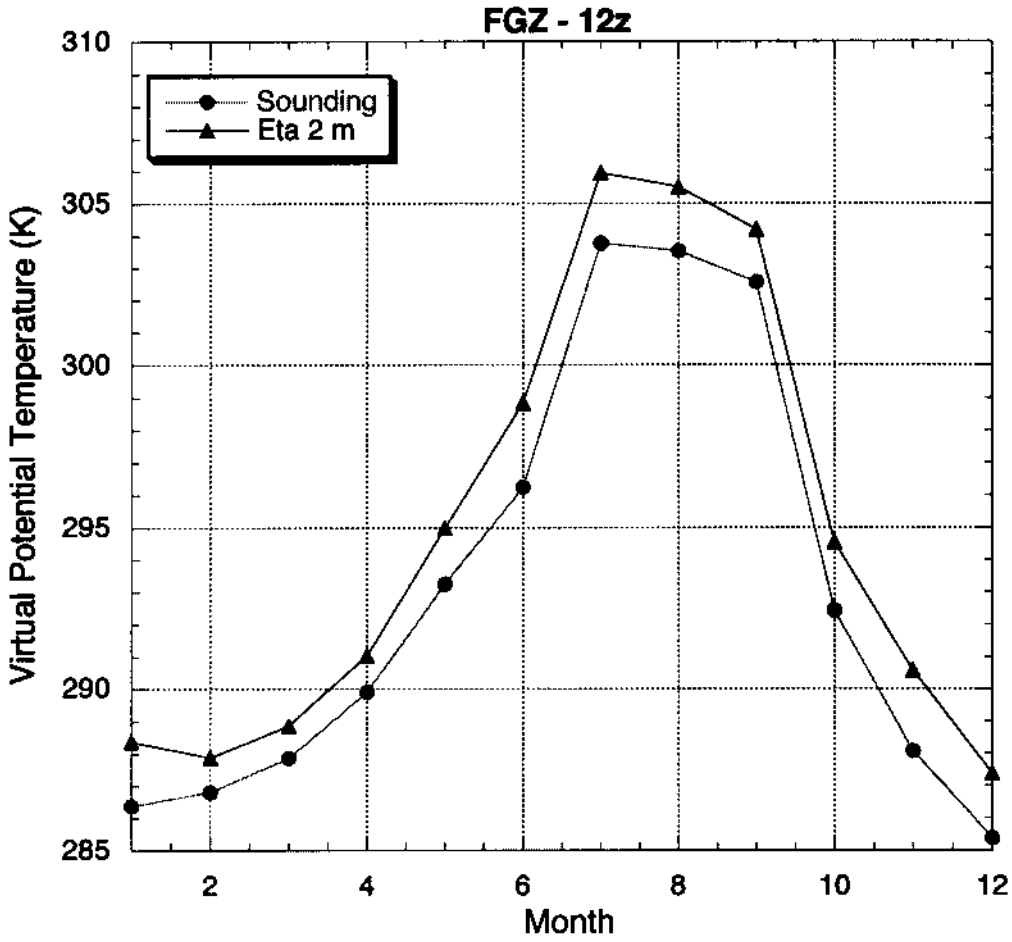

Figure 4-17b A 12 UTC monthly mean time series plot of sounding surface and Eta 2 m θ_v for Flagstaff, AZ (FGZ). This does not indicate a seasonal transition in the Eta 2m.

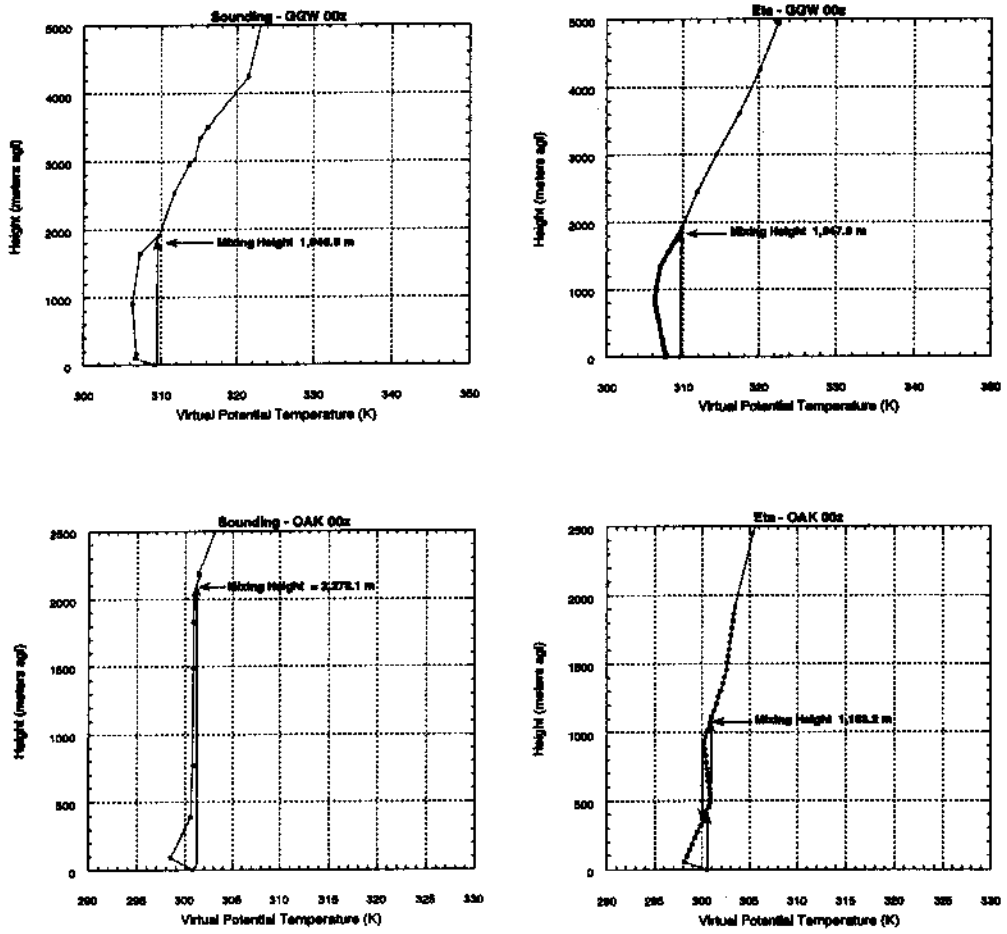

Figure 4-18a The top two θ_v profiles are 00 UTC examples of how the Eta's vertical structure can be similar to that of the sounding and similar mixing height values can be computed. The bottom two θ_v profiles are 00 UTC examples of how Eta's vertical structure can be different than that of the sounding and mixing height values determined can be quite different. Mixing height values are determined using the Stull method where parcel ascent is performed using relative maxima and minima.

interesting to note the higher vertical resolution of the Eta between 400 and ~750 meters. The Eta and sounding have similar values of θ_v at 400 and 750 meters, but in between, the Eta has several additional levels that the sounding does not have. Here, the Eta is indicating a structural feature in the θ_v profile that the sounding is missing due to its coarse resolution.

Figure 4-18b is a similar example of comparing sounding and Eta θ_v profiles. In this case though (top two plots), a similar mixing height value can be determined, as low level structure of θ_v is quite close between the sounding and the Eta. However, from 300 meters up to 2500 meters, the sounding and Eta θ_v profiles change considerably. The bottom two plots in Figure 4-18b illustrate another example of when different mixing height values can be determined. Here again, where sounding and Eta have similar levels, θ_v values are quite close. But elsewhere, where the Eta has several levels that the sounding does not, the Eta appears to be resolving a structural feature in the θ_v profile due to its finer vertical resolution.

This discussion highlights the different features between the Eta output and the sounding data. Surface values of θ_v and θ show considerable differences between the sounding and Eta that contributes to how well mixing height values correspond. As discussed earlier, this is most likely related to the lack of data used in model assimilation to correct surface first guess values.

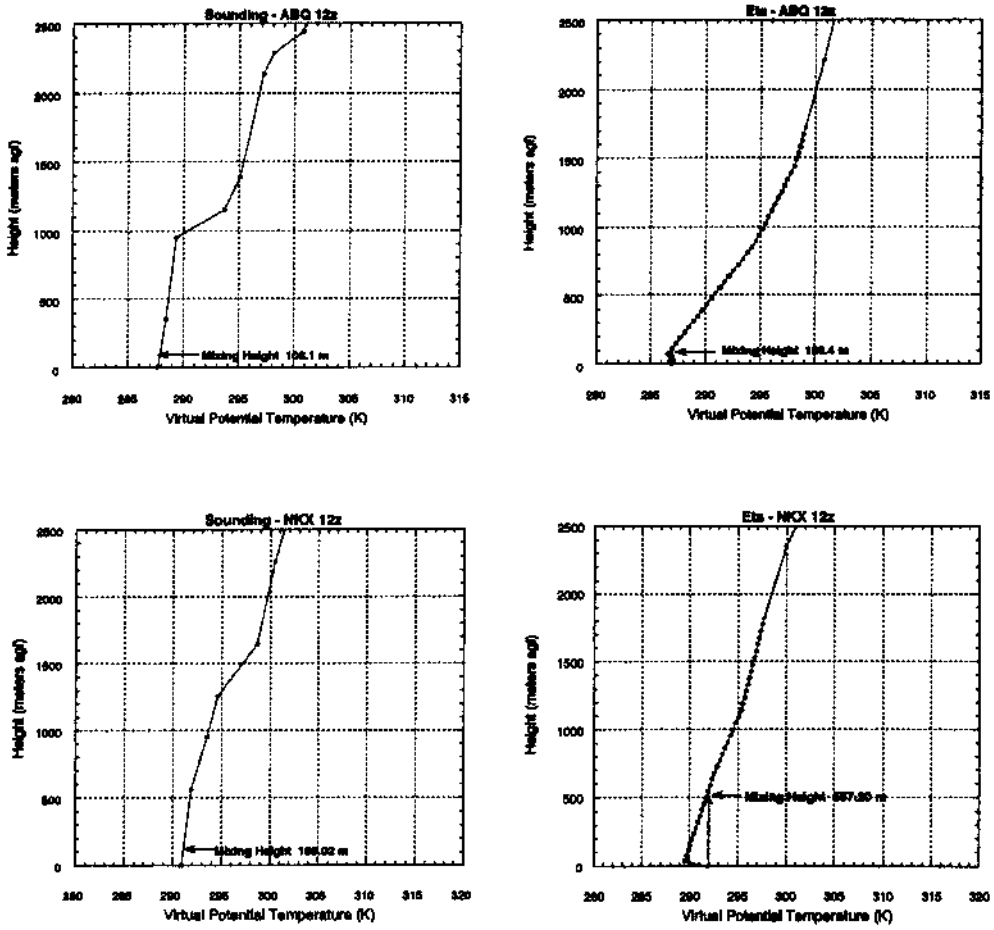

Figure 4-18b Same as 4-18a illustrating 12 UTC.

Another important reason as to why mixing height values differ between sounding and Eta estimates is related to the how well the vertical profile structures match. As described above, sometimes the Eta output can show a considerable difference in profile structure when compared to the sounding. However, at other times the Eta profile appears to be different because it has a finer vertical resolution, even though in reality it is quite similar to the sounding at similar altitude levels.

The results shown, based on Eta and sounding differences, explain why mixing height values computed from the Stull method for each data set may also be different. When profile structure is similar between the sounding and the Eta, mixing height values are very close. However when θ_v profiles are different, mixing height values are only different due to coarse sounding resolution or the Eta misrepresenting the θ_v structure, not because of methodology.

Spatial analysis of mixing height computed from the Eta

Monthly mean mixing height values were computed over the western U.S. for both 00 and 12 UTC in order to illustrate the spatial coverage that can be provided from the NCEP Eta model. Figures 4-19a through 4-19l are spatial plots of mixing height for both 00 and 12 UTC over the West. It should be emphasized that different scales were used for 00 and 12 UTC. This was performed because mixing heights are almost always at 100 meters agl or lower at 12 UTC, and at 00 UTC heights are typically 1000 meters agl or much higher. The advantage of using model output to compute mixing height is that the spatial coverage based on a uniform grid is much more comprehensive than station sounding data.

A general observation from Figures 4-19a through 4-19l is the presence of seasonal variability of mixing height over both land and sea. Over land, higher heights are depicted during the warmer months (i.e., June at 00 UTC; Figure 4-19f) and lower heights during the cooler months (i.e., January at 00 UTC; Figure 4-19a), as mixed layer growth is strongly governed by the amount of surface heating that occurs. Over the ocean, higher mixing heights are observable during the cooler months, especially at 12 UTC (i.e., February at 12 UTC; Figure 4-19b), and lower heights exist during the warmer months (i.e., July at 12 UTC; Figure 4-19g). Even though the Pacific Ocean near the West Coast of the U.S. is quite cold during the cooler months, overlying air can still be much cooler than that of water. The water acts as a heat source to the above air, and thus boundary layer development tends to be more active over the eastern Pacific Ocean during the cooler seasons. This is more noticeable at 12 UTC because the air is much cooler than at 00 UTC even though the ocean is a lagged heat source (water increases and loses heat more slowly than land). Therefore, the ocean surface is still relatively warm compared to the above air (i.e., March at 12 UTC; Figure 4-19c).

Other seasonal patterns that are interesting to note occur over land regions. For example, in April at 00 UTC (i.e., Figure 4-19d), higher mixing height values begin to appear in the desert southwest and then intensify in May and June (i.e., Figures 4-19; e and f). June tends to be the driest time of year in this region and solar heating at the surface is at its peak. However, in July and August (i.e., Figures 4-19; g and h), higher heights occur in the Great Basin region, and mixing height values over the southwest are somewhat suppressed. These patterns seem to be indicative of the onset and occurrence

of the southwest monsoon, as July and August tend to be the wettest time of the year in Arizona and New Mexico.

Another spatial pattern that stands out in Figures 4-19a through 4-19l is the diurnal variability of mixing height. Even though these plots are monthly means, the daytime growth and nighttime suppression of the mixed layer is evident when comparing 00 UTC and 12 UTC (i.e., July; Figure 4-19g and August; Figure 4-19h). July and August are the driest months of the year over the Great Basin. Mixing heights can be as high as 5000 meters agl at 00 UTC and below 100 meters agl at 12 UTC. This pattern also shows up over the desert southwest during the months of May and June (i.e., Figures 4-19; e and f) as it is their driest time of year prior to the onset of the Southwest Monsoon in early July.

Some other interesting features that can be noticed in Figures 4-19a through 4-19l, are elevation changes throughout the western U.S. A first example would be the 00 UTC height changes that outline the California Central Valley and Sierra-Nevada Mountains (i.e., April; Figures 4-19d and May; Figure 4-19e). The Uinta Montains in Utah east of Salt Lake City also stand nicely in May, June, and July at 12 UTC (i.e., Figures 4-19; e, f, and g). This may be a depiction of surrounding areas, that are at a much lower elevation, experiencing morning inversions due to strong radiational cooling whereas the Uinta Range is approximately 3,000 meters or higher, and therefore does not receive such a dramatic diurnal temperature change. Another interesting note is how the 00 UTC mixing heights outline the entire Pacific Coast and the mid-western Plains while highlighting the complex terrain of the interior western U.S. (i.e., August; Figure 4-19h).

The ability to examine these seasonal and diurnal patterns suggests that the Eta model physics used to determine PBL structure is performing sufficiently to produce mixing heights. In this study, only spatial patterns are analyzed. However temporally, this kind of geographically coverage of mixing height can be provided every 6 hours out to 48 hours twice daily.

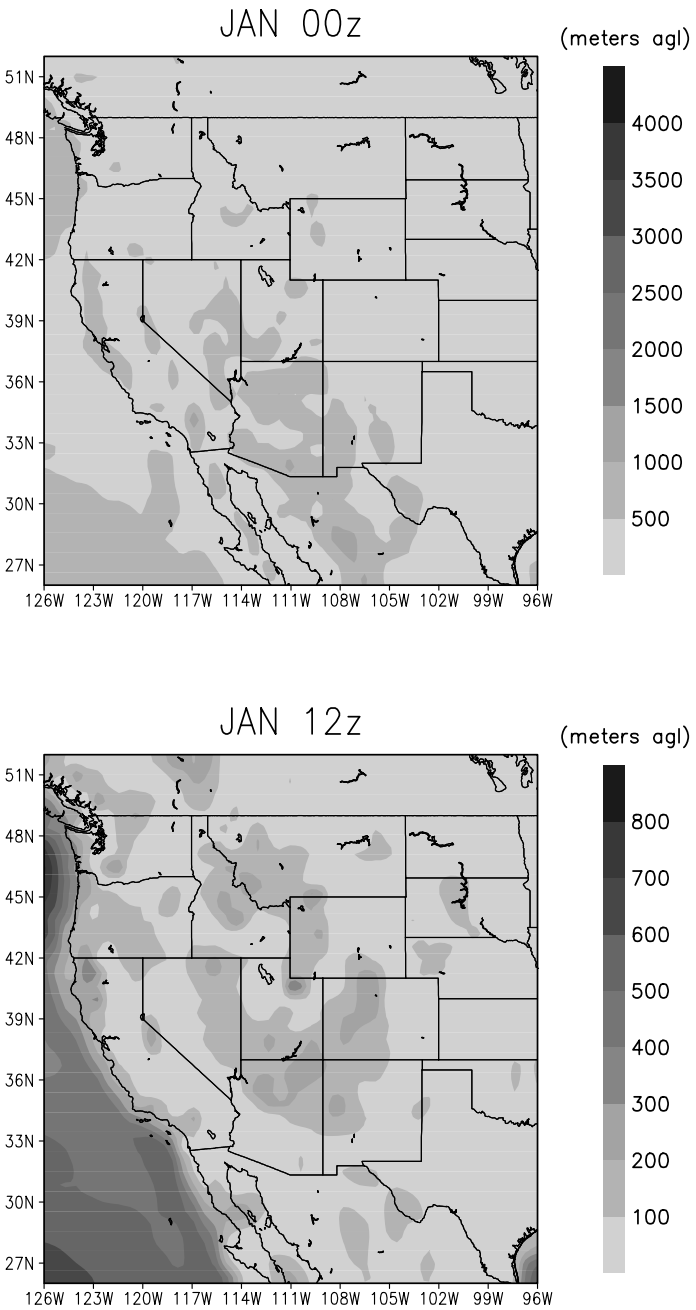

Figure 4-19a Geographical plots of mean monthly mixing height for the month of January for both 00 and 12 UTC indicating the spatial coverage that can be provided by using NCEP Eta model output.

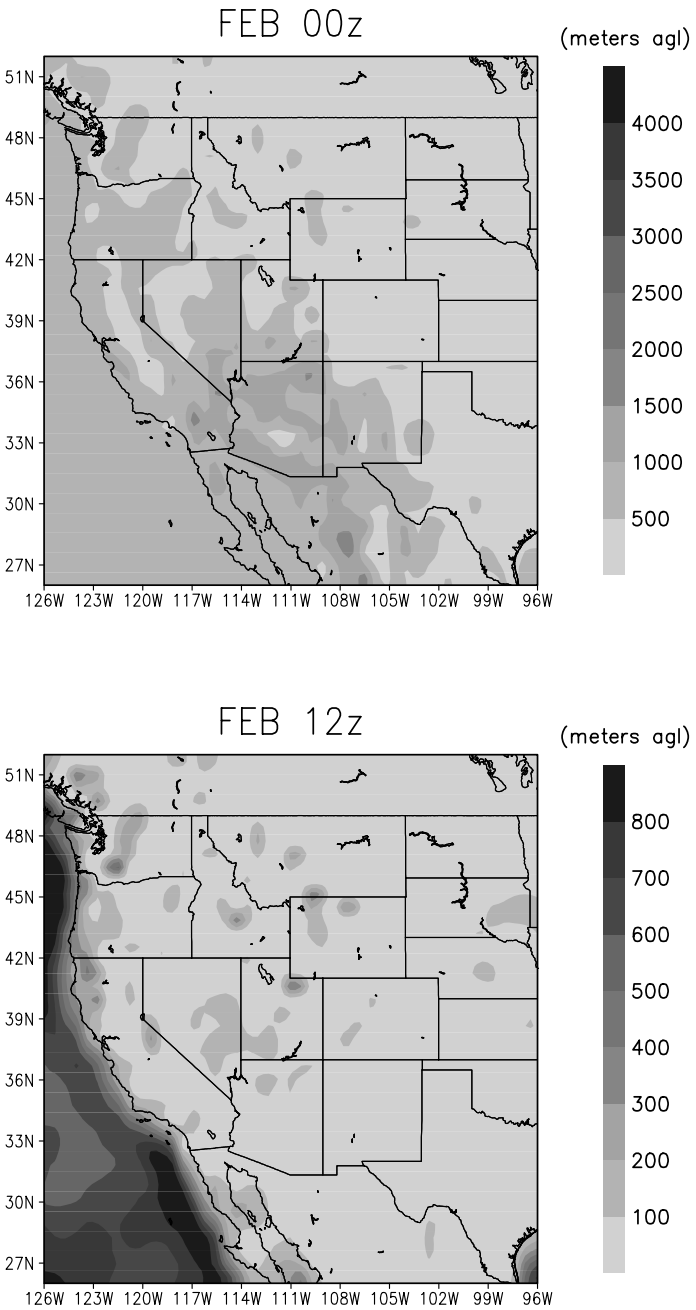

Figure 4-19b Same as 4-19a illustrating February.

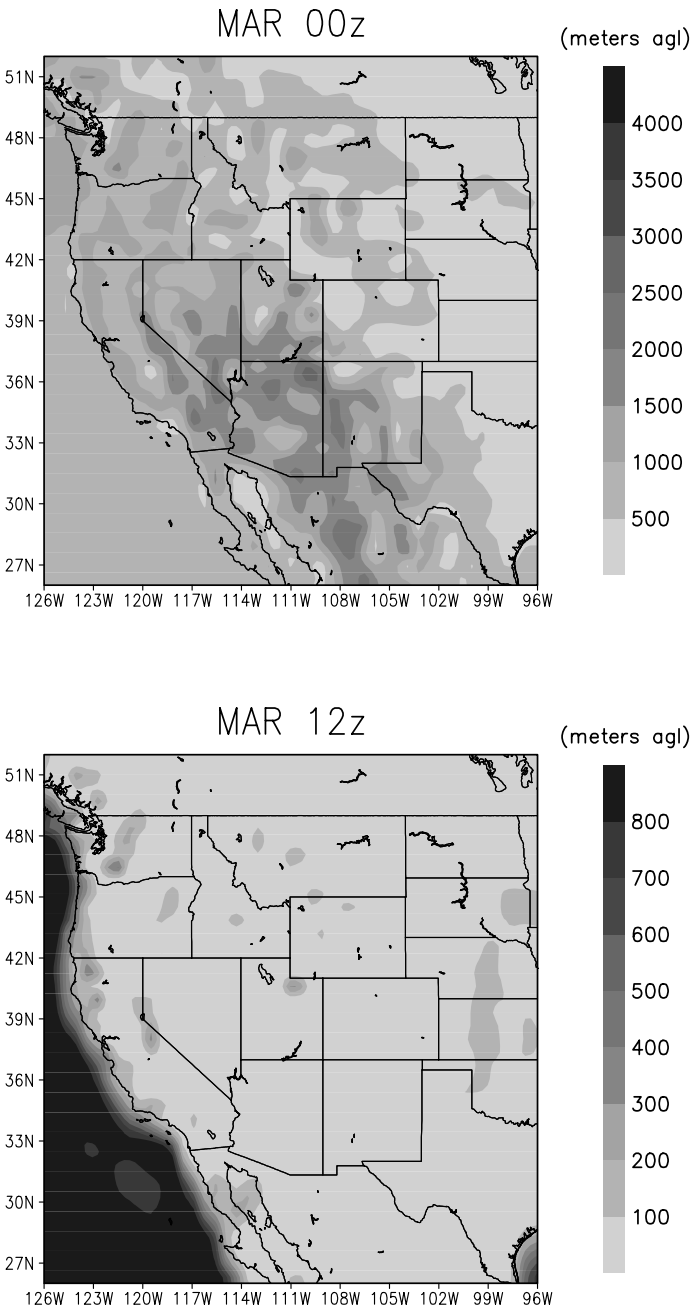

Figure 4-19c Same as 4-19a illustrating March.

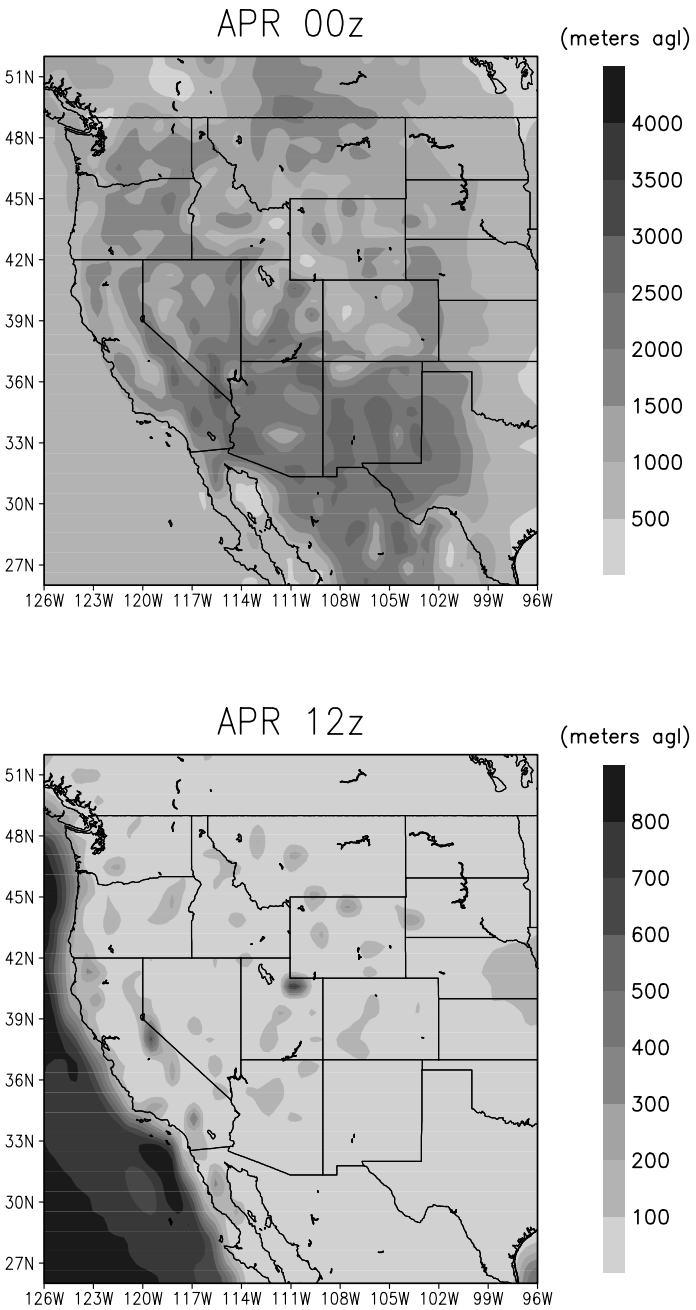

Figure 4-19d Same as 4-19a illustrating April.

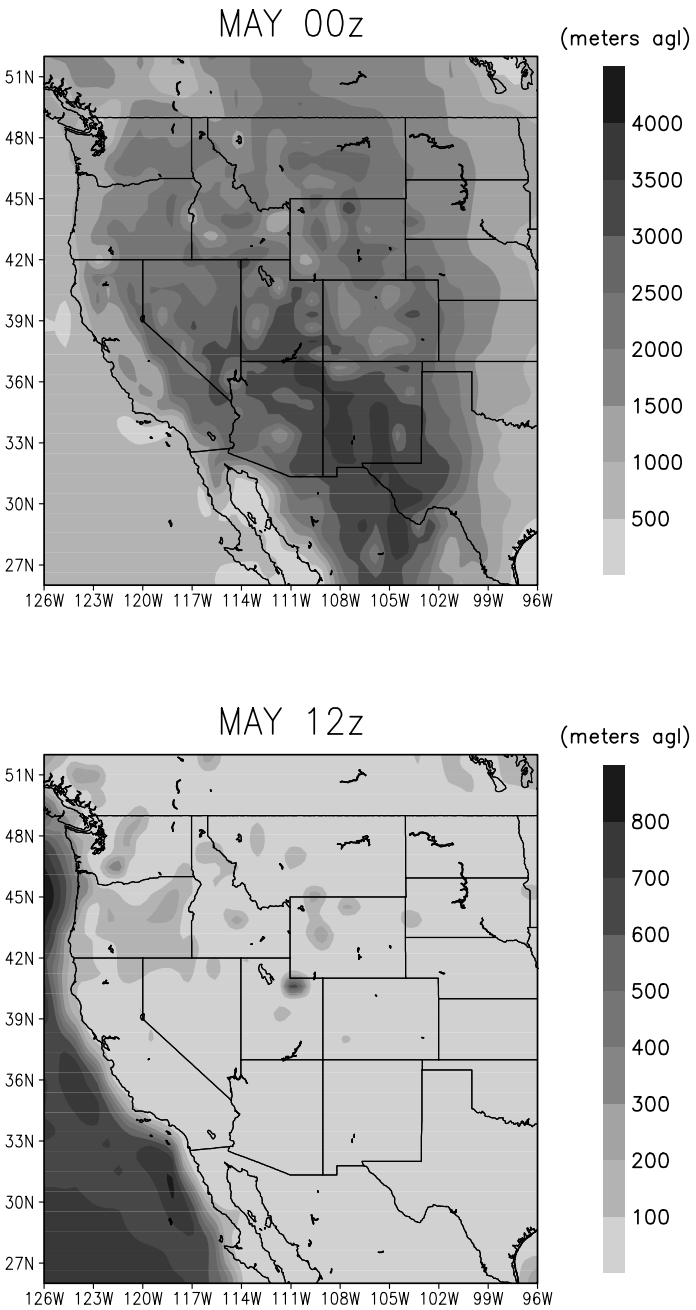

Figure 4-19e Same as 4-19a illustrating May.

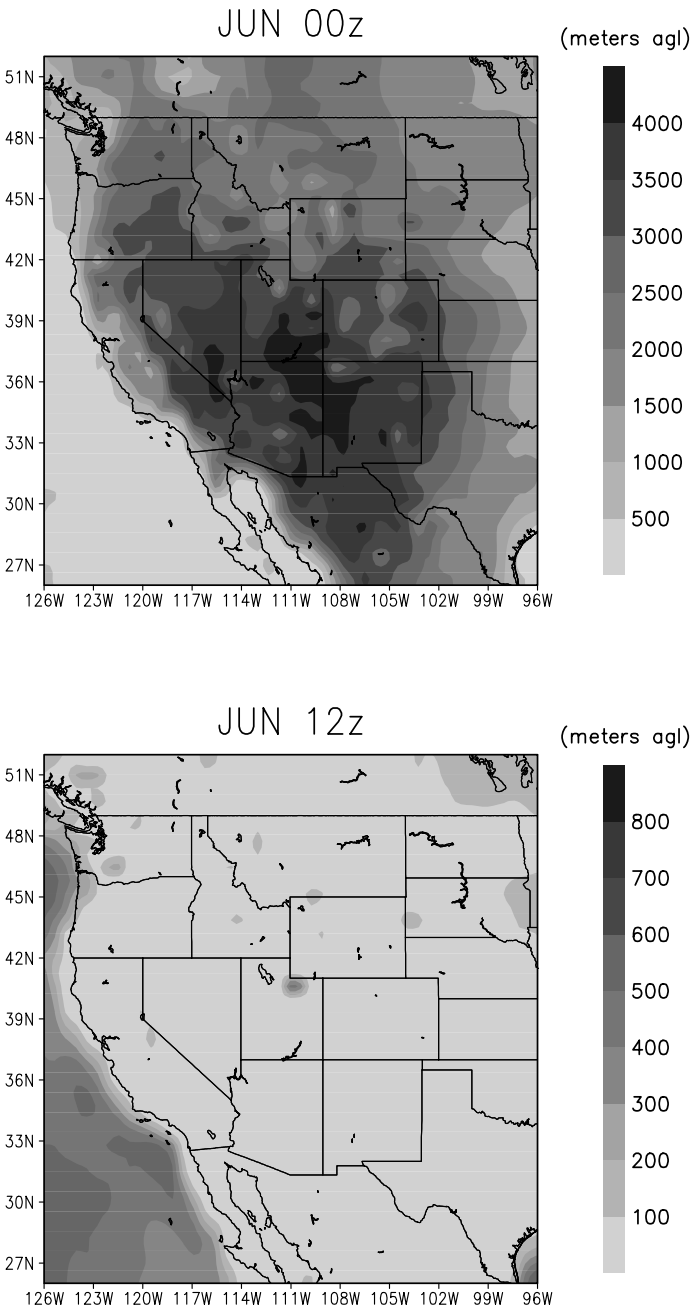

Figure 4-19f Same as 4-19a illustrating June.

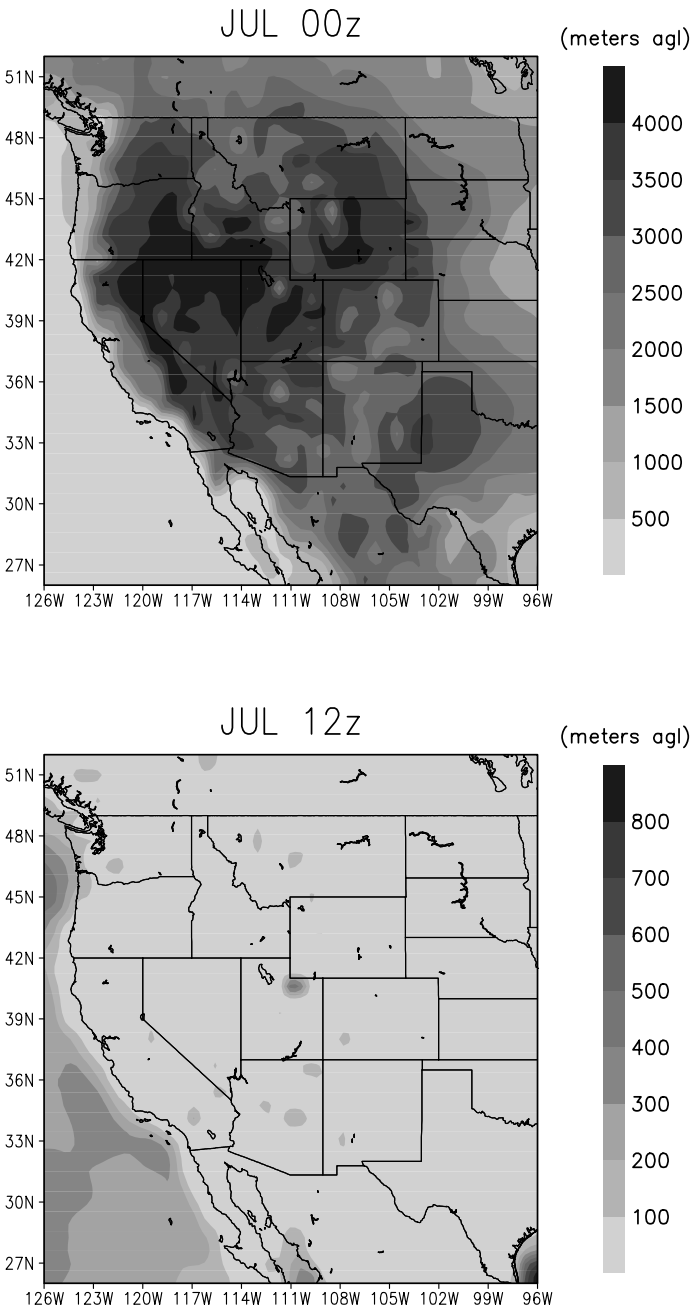

Figure 4-19g Same as 4-19a illustrating July.

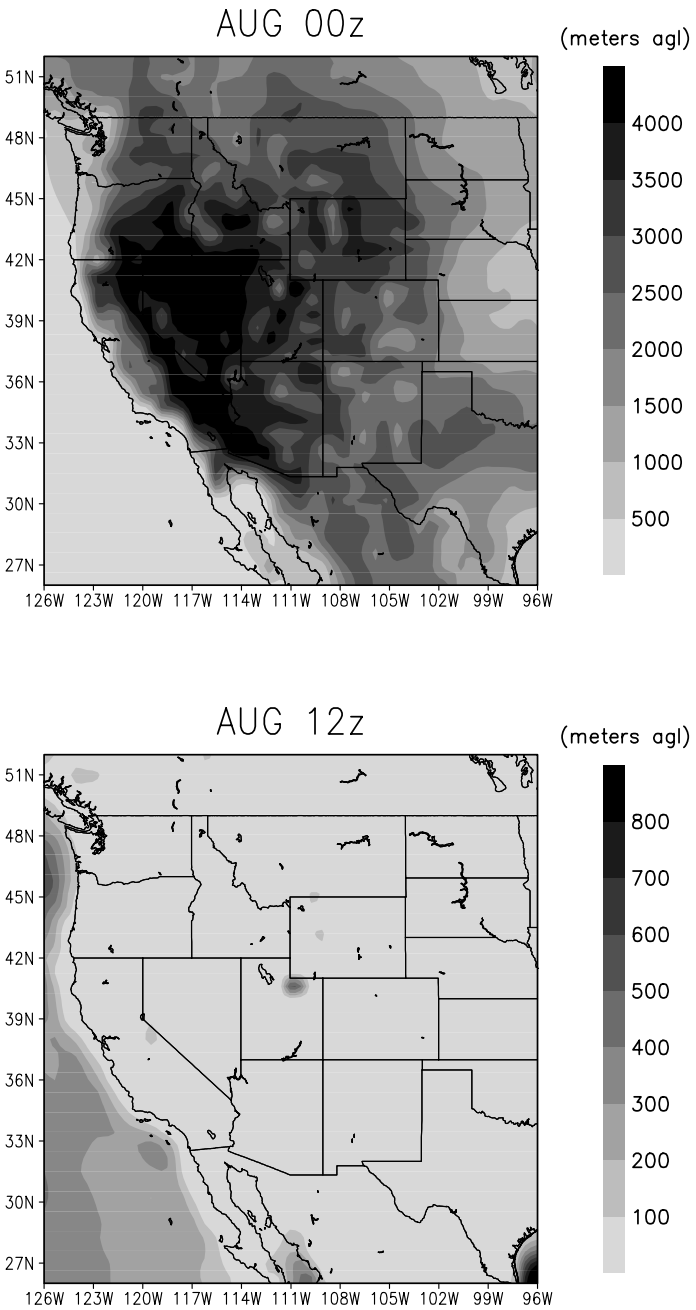

Figure 4-19h Same as 4-19a illustrating August.

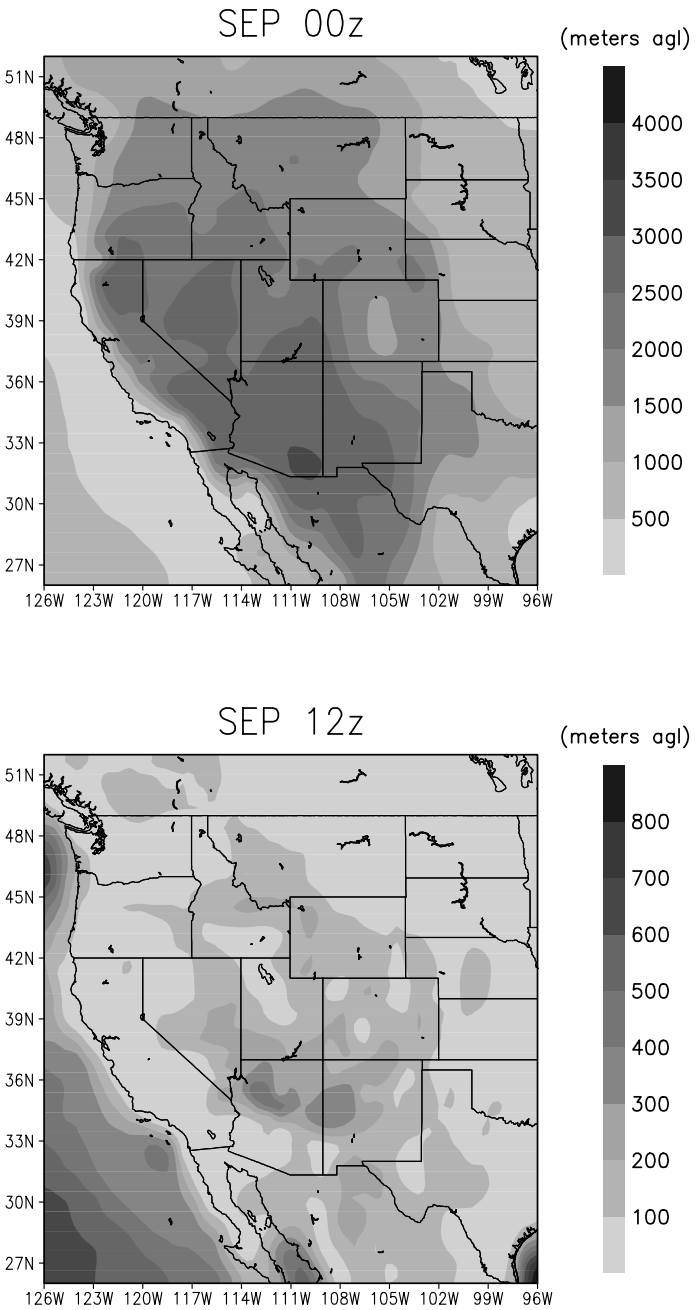

Figure 4-19i Same as 4-19a illustrating September.

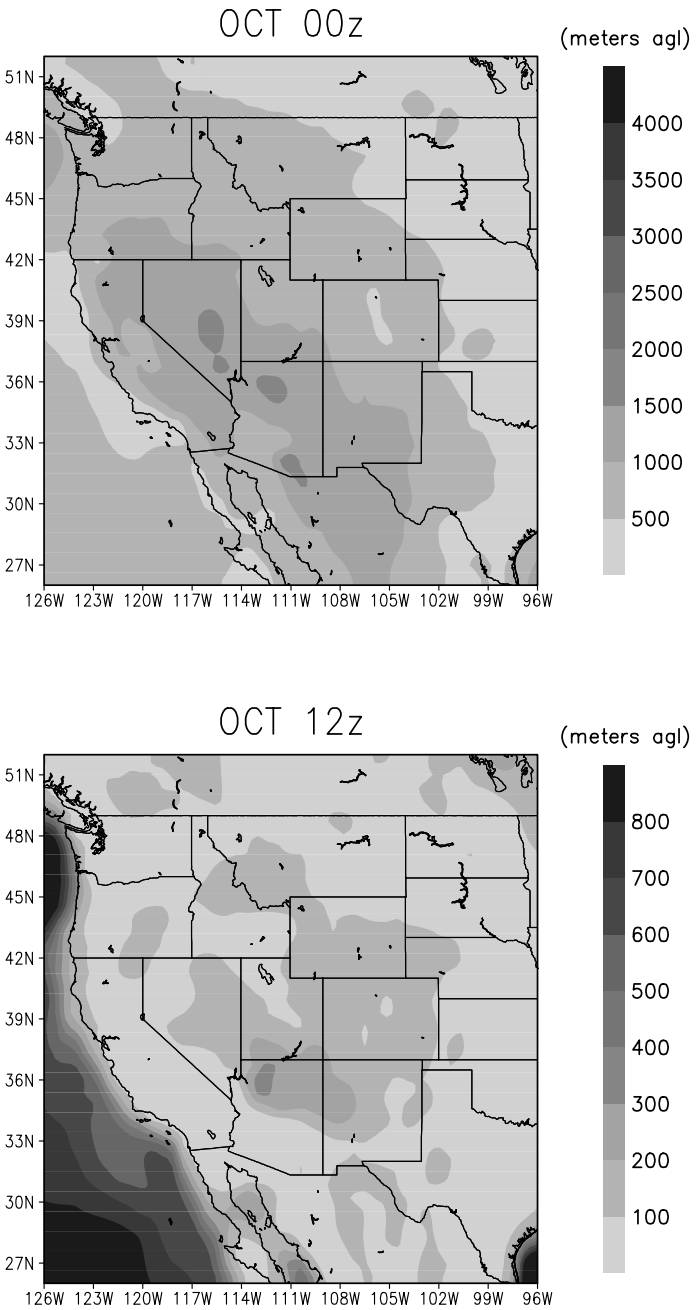

Figure 4-19j Same as 4-19a illustrating October.

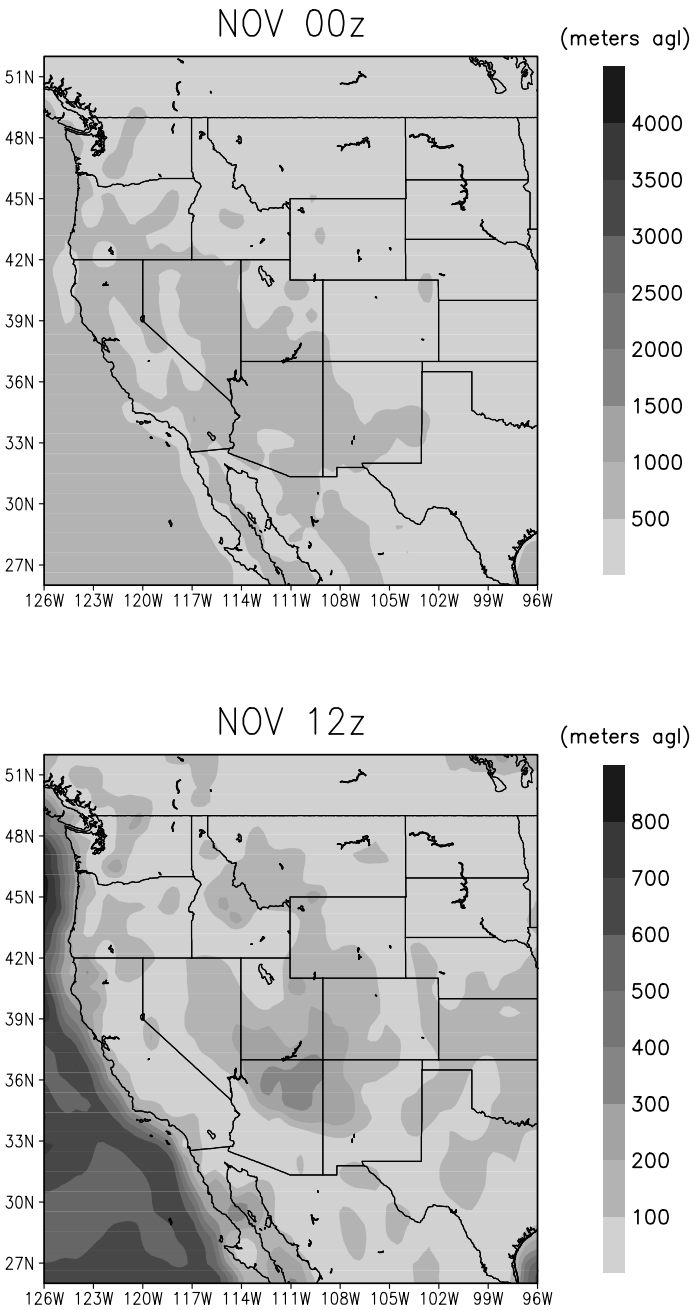

Figure 4-19k Same as 4-19a illustrating November.

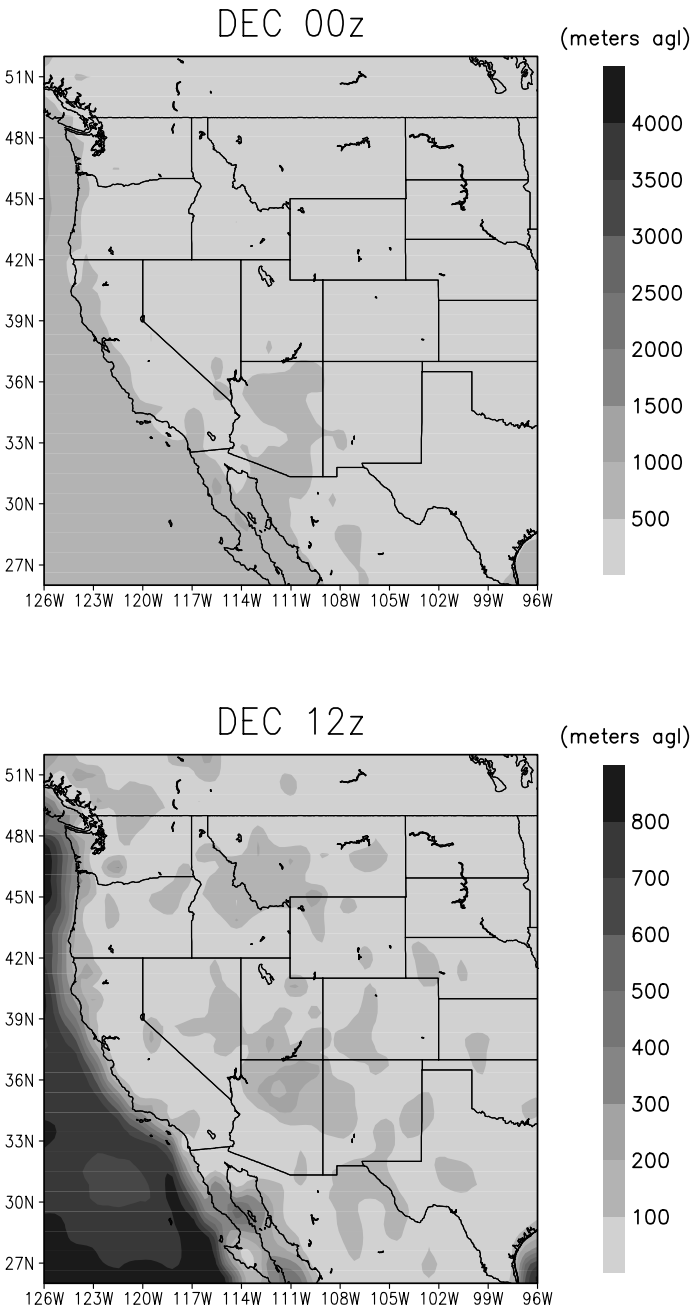

Figure 4-19l Same as 4-19a illustrating December.

CHAPTER FIVE

DISCUSSION AND CONCLUSIONS

The results of this study are based upon the mixing height methodology comparison of Stull and Holzworth, the comparison of Eta mixing heights to sounding heights using the Stull method, and the examination of the spatial coverage of mixing height using the Eta model. From the methodology comparison, it is evident that significant differences can exist in computed mixing height values, especially at 12 UTC. This is largely due to important distinguishing concepts that lie within the procedures themselves. For instance, the Stull method incorporates moisture by using θ_v, whereas the Holzworth technique solely uses θ. In many instances, the use of θ is probably sufficient, but as pointed out in Chapter 4, important cases do arise when moisture needs to be accounted for in mixing height estimation (e.g., the existence of sharp moisture gradients at the surface; i.e., Figure 4-4). A second issue of concern that arises in methodology is the utilization of the entire profile. The Stull method tracks all possible parcel movements (negatively and positively buoyant), whereas the Holzworth technique only examines the ascent of the surface parcel. This can generate misleading mixing height values if only the surface parcel is used for estimation because significant instability can be elevated (i.e., Figure 4-3). A third issue is the use of the $T+5\,^{\circ}C$ concept at 12 UTC by the Holzworth method, which can be quite subjective; an arbitrary $5\,^{\circ}C$ can be very inconsistent from day to day. This approach often produces mixing height values that are excessively high given current observations (i.e., Figure 4-8), which is similar to the findings by Goldman (1980). Estimated heights from the

Holzworth method, especially at 12 UTC, can produce misleading values of mean transport wind as a result of mixing height overestimates (i.e., Figure 4-9).

Even though the Stull method examines the entire sounding profile and tracks all relevant parcel movements, computed mixing height values computed are only an estimate of the true dispersion level as with the Holzworth technique. During instances of strong vertical motions or horizontal advection, the atmospheric structure is constantly changing, and height values computed from the Stull method can be inaccurate. Misrepresentation of mixing height occurs because profiles used are only snapshots in time, and levels to which parcels are tracked may be unrealistic, especially when height estimation is performed using spatially and temporally coarse radiosonde data. These potential drawbacks of the Stull method can be remedied to some extent when model output is used, as it accounts for atmospheric processes (i.e., vertical motions) and provides much better spatial and temporal representation of values.

The inaccuracies that can develop using the Stull procedure, during the presence of strong vertical motions or horizontal advection, also occur when the Holzworth method is used. Therefore, it is suggested that the Stull method be used over the Holzworth technique for smoke and air quality management planning. The Stull technique is clearly more comprehensive in its overall assessment of instability. It always accounts for moisture and does not require the use of arbitrary concepts (e.g., $T+5\,^{\circ}C$). Further, similar to the Holzworth method, the Stull procedure can easily be employed operationally and used with various data sources (e.g., sounding or model output).

Based upon the results of comparing Eta output to sounding data, the Eta appears to perform reasonably well using the Stull method. Even though there are occurrences when the model height values are not in agreement with observed height values, the overall diurnal trends between the two are fairly consistent. This suggests that the Stull method in combination with Eta output can provide useful operational guidance.

Time series analysis of model and sounding height differences for the Stull method shown in Chapter 4 (i.e., Figures 4-16a through 4-17c) provided a generalized view of the accuracy of deriving point location forecasts of mixing height from the Eta model. However, structural differences were more clearly seen between the sounding and Eta when individual profile examples were analyzed. Mixing height values computed from the model were closer to sounding values when the θ_v structural profile from the Eta was consistent to that of the co-located sounding (i.e., Figures 4-18a and 4-18b). Low-level structural differences between the Eta and sounding profiles seem to occur as a result of the model assimilation process. For some areas, observed values that are too far below model terrain can not be used effectively to correct model first guess surface values (i.e., Table 3-4).

Differences in Eta and sounding structure also seem to exist because of vertical resolution. The Eta showed similar values of θ_v when compared to the sounding at corresponding altitude levels, but the Eta also appeared to resolve more structural detail because of its finer vertical resolution. Further, it should be reemphasized here that the Eta output used in this study is at 80 km horizontal resolution, and therefore individual grid point estimates of vertical structure can be more subject to error than if a finer horizontal resolution scale were to be used.

The results based on Eta and sounding differences also explain why mixing height values computed from the Stull method can be different. When profile structure is similar between the sounding and the Eta, mixing height values are very close. However, when θ_v profiles are different, mixing height values are only different due to coarse sounding resolution or the Eta misrepresenting the θ_v structure, not because of methodology.

The spatial coverage of mixing height that can be provided using the NCEP Eta model output as a data source is much more comprehensive over large geographical areas than sounding measurements at upper air stations (i.e., Figures 1-2 and 1-3). The output can be used to assess large-scale patterns of mixing height and reasonable point location forecasts as described in Chapter 4. The ability of the model physics to capture diurnal and seasonal variability is quite encouraging and promotes the value of model output for prediction. Further, only initializations were used in this study, but forecast output is available twice daily in 6-hour intervals out to 48 hours. Therefore, not only does the model output provide much better spatial representation, but it also can provide extended prediction of mixing height.

Monitoring dispersion and transport of resultant wildfire smoke can be crucial to decision-makers and burn planners, especially when pollutants have the potential to affect sensitive receptors such as human-populated areas. Thus, this research was performed to improve mixing height and mean transport wind forecasts that are made available for the fire weather and smoke management agencies. These forecasts are currently limited spatially to upper air station locations, unless model derived soundings are used, and temporally prediction rarely exceeds 12 hours. Mixing height determination using model

output can be highly beneficial for burn planning and wildfire suppression. Spatially, values can be generated for a large geographical area (e.g., western U.S.) providing a synoptic scale depiction of variability. Temporally, forecasts can be produced twice daily at 00 and 12 UTC every 6 hours for a period of 48 hours. Point location forecasts (e.g., Reno, NV) of mixing height and transport wind can also be extracted and examined individually if desired. Depending on agency needs, tailored forecast products of mixing height and mean transport wind using model output can be made conveniently available. For example, short-term trends and changes in mixing height may be more important than the actual height values. This guidance can be used to assist in burn planning efforts, wildfire suppression, and other specific air quality studies where knowledge of the mixed layer is needed.

The results of this research can be applied to a variety of future work. NCEP Eta model physics and resolution are constantly being updated, and can only improve point location forecasts and spatial detail in mixing height estimated values. Mixing height values could be computed using output from another numerical model besides the Eta and compared to actual observations. This would indicate whether or not other models could provide satisfactory prediction of PBL structure and mixing height. It would be especially worth while to examine mixing height computations at higher model resolution (e.g., mesoscale models using a 12 km or less grid) and compare these results to the 80 km derived values analyzed in this study. Finally, attaining larger climatologies (beyond two years) of mixing height generated from model output would be useful. Another interesting study would be to analyze the spatial patterns on a more seasonal basis and associate mixing height behavior to relevant synoptic patterns.

REFERENCES

Baxter, R., 1991: Determination of mixing heights form data collected during the 1985 SCCCAMP field program. *J. Appl. Meteor*., **30**, 598-605.

Berman, S., et al., 1999: Spatial and temporal variation in the mixing depth over the northeastern United States during the summer of 1995. *J. Appl. Meteor*., **38**, 1661-1673.

Beyrich, F., 1997: Mixing height estimation from sodar data – a critical discussion. *Atmos. Environ*., **31**, 3941-3953.

Caiazza, R., C.D. Bedford, and R. Wooley, 1992: A unique atmospheric stability classification situation at a Lake Ontario shoreline. *Proceedings of the 10th Symposium on Turbulence and Diffusion*, September 29-October 2, 1992, Portland, OR, 314-317.

Capuano, M.E., and M.K. Atchison, 1984: Worldwide mean mixed layer heights based on an 8-year study period. *Proceedings of the Fourth Joint Conference on Applications of Air Pollution Meteorology*, October 16-19, 1984, Portland, OR, 198-201.

Coulter, R.L., 1979: A comparison of three methods for measuring mixing-layer height. *J. Appl. Meteor*., **18**, 1495-1499.

Dayan, U., and J. Rodnizki, 1999: The temporal behavior of the atmospheric boundary layer in Israel. *J. Appl. Meteor*., **38**, 830-836.

Fairfall, C.W., 1991: The humidity and temperature sensitivity of clear-air radars in the convective boundary layer. *J. Appl. Meteor*., **30**, 1064-1074.

Garrett, A.J., 1981: Comparison of observed mixed-layer depths to model estimates using observed temperatures and winds, and MOS forecasts. *J. Appl. Meteor*., **20**, 1277-1283.

Goldman, A.D., 1980: A physically realistic method of calculating mixing heights over rural areas for use in atmospheric dispersion models. *Proceedings of the 2nd Joint Conference on Applications of Air Pollution Meteorology*, March 24-27, 1980, New Orleans, LA, 781-786.

Heffter, J.L., 1980: *Air Resources Laboratories Atmospheric Transport and Dispersion Model*. NOAA. Tech. Memo. ERL ARL-81, 24 pp.

Holzworth, G.C., 1964: Estimates of mean maximum mixing depths in the contiguous

United States. *Mon. Wea. Rev.*, **92**, 235-242.

____ 1967: Mixing depths, wind speeds and air pollution potential for selected locations in the United States. *J. Appl. Meteor*., **6**, 1039-1044.

____ 1972: Mixing Heights, Wind Speeds, and Potential for Urban Air Pollution Throughout the Contiguous United States, Meteorology Laboratory, EPA, Research Triangle Park, NC, 27711, 118 pp.

Huschke, R.E., 1959: *Glossary of Meteorology*. American Meteorological Society, 638 pp.

Lena, F., and Desiato, F., 1998: Intercomparison of nocturnal mixing height estimate methods for urban air pollution modelling. *Atmos. Environ*., **33**, 2385-2393.

Marsik, F.J., et al., 1995: Comparison of methods for estimating mixing height used during the 1992 Atlanta field intensive. *J. Appl. Meteor*., **34**, 1802-1814.

McNulty, B.L., and M. Cairns, 1999: A comparison of the Eta model-derived surface data with ASOS temperature and winds, Western Region Technical Attachment, WR99-10, pp.

National Centers for Environmental Prediction, 2000: EMC: Mesoscale Model Branch Hompage, http://www.emc.ncep.noaa.gov/mmb/mesoscale.html.

National Weather Service, 2000: Seattle Forecast Office Homepage, http://www.seawfo.noaa.gov.

Nutter, P.A., and J. Manobianco, 1999: Evaluation of the 29-km Eta model. Part I: Objective verification at three selected stations. *Wea. Forecasting*, **14**, 5-17.

Nutter, P.A., and J. Manobianco, 1999: Evaluation of the 29-km Eta model. Part II: Subjective verification over Florida. *Wea. Forecasting*, **14**, 18-37.

Olesen, H.R., A.B. Jensen, and N. Brown, 1987: An operational procedure for mixing height estimation. *Riso Nat. Lab. MST-Luft-A96*. 2nd edition 1992, 182 pp.

Piringer, M., Baurmann, K., and Langer, M., 1997: A comparison of estimate and modelled mixing heights. *Proceedings of the 12th Symposium on Boundary Layers and Turbulence*, July 28-August 1, 1997, Vancouver, BC, 46-47.

Rogers, E., and Coauthors, 1997: Changes to the NCEP operational "Early" Eta analysis / forecast system. NWS Technical Procedures Bulletion No. 447, NOAA/NWS, Washington, DC [available at http://www.nws.noaa.gov/om/447body.htm]

Seibert, P., F. Beyrich, S. Gryning, S. Joffre, A. Rasmussen, and P. Tercier, 1997: A comparison of practical methods for the determination of mixing heights. *Proceedings of the 12th Symposium on Boundary Layers and Turbulence*, July 28-August 1, 1997, 271-272.

Staudenmaier, M., 1996b: The initialization procedure in the Meso Eta model. Western Region Technical Attachment, WR96-30, 11 pp.

Stull, R.B., 1988: *An Introduction to Boundary Layer Meteorology*. Kluwer Academic Publishers, 666 pp.

____, R.B., 1991: Static stability-an update. *Bull. Amer. Meteor*., **72**, 1521-1529.

Ulke, A.G., and N.A. Mazzeo, 1998: Climatological aspects of the daytime mixing height in Buenos Aires, Argentina. *Atmos. Environ*., **32**, 1615-1622.

Wallace, J.M., and P.V. Hobbs, 1977: *Atmospheric Science An Introductory Survey*. Academic Press, 467 pp.

APPENDIX

Monthly mean corrections for 2 meter agl NCEP Eta
potential temperature and virtual potential temperature

θ_{EO} 2 m Eta original potential temperature
θ_{EC} 2 m Eta corrected potential temperature
θ_{VEO} 2 m Eta original virtual potential temperature
θ_{VEC} 2 m Eta corrected virtual potential temperature
θ_{S} Sounding surface potential temperature
θ_{VS} Sounding surface virtual potential temperature

Table A
00 UTC

Month	Station ID	θ_{VEO}	θ_{VS}	θ_{VEC}	$\theta_{VEC} - \theta_{VS}$	θ_{EO}	θ_{S}	θ_{EC}	$\theta_{EC} - \theta_{S}$
JAN	UIL	282.63	280.81	281.62	0.82	281.62	280.81	280.65	0.82
	GEG	280.25	280.59	280.32	-0.27	279.56	280.59	279.64	-0.27
	TFX	281.32	281.95	281.49	-0.46	280.83	281.95	281.02	-0.46
	GGW	273.12	269.88	271.22	1.34	272.72	269.88	270.92	1.34
	BOI	285.60	286.73	286.07	-0.66	284.99	286.73	285.37	-0.66
	MFR	289.29	284.74	286.23	1.49	288.45	284.74	285.45	1.49
	RIW	288.09	289.21	288.18	-1.03	287.62	289.21	287.72	-1.03
	REV	292.24	294.96	293.69	-1.26	291.48	294.96	293.04	-1.26
	SLC	291.16	289.98	290.73	0.75	290.55	289.98	290.03	0.75
	OAK	287.11	286.35	286.78	0.43	285.81	286.35	285.51	0.43
	DNR	291.95	293.78	292.42	-1.36	291.47	293.78	291.94	-1.36
	FGZ	299.55	299.73	299.56	-0.17	298.82	299.73	298.87	-0.17
	ABQ	295.19	298.67	297.05	-1.62	294.59	298.67	296.59	-1.62
	NKX	289.76	291.16	290.55	-0.60	288.32	291.16	289.28	-0.60
FEB	TUS	298.08	299.83	299.17	-0.66	297.24	299.83	298.51	-0.66
	UIL	283.83	281.74	282.44	0.70	282.75	281.74	281.55	0.70
	GEG	283.51	284.13	283.71	-0.42	282.66	284.13	282.92	-0.42
	TFX	285.70	289.14	287.59	-1.55	285.05	289.14	287.19	-1.55
	GGW	279.86	281.00	280.11	-0.89	279.26	281.00	279.56	-0.89
	BOI	286.32	287.43	286.91	-0.52	285.63	287.43	286.24	-0.52
	MFR	287.66	286.01	286.76	0.74	286.86	286.01	285.93	0.74
	RIW	288.04	291.69	289.40	-2.29	287.53	291.69	288.91	-2.29
	REV	291.37	293.13	292.23	-0.90	290.56	293.13	291.46	-0.90
	SLC	291.63	290.66	291.44	0.78	290.96	290.66	290.77	0.78
	OAK	286.40	286.24	286.37	0.13	285.09	286.24	285.09	0.13
	DNR	292.79	296.89	295.12	-1.77	292.26	296.89	294.64	-1.77
	FGZ	299.79	298.49	299.21	0.72	299.08	298.49	298.72	0.72
	ABQ	296.28	300.06	298.80	-1.26	295.66	300.06	298.31	-1.26

	NKX	289.28	290.03	289.50	-0.53	287.83	290.03	288.24	-0.53
	TUS	298.13	298.83	298.30	-0.53	297.32	298.83	297.59	-0.53
MAR	UIL	284.27	282.32	282.99	0.67	283.16	282.32	282.04	0.67
	GEG	286.69	288.00	286.88	-1.12	285.70	288.00	286.11	-1.12
	TFX	287.61	289.97	288.56	-1.42	286.89	289.97	288.01	-1.42
	GGW	282.52	283.03	282.42	-0.61	281.80	283.03	281.70	-0.61
	BOI	289.93	292.66	291.77	-0.89	289.09	292.66	291.21	-0.89
	MFR	291.15	289.22	290.06	0.85	290.20	289.22	289.29	0.85
	RIW	292.54	295.91	293.83	-2.08	291.86	295.91	293.29	-2.08
	REV	296.87	298.60	297.81	-0.79	295.84	298.60	297.22	-0.79
	SLC	296.32	295.60	296.00	0.41	295.45	295.60	295.24	0.41
	OAK	289.03	288.38	288.82	0.44	287.66	288.38	287.50	0.44
	DNR	296.42	300.09	297.95	-2.14	295.74	300.09	297.35	-2.14
	FGZ	305.69	303.08	304.41	1.33	304.90	303.08	303.77	1.33
	ABQ	301.60	303.96	302.84	-1.12	300.82	303.96	302.12	-1.12
	NKX	289.85	290.95	290.37	-0.58	288.34	290.95	289.13	-0.58
	TUS	301.64	302.58	301.86	-0.72	300.69	302.58	301.03	-0.72
APR	UIL	286.52	284.76	285.52	0.76	285.40	284.76	284.62	0.76
	GEG	292.58	292.14	292.52	0.39	291.50	292.14	291.50	0.39
	TFX	293.99	294.93	294.24	-0.69	293.13	294.93	293.52	-0.69
	GGW	292.34	293.23	292.52	-0.71	291.36	293.23	291.70	-0.71
	BOI	294.52	295.27	294.73	-0.54	293.54	295.27	293.90	-0.54
	MFR	294.78	292.18	293.39	1.21	293.77	292.18	292.66	1.21
	RIW	297.00	298.44	297.31	-1.12	296.11	298.44	296.61	-1.12
	REV	298.16	298.85	298.39	-0.46	297.15	298.85	297.56	-0.46
	SLC	299.23	297.21	298.12	0.91	298.25	297.21	297.26	0.91
	OAK	290.89	290.03	290.60	0.57	289.46	290.03	289.22	0.57
	DNR	299.92	300.56	300.00	-0.56	299.05	300.56	299.22	-0.56
	FGZ	305.67	302.28	302.90	0.62	304.83	302.28	302.34	0.62
	ABQ	305.26	306.42	305.66	-0.75	304.57	306.42	305.06	-0.75
	NKX	290.21	291.85	290.92	-0.93	288.70	291.85	289.69	-0.93
	TUS	303.77	303.90	303.74	-0.16	302.96	303.90	302.91	-0.16
MAY	UIL	289.47	286.75	287.76	1.02	288.11	286.75	286.48	1.02
	GEG	299.25	295.93	297.34	1.41	297.96	295.93	296.45	1.41
	TFX	302.23	301.06	302.25	1.19	301.11	301.06	301.22	1.19
	GGW	300.92	299.13	300.29	1.15	299.68	299.13	299.24	1.15
	BOI	302.20	300.24	301.90	1.66	300.93	300.24	300.82	1.66
	MFR	299.64	294.25	295.71	1.46	298.44	294.25	294.46	1.46
	RIW	306.36	306.70	306.39	-0.31	305.25	306.70	305.37	-0.31
	REV	305.27	305.14	305.26	0.12	304.09	305.14	304.09	0.12
	SLC	307.94	304.57	305.71	1.14	306.78	304.57	304.78	1.14
	OAK	292.69	290.45	291.40	0.95	291.12	290.45	289.95	0.95
	DNR	309.49	309.49	309.49	0.00	308.26	309.49	308.26	0.00
	FGZ	314.77	311.06	312.19	1.13	313.84	311.06	311.48	1.13
	ABQ	314.35	313.66	314.33	0.67	313.45	313.66	313.46	0.67
	NKX	292.41	293.65	293.06	-0.59	290.68	293.65	291.62	-0.59

	TUS	311.47	312.28	311.53	-0.75	310.48	312.28	310.53	-0.75
JUN	UIL	292.52	288.58	289.37	0.79	290.86	288.58	287.96	0.79
	GEG	304.36	301.29	302.40	1.12	302.88	301.29	301.08	1.12
	TFX	304.97	301.68	304.37	2.69	303.52	301.68	303.02	2.69
	GGW	303.84	301.37	302.40	1.03	302.29	301.37	301.03	1.03
	BOI	308.85	305.93	307.15	1.22	307.34	305.93	305.91	1.22
	MFR	308.88	302.36	303.67	1.30	307.40	302.36	302.51	1.30
	RIW	311.66	310.79	311.72	0.94	310.40	310.79	310.49	0.94
	REV	313.67	312.01	313.25	1.24	312.17	312.01	311.86	1.24
	SLC	315.09	310.25	311.84	1.58	313.71	310.25	310.63	1.58
	OAK	298.96	292.62	294.23	1.61	296.97	292.62	292.60	1.61
	DNR	316.45	314.66	315.77	1.10	315.12	314.66	314.43	1.10
	FGZ	322.88	316.07	316.69	0.62	321.87	316.07	315.88	0.62
	ABQ	321.42	319.65	320.81	1.16	320.32	319.65	319.93	1.16
	NKX	295.86	295.77	295.87	0.10	293.86	295.77	293.92	0.10
	TUS	319.84	316.64	317.75	1.11	318.60	316.64	316.99	1.11
JUL	UIL	295.31	291.73	292.78	1.05	293.37	291.73	291.13	1.05
	GEG	312.05	307.65	309.16	1.52	310.66	307.65	307.95	1.52
	TFX	313.66	311.14	312.66	1.52	312.18	311.14	311.27	1.52
	GGW	312.83	308.81	310.20	1.38	311.26	308.81	308.51	1.38
	BOI	318.17	315.10	316.64	1.54	316.84	315.10	315.20	1.54
	MFR	315.88	309.11	310.51	1.40	314.48	309.11	309.01	1.40
	RIW	321.92	320.01	321.76	1.75	320.58	320.01	320.46	1.75
	REV	321.97	319.98	320.94	0.96	320.76	319.98	319.75	0.96
	SLC	323.54	318.84	319.97	1.13	321.92	318.84	318.45	1.13
	OAK	303.16	294.72	295.60	0.87	301.05	294.72	293.87	0.87
	DNR	321.40	318.88	320.58	1.69	319.40	318.88	318.66	1.69
	FGZ	326.15	316.75	318.86	2.11	324.27	316.75	317.05	2.11
	ABQ	320.89	319.95	320.92	0.96	318.77	319.95	318.81	0.96
	NKX	299.61	300.00	299.62	-0.37	297.21	300.00	297.32	-0.37
	TUS	320.48	315.29	317.26	1.97	318.23	315.29	315.25	1.97
AUG	UIL	296.71	293.25	294.07	0.82	294.68	293.25	292.36	0.82
	GEG	312.19	308.36	310.05	1.69	310.70	308.36	308.85	1.69
	TFX	313.49	312.60	313.29	0.69	311.99	312.60	311.86	0.69
	GGW	311.92	310.07	310.98	0.91	310.33	310.07	309.38	0.91
	BOI	317.80	314.37	315.94	1.57	316.67	314.37	314.67	1.57
	MFR	316.01	308.49	309.63	1.15	314.73	308.49	308.35	1.15
	RIW	319.18	318.51	319.19	0.68	317.86	318.51	317.87	0.68
	REV	321.27	319.03	320.24	1.22	320.10	319.03	318.98	1.22
	SLC	321.84	317.22	318.08	0.86	320.32	317.22	316.67	0.86
	OAK	303.90	296.26	297.56	1.29	301.70	296.26	295.53	1.29
	DNR	318.87	316.17	318.00	1.83	316.96	316.17	316.09	1.83
	FGZ	324.36	316.68	318.38	1.69	322.54	316.68	316.73	1.69
	ABQ	319.06	319.36	319.08	-0.28	316.80	319.36	316.98	-0.28
	NKX	300.91	300.80	300.93	0.14	298.32	300.80	298.43	0.14
	TUS	321.23	317.04	318.53	1.49	319.08	317.04	316.70	1.49

SEP	UIL	294.17	293.09	293.77	0.67	292.35	293.09	292.03	0.67
	GEG	304.53	304.58	304.53	-0.05	302.91	304.58	303.01	-0.05
	TFX	308.70	308.18	308.71	0.53	307.34	308.18	307.37	0.53
	GGW	306.15	305.51	306.10	0.59	304.67	305.51	304.71	0.59
	BOI	310.15	308.98	309.86	0.88	308.71	308.98	308.42	0.88
	MFR	310.66	303.96	307.00	3.04	309.27	303.96	305.76	3.04
	RIW	313.29	312.34	313.17	0.83	311.97	312.34	311.85	0.83
	REV	312.78	313.29	312.83	-0.46	311.25	313.29	311.37	-0.46
	SLC	313.82	311.70	312.82	1.12	312.24	311.70	311.21	1.12
	OAK	301.68	297.73	299.14	1.42	299.35	297.73	297.57	1.42
	DNR	315.98	314.59	315.64	1.05	314.51	314.59	314.21	1.05
	FGZ	318.21	315.64	317.10	1.46	316.43	315.64	315.38	1.46
	ABQ	318.88	318.22	318.70	0.48	317.25	318.22	317.12	0.48
	NKX	301.62	301.90	301.63	-0.26	298.84	301.90	298.91	-0.26
	TUS	317.85	316.16	317.53	1.37	315.61	316.16	315.38	1.37
OCT	UIL	287.85	287.53	287.75	0.21	286.39	287.53	286.34	0.21
	GEG	291.26	293.24	292.14	-1.10	290.17	293.24	291.22	-1.10
	TFX	294.40	297.12	295.41	-1.71	293.54	297.12	294.63	-1.71
	GGW	290.91	293.05	291.07	-1.98	289.93	293.05	290.18	-1.98
	BOI	297.60	298.41	297.66	-0.75	296.79	298.41	296.85	-0.75
	MFR	299.44	294.64	296.33	1.69	298.49	294.64	295.34	1.69
	RIW	301.07	302.48	301.26	-1.22	300.21	302.48	300.39	-1.22
	REV	302.55	304.71	303.43	-1.28	301.62	304.71	302.33	-1.28
	SLC	302.59	301.77	302.47	0.69	301.62	301.77	301.51	0.69
	OAK	295.19	294.21	295.02	0.81	293.49	294.21	293.44	0.81
	DNR	303.84	305.31	304.28	-1.03	302.94	305.31	303.45	-1.03
	FGZ	307.33	308.64	307.82	-0.83	306.29	308.64	306.93	-0.83
	ABQ	307.37	309.18	307.87	-1.31	306.23	309.18	306.94	-1.31
	NKX	297.30	298.05	297.46	-0.59	295.20	298.05	295.53	-0.59
	TUS	307.42	309.82	309.06	-0.76	306.03	309.82	307.90	-0.76
NOV	UIL	285.87	284.66	285.44	0.79	284.64	284.66	284.24	0.79
	GEG	286.03	286.28	286.01	-0.27	285.11	286.28	285.09	-0.27
	TFX	286.40	287.63	286.71	-0.92	285.76	287.63	286.13	-0.92
	GGW	282.21	281.75	282.23	0.48	281.56	281.75	281.57	0.48
	BOI	290.29	291.33	290.58	-0.75	289.55	291.33	289.87	-0.75
	MFR	292.17	287.89	289.24	1.35	291.22	287.89	288.22	1.35
	RIW	291.25	292.83	291.61	-1.22	290.71	292.83	291.10	-1.22
	REV	296.03	297.99	296.99	-1.00	295.16	297.99	296.24	-1.00
	SLC	294.79	294.00	294.67	0.67	294.08	294.00	293.95	0.67
	OAK	289.95	289.92	289.94	0.02	288.44	289.92	288.44	0.02
	DNR	294.82	296.97	295.05	-1.92	294.26	296.97	294.44	-1.92
	FGZ	301.85	302.92	302.28	-0.64	301.00	302.92	301.58	-0.64
	ABQ	298.88	301.13	299.83	-1.30	298.13	301.13	299.11	-1.30
	NKX	293.10	294.61	293.82	-0.79	291.40	294.61	292.32	-0.79
	TUS	301.43	303.61	302.77	-0.84	300.37	303.61	302.13	-0.84
DEC	UIL	282.67	280.22	281.32	1.10	281.66	280.22	280.32	1.10

	GEG	279.10	279.06	279.11	0.04	278.46	279.06	278.46	0.04
	TFX	282.06	282.33	282.10	-0.23	281.56	282.33	281.62	-0.23
	GGW	276.96	276.15	276.84	0.70	276.50	276.15	276.42	0.70
	BOI	283.62	282.58	283.56	0.97	283.08	282.58	282.97	0.97
	MFR	287.58	282.02	283.72	1.70	286.85	282.02	282.96	1.70
	RIW	286.33	284.09	286.10	2.02	285.90	284.09	285.68	2.02
	REV	289.49	291.24	290.45	-0.79	288.84	291.24	289.89	-0.79
	SLC	288.28	285.25	287.11	1.86	287.79	285.25	286.59	1.86
	OAK	286.51	285.61	286.44	0.83	285.36	285.61	285.31	0.83
	DNR	290.24	289.98	290.18	0.20	289.81	289.98	289.75	0.20
	FGZ	296.23	297.29	296.60	-0.69	295.56	297.29	296.06	-0.69
	ABQ	293.21	295.28	293.42	-1.86	292.65	295.28	292.95	-1.86
	NKX	289.48	291.03	290.46	-0.57	288.23	291.03	289.49	-0.57
	TUS	294.68	295.94	295.25	-0.69	293.79	295.94	294.52	-0.69

Table B
12 UTC

Month	Station ID	θ_{VEO}	θ_{VS}	θ_{VEC}	$\theta_{VEC} - \theta_{VS}$	θ_{EO}	θ_{S}	θ_{EC}	$\theta_{EC} - \theta_{S}$
JAN	UIL	281.31	278.08	279.18	1.09	285.39	282.22	283.29	1.08
	GEG	277.64	277.30	277.55	0.26	282.15	281.82	282.07	0.25
	TFX	277.99	278.06	277.99	-0.06	282.78	282.86	282.78	-0.08
	GGW	269.84	265.97	267.93	1.97	274.61	270.80	272.67	1.87
	BOI	283.04	281.73	282.57	0.84	287.74	286.21	287.14	0.93
	MFR	285.43	278.96	280.38	1.43	289.98	283.24	284.49	1.26
	RIW	284.61	283.10	284.41	1.30	289.56	288.02	289.35	1.33
	REV	288.05	288.60	288.18	-0.42	292.73	293.22	292.84	-0.38
	SLC	288.28	285.42	286.63	1.21	293.09	289.99	291.20	1.21
	OAK	282.83	281.07	281.97	0.90	286.68	284.94	285.82	0.89
	DNR	288.03	285.79	287.61	1.83	293.01	290.64	292.45	1.81
	FGZ	291.97	286.38	288.37	1.99	296.75	291.34	293.26	1.93
	ABQ	288.86	288.10	288.82	0.72	293.73	292.84	293.69	0.85
	NKX	286.83	283.59	285.02	1.43	290.60	287.55	289.00	1.45
FEB	TUS	288.93	285.34	286.92	1.58	293.39	289.87	291.42	1.55
	UIL	282.06	278.92	279.97	1.05	286.09	283.07	283.94	0.87
	GEG	279.25	279.31	279.25	-0.06	283.68	283.79	283.68	-0.10
	TFX	279.41	282.18	280.52	-1.66	284.15	286.93	285.26	-1.66
	GGW	274.29	275.77	274.72	-1.05	278.97	280.40	279.35	-1.05
	BOI	281.41	282.38	281.75	-0.63	286.12	286.89	286.38	-0.52
	MFR	283.59	280.84	281.81	0.98	288.16	285.14	286.08	0.94
	RIW	281.37	284.01	282.66	-1.35	286.35	288.89	287.59	-1.30
	REV	285.74	288.23	287.29	-0.94	290.43	292.88	291.79	-1.09
	SLC	286.32	286.38	286.32	-0.06	291.18	290.91	291.13	0.22
	OAK	282.38	281.36	281.93	0.57	286.25	285.25	285.80	0.56
	DNR	284.97	286.10	285.30	-0.80	290.02	290.94	290.22	-0.71
	FGZ	288.76	286.80	287.89	1.09	293.62	291.76	292.79	1.03
	ABQ	285.47	289.30	287.68	-1.62	290.41	294.05	292.35	-1.70
	NKX	285.40	283.27	284.08	0.80	289.16	287.20	287.94	0.74
	TUS	286.43	286.85	286.43	-0.42	290.96	291.28	290.96	-0.32
MAR	UIL	281.23	277.50	278.26	0.76	285.20	281.66	284.01	2.35
	GEG	279.65	279.96	279.62	-0.34	284.00	284.44	284.00	-0.44
	TFX	278.55	281.10	279.80	-1.30	283.27	285.81	285.55	-0.27
	GGW	273.69	274.96	274.04	-0.93	278.40	279.61	279.52	-0.09
	BOI	281.97	284.17	283.09	-1.08	286.59	288.63	287.90	-0.73
	MFR	283.28	281.02	281.60	0.57	287.84	285.26	285.97	0.72
	RIW	281.95	285.73	284.44	-1.28	286.97	290.57	290.04	-0.53
	REV	286.38	290.48	289.44	-1.04	290.98	295.10	294.10	-1.00
	SLC	287.02	288.10	287.09	-1.01	291.83	292.66	291.92	-0.73
	OAK	282.44	281.94	282.27	0.34	286.28	285.82	286.05	0.23
	DNR	286.01	288.20	286.94	-1.26	291.06	292.94	292.00	-0.94

	FGZ	289.09	287.86	288.86	1.00	293.92	292.81	293.58	0.78
	ABQ	287.62	293.27	291.36	-1.92	292.53	297.91	297.88	-0.03
	NKX	284.98	284.00	284.75	0.75	288.75	287.86	288.06	0.20
	TUS	286.46	289.63	288.24	-1.40	290.91	294.05	293.55	-0.50
APR	UIL	281.55	276.41	277.62	1.22	285.60	280.61	281.79	1.18
	GEG	281.83	281.59	281.81	0.22	286.19	286.06	286.18	0.12
	TFX	282.21	284.66	283.82	-0.85	286.84	289.24	288.46	-0.79
	GGW	280.08	282.21	281.28	-0.93	284.53	286.62	285.71	-0.91
	BOI	283.97	285.30	284.62	-0.68	288.59	289.69	289.11	-0.58
	MFR	285.09	281.71	282.88	1.17	289.60	285.92	287.13	1.20
	RIW	285.65	289.78	288.20	-1.58	290.47	294.44	293.00	-1.44
	REV	287.70	291.51	290.33	-1.18	292.36	296.10	295.01	-1.09
	SLC	289.65	290.27	289.62	-0.65	294.41	294.68	294.37	-0.31
	OAK	283.15	282.69	283.03	0.34	287.01	286.53	286.90	0.37
	DNR	288.71	290.65	289.74	-0.92	293.56	295.23	294.32	-0.91
	FGZ	291.41	289.89	291.03	1.14	296.18	294.77	295.90	1.12
	ABQ	289.01	295.00	293.15	-1.85	293.82	299.64	297.95	-1.70
	NKX	285.14	284.04	284.88	0.84	288.91	287.96	288.72	0.76
	TUS	287.15	290.79	289.40	-1.39	291.67	295.16	293.83	-1.33
MAY	UIL	283.98	280.05	281.52	1.48	287.83	284.00	285.44	1.43
	GEG	285.38	285.98	285.50	-0.48	289.55	290.18	289.66	-0.52
	TFX	286.41	289.45	288.31	-1.14	290.85	293.79	292.68	-1.10
	GGW	284.65	287.24	286.13	-1.11	288.88	291.36	290.30	-1.06
	BOI	289.57	289.80	289.63	-0.17	293.92	293.95	293.93	-0.02
	MFR	288.18	285.00	286.19	1.20	292.50	288.96	290.10	1.14
	RIW	290.58	295.93	294.78	-1.15	295.25	300.32	299.23	-1.09
	REV	291.28	295.24	294.39	-0.85	295.78	299.67	298.70	-0.97
	SLC	294.45	295.53	294.49	-1.04	299.00	299.64	298.99	-0.65
	OAK	283.52	284.15	283.72	-0.42	287.32	287.86	287.45	-0.41
	DNR	294.55	297.30	296.12	-1.18	299.19	301.54	300.45	-1.09
	FGZ	295.07	293.24	294.97	1.72	299.75	298.02	299.69	1.67
	ABQ	293.83	301.14	299.31	-1.83	298.51	305.58	303.82	-1.77
	NKX	286.64	287.34	286.81	-0.53	290.23	290.94	290.40	-0.53
	TUS	291.85	296.65	294.60	-2.06	296.25	301.06	299.00	-2.06
JUN	UIL	286.50	283.50	284.39	0.89	290.11	287.20	288.12	0.92
	GEG	288.99	289.63	289.17	-0.46	292.99	293.62	293.18	-0.44
	TFX	291.32	293.03	292.17	-0.85	295.42	297.02	296.19	-0.83
	GGW	289.08	291.25	290.24	-1.00	293.00	295.01	294.04	-0.97
	BOI	292.49	294.18	293.52	-0.66	296.72	298.08	297.50	-0.58
	MFR	291.72	289.13	290.28	1.15	295.86	292.90	294.05	1.15
	RIW	294.57	300.15	298.08	-2.07	299.05	304.27	302.24	-2.03
	REV	296.02	300.91	300.28	-0.63	300.31	305.08	304.46	-0.62
	SLC	299.28	300.10	299.54	-0.56	303.70	303.91	303.72	-0.19
	OAK	286.10	285.74	286.21	0.47	289.70	289.31	289.79	0.48
	DNR	298.15	301.24	300.10	-1.14	302.63	305.16	303.99	-1.17
	FGZ	299.50	296.25	298.84	2.58	304.08	300.94	303.56	2.62

	ABQ	299.18	305.88	304.64	-1.24	303.64	310.15	308.71	-1.45
	NKX	288.85	289.44	289.04	-0.40	292.29	292.83	292.46	-0.37
	TUS	296.73	302.48	300.88	-1.60	300.88	306.56	304.77	-1.79
JUL	UIL	288.55	285.21	286.11	0.91	291.98	288.76	289.63	0.87
	GEG	292.62	293.63	293.08	-0.54	296.50	297.44	296.89	-0.54
	TFX	293.97	296.47	295.80	-0.68	297.97	300.32	299.64	-0.68
	GGW	292.43	295.52	294.63	-0.89	296.15	298.98	298.17	-0.82
	BOI	296.30	299.58	298.64	-0.94	300.56	303.35	302.36	-0.99
	MFR	293.96	293.61	293.93	0.31	297.99	297.14	297.76	0.62
	RIW	300.32	305.98	304.64	-1.34	304.60	309.81	308.40	-1.41
	REV	299.05	305.95	304.66	-1.29	303.34	310.11	309.19	-0.92
	SLC	304.58	307.14	305.71	-1.43	308.77	310.61	309.49	-1.12
	OAK	286.63	287.34	286.85	-0.50	290.23	290.77	290.35	-0.42
	DNR	304.70	306.63	306.01	-0.62	308.64	309.96	309.44	-0.52
	FGZ	306.96	303.78	305.94	2.16	310.62	307.69	309.72	2.04
	ABQ	305.11	309.91	308.77	-1.14	308.72	313.01	312.07	-0.95
	NKX	291.76	292.79	292.25	-0.54	294.91	295.79	295.29	-0.49
	TUS	303.46	307.04	305.28	-1.76	306.47	309.59	308.00	-1.58
AUG	UIL	289.47	285.50	286.65	1.15	292.81	288.99	290.03	1.04
	GEG	292.17	294.34	293.32	-1.03	296.10	298.18	297.16	-1.03
	TFX	294.20	297.91	296.97	-0.95	298.24	301.69	300.81	-0.88
	GGW	292.35	296.53	295.70	-0.84	296.10	300.04	299.11	-0.93
	BOI	295.73	299.84	299.17	-0.67	300.06	303.67	302.95	-0.72
	MFR	293.57	293.88	293.62	-0.25	297.66	297.34	297.64	0.29
	RIW	299.24	305.12	304.26	-0.86	303.56	308.91	307.84	-1.07
	REV	298.13	305.33	303.63	-1.70	302.50	309.45	307.81	-1.64
	SLC	303.62	306.79	305.52	-1.27	307.85	310.34	309.03	-1.32
	OAK	288.01	288.27	288.05	-0.22	291.51	291.60	291.52	-0.07
	DNR	303.15	305.52	304.88	-0.65	307.15	308.94	308.35	-0.59
	FGZ	306.13	303.54	305.52	1.98	309.85	307.48	309.29	1.81
	ABQ	304.63	309.31	308.55	-0.77	308.27	312.57	311.48	-1.10
	NKX	293.21	293.32	293.23	-0.09	296.24	296.22	296.24	0.02
	TUS	303.87	306.87	305.34	-1.53	306.99	309.49	307.99	-1.50
SEP	UIL	288.58	284.23	285.99	1.76	291.97	287.90	289.54	1.64
	GEG	290.60	290.46	290.59	0.13	294.48	294.43	294.48	0.04
	TFX	295.29	295.03	295.29	0.26	299.45	299.13	299.45	0.32
	GGW	291.94	291.83	291.94	0.11	295.94	295.78	295.94	0.15
	BOI	297.35	297.56	297.35	-0.22	301.52	301.33	301.51	0.18
	MFR	294.89	290.04	292.47	2.42	298.98	293.74	296.16	2.42
	RIW	300.93	301.49	300.93	-0.55	305.31	305.55	305.29	-0.26
	REV	298.88	302.09	299.62	-2.47	303.01	306.10	303.72	-2.38
	SLC	302.83	301.77	302.77	1.00	306.91	305.34	306.76	1.42
	OAK	290.14	289.53	290.17	0.64	293.38	292.78	293.39	0.62
	DNR	302.91	301.56	302.88	1.32	307.24	305.43	307.17	1.74
	FGZ	304.19	302.57	304.19	1.63	307.97	306.54	307.97	1.43
	ABQ	305.34	307.12	305.41	-1.72	309.32	310.77	309.37	-1.40

	NKX	296.27	294.72	295.52	0.81	299.04	297.52	298.25	0.73
	TUS	303.88	304.97	303.98	-0.99	307.12	307.88	307.19	-0.69
OCT	UIL	285.15	281.98	283.12	1.14	288.80	285.82	286.89	1.07
	GEG	282.52	282.52	282.52	0.00	286.78	286.83	286.78	-0.05
	TFX	286.25	287.88	286.56	-1.32	290.82	292.33	291.07	-1.26
	GGW	283.29	283.17	283.31	0.14	287.66	287.52	287.68	0.16
	BOI	286.99	287.51	287.06	-0.46	291.74	291.88	291.76	-0.12
	MFR	286.93	283.71	285.65	1.94	291.60	287.75	289.71	1.96
	RIW	292.41	292.62	292.44	-0.18	297.24	297.15	297.25	0.10
	REV	289.36	294.65	292.05	-2.60	294.00	299.14	296.52	-2.62
	SLC	293.67	291.61	293.75	2.14	298.42	295.89	298.42	2.53
	OAK	285.01	285.53	285.13	-0.40	288.73	289.16	288.84	-0.32
	DNR	295.40	292.82	295.40	2.58	300.29	297.29	300.01	2.71
	FGZ	294.32	292.42	294.54	2.12	299.01	297.14	299.22	2.09
	ABQ	297.39	298.04	297.52	-0.52	301.97	302.33	302.01	-0.32
	NKX	291.98	289.47	290.80	1.32	295.36	293.12	294.39	1.27
	TUS	294.28	295.85	294.72	-1.13	298.41	299.96	298.90	-1.05
NOV	UIL	284.30	280.97	281.62	0.65	288.16	284.91	285.61	0.70
	GEG	282.19	281.27	281.86	0.59	286.50	285.64	286.20	0.56
	TFX	282.90	284.05	282.92	-1.12	287.56	288.68	287.56	-1.11
	GGW	278.21	276.45	277.56	1.11	282.78	281.03	282.13	1.10
	BOI	286.39	284.58	286.03	1.46	291.01	288.99	290.50	1.50
	MFR	288.25	282.56	284.01	1.45	292.65	286.64	288.05	1.41
	RIW	286.92	285.95	286.71	0.76	291.81	290.75	291.58	0.84
	REV	290.66	291.24	290.72	-0.52	295.23	295.77	295.25	-0.52
	SLC	290.67	288.23	289.67	1.44	295.42	292.73	294.21	1.48
	OAK	285.57	283.97	284.82	0.85	289.22	287.64	288.45	0.81
	DNR	290.31	288.14	289.59	1.45	295.26	292.86	294.32	1.45
	FGZ	294.74	288.09	290.57	2.48	299.39	293.00	295.38	2.38
	ABQ	293.19	291.95	293.04	1.09	297.92	296.52	297.72	1.21
	NKX	289.77	286.18	287.52	1.34	293.34	289.96	291.22	1.26
	TUS	293.18	289.73	291.56	1.83	297.44	294.07	295.66	1.58
DEC	UIL	281.34	277.25	278.27	1.02	285.39	281.40	282.40	1.00
	GEG	275.77	275.65	275.79	0.15	280.32	280.21	280.34	0.13
	TFX	278.44	279.77	278.84	-0.92	283.21	284.55	283.69	-0.86
	GGW	273.09	270.97	272.48	1.51	277.81	275.74	277.22	1.48
	BOI	279.59	277.27	278.80	1.53	284.37	281.89	283.48	1.59
	MFR	282.76	276.35	278.30	1.95	287.40	280.71	282.50	1.79
	RIW	281.83	278.39	281.52	3.14	286.81	283.35	286.44	3.09
	REV	284.22	284.40	284.25	-0.15	289.01	289.12	289.03	-0.09
	SLC	284.15	280.18	281.81	1.63	289.08	284.90	286.54	1.64
	OAK	281.22	279.43	280.35	0.93	285.24	283.49	284.40	0.91
	DNR	286.08	282.64	284.30	1.66	291.11	287.55	289.07	1.53
	FGZ	289.53	285.39	287.38	2.00	294.38	290.37	292.37	2.01
	ABQ	286.88	285.91	286.78	0.87	291.79	290.65	291.67	1.02
	NKX	286.05	282.14	283.74	1.61	290.01	286.35	287.85	1.50

	TUS	287.16	285.27	286.39	1.11	291.64	289.70	290.84	1.14